Impacts of ionospheric plasma on magnetic reconnection and Earth's magnetosphere dynamics

S. Toledo-Redondo[1,2], M. André[3], N. Aunai[4], C. R. Chappell[5], J. Dargent[6], S. A. Fuselier[7,8], A. Glocer[9], D. B. Graham[3], S. Haaland[10,11,12], M. Hesse[13], L., M. Kistler[14], B. Lavraud[2,15], W. Li[16], T. E. Moore[8], P. Tenfjord[11], and S. K. Vines[17]

[1]Department of Electromagnetism and Electronics, University of Murcia, Murcia, Spain.

[2] Institut de Recherche en Astrophysique et Planétologie, Université de Toulouse, CNRS, UPS, CNES, Toulouse, France.

[3]Swedish Institute of Space Physics, Uppsala, Sweden,

[4]Laboratoire de Physique des Plasmas, Paris, France,

[5]Physics and Astronomy Department, Vanderbilt University, Nashville, TN, USA,

[6]Physics Department E. Fermi, University of Pisa, Pisa, Italy,

[7]Southwest Research Institute, San Antonio, TX, USA,

[8]Department of Physics and Astronomy, University of Texas at San Antonio, San Antonio, TX, USA,

[9]NASA Goddard Space Flight Center, Greenbelt, MD, USA,

[10]Max-Planck Institute for Solar Systems Research, Göttingen, Germany,

[11]Space Plasma Physics Group, University of Bergen, Bergen, Norway,

[12]The University Centre in Svalbard Longyearbyen, Norway,

[13] Science Directorate, NASA Ames Research Center, Moffett Field, CA,

[14]Institute for the Study of Earth Oceans and Space, University of New Hampshire, Durham, NH, USA,

[15]Laboratoire d'Astrophysique de Bordeaux, Univ. Bordeaux, CNRS, B18N, allée Geoffroy Saint-Hilaire, 33615 Pessac, France

[16]State Key Laboratory of Space Weather, National Space Science Center, Beijing, China,

[17]Johns Hopkins University Applied Physics Laboratory, Laurel, MD, USA,

Corresponding author: Sergio Toledo-Redondo (Sergio.Toledo@um.es)

Key Points:

- Ionospheric plasma contributes a significant part of the magnetospheric density in the regions where magnetic reconnection is most frequent
- Cold and heavy ions of ionospheric origin reduce magnetic reconnection efficiency and modify energy conversion mechanisms
- The presence of ionospheric ions and their effects on reconnection and magnetospheric dynamics are enhanced during geomagnetic storms

Abstract

Ionospheric ions (mainly H^+, He^+ and O^+) escape from the ionosphere and populate the Earth's magnetosphere. Their thermal energies are usually low when they first escape the ionosphere, typically a few eV to tens of eV, but are energized in their journey through the magnetosphere. The ionospheric population is variable, and it makes significant contributions to the magnetospheric mass density in key regions where magnetic reconnection is at work. Solar wind – magnetosphere coupling occurs primarily

via magnetic reconnection, a key plasma process that enables transfer of mass and energy into the near-Earth space environment. Reconnection leads to the triggering of magnetospheric storms, aurorae, energetic particle precipitation and a host of other magnetospheric phenomena. Several works in the last decades have attempted to statistically quantify the amount of ionospheric plasma supplied to the magnetosphere, including the two key regions where magnetic reconnection proceeds: the dayside magnetopause and the magnetotail. Recent in-situ observations by the Magnetospheric Multiscale spacecraft and associated modelling have advanced our current understanding of how ionospheric ions alter the magnetic reconnection process at meso- and small-scales, including its onset and efficiency. This article compiles the current understanding of the ionospheric plasma supply to the magnetosphere. It reviews both the quantification of these sources and their effects on the process of magnetic reconnection. It also provides a global description of how the ionospheric ion contribution modifies the way the solar wind couples to the Earth's magnetosphere and how these ions modify the global dynamics of the near-Earth space environment.

Plain Language Summary

Above the neutral atmosphere, space is filled with charged particles, which are tied to the Earth´s magnetic field. The particles come from two sources, the solar wind and the upper Earth's atmosphere. Most of the solar wind particles are deflected by the Earth´s magnetic field, but some can penetrate into near-Earth space. The upper ionized layer of the atmosphere is continuously ejecting particles into space, which have low energies and are difficult to measure. We investigate the relative importance of the two charged particle sources for the dynamics of plasma processes in near-Earth space. In particular, we consider the effects of these sources in magnetic reconnection. Magnetic reconnection allows initially separated plasma regions to become magnetically connected and mix, and converts magnetic energy to kinetic energy of charged particles. Magnetic reconnection is the main driver of geomagnetic activity in the near-Earth space, and is responsible for the release of energy that drives a variety of space weather effects. We highlight the fact that plasma from the ionized upper atmosphere contributes a significant part of the density in the key regions where magnetic reconnection is at work, and that this contribution is larger when the geomagnetic activity is high.

1 Introduction

Magnetospheric plasma composition and circulation, as well as the sources and sinks of plasma populations in the magnetosphere, have been extensively studied since the beginning of the space era in the late 1950s. Magnetospheric ions of ionospheric origin, or ionospheric-originating ions, however, are difficult to characterize. Their initial low thermal and kinetic energies prevent them from reaching spacecraft particle detectors and therefore remain invisible until energized, usually far away from the ionosphere. Nevertheless, using various direct and indirect techniques, past and recent studies have demonstrated that these particles are important to the dynamics of the Earth's magnetosphere. These particles (H^+), along with heavy ions species such as O^+ and He^+, often dominate the magnetospheric mass-density. In the past years, several review works have addressed the current understanding of these ionospheric ions in the Earth's magnetosphere. Kronberg et al. (2014) reviewed the production and circulation of ionospheric heavy ions in the nightside and inner magnetosphere, highlighting their consequences for the plasma sheet, ring current and radiation belts. Chappell (2015) provided a historical review on the sources and transport of ionospheric ions towards the magnetosphere, highlighting their main role as a magnetospheric plasma source together with the solar wind. Welling et al. (2015) made a thorough review of the Earth's magnetosphere plasma sources, transport and losses. Kistler (2016) analyzed the effects of O^+ coming from the ionosphere in magnetotail dynamics. Yamauchi (2019) reviewed the terrestrial ion escape and circulation in space using knowledge gained from the

Cluster space mission. Finally, Yau et al. (2020) and André et al. (2020) briefly reviewed the escape of ionospheric ions in the polar regions and their impact on magnetic reconnection.

In this work, we discuss the implications of ionospheric ions for magnetic reconnection occurring in the magnetosphere. We focus on the two main regions where magnetic reconnection plays a major role: the dayside magnetopause and the Earth's magnetotail. In Section 2 we present a summary of the plasma sources and the transport mechanisms that are relevant for bringing ionospheric plasma to these outer magnetospheric regions where magnetic reconnection operates. Section 3 presents a review of observational works that attempted to quantify the amount of ionospheric ions that are present near the reconnecting regions. Section 4 focuses on how these changes in magnetospheric composition and plasma properties affect magnetic reconnection, both at the dayside and the tail. In this section, we review the most relevant numerical simulations and spacecraft observations of magnetic reconnection. In Section 5, we discuss the implications of having the ionospheric source of plasma in the magnetosphere, and compile a list of open questions on the subject. Finally, in section 6, we summarize and highlight the main points of this review.

2 Sources and transport of ionospheric ions to the main reconnection regions

2.1 The ionosphere as a source of plasma

The upper atmosphere is partially ionized, and is known as the ionosphere (Figure 1). Ionization occurs through photoionization by solar EUV emission and other radiation, and sometimes also by precipitating charged particles, such as accelerated electrons that generate auroras. At the altitudes where collisions with neutrals in the atmosphere dominate, the energy of charged particles in the ionosphere is of the order 0.1 eV (Kelley, 2009).

At higher altitudes (a few hundred km) the density is lower and the plasma becomes essentially collisionless. Here low-mass electrons can move to even higher altitudes and create an ambipolar electric field, pulling positive ions upward (cyan arrows in Figure 1). The typical dynamics of the ionosphere make ions flow upward along the geomagnetic field. While the heavier ions, O^+, N^+, NO^+ typically do not reach escape velocity and return to the ionosphere because of the gravitational force, light ions, H^+ and He^+ can escape upward into the magnetosphere and have been called the 'classical' polar wind (Banks and Holzer, 1969; Banks, et al., 1971; Schunk et al. 1975). The polar wind occurs from mid latitudes (above ~50^o latitude) all the way to the magnetic poles. Therefore, it supplies the plasmasphere, the outer magnetosphere and the plasma sheet (see colored regions of Figure 1). Ionospheric ions, including heavy ions, are also energized by other mechanisms than an ambipolar electric field, such as waves, which can also make them escape upward into the magnetosphere, constituting what is often called 'non-classical' polar wind or energetic polar wind. In contrast to the escape of a few neutral particles in the upper atmosphere, corresponding to the high energy tail of a Maxwellian velocity distribution in thermodynamic equilibrium, there is no need to heat the whole atmosphere in order for the charged particles to escape. A major part of the mass outflow from the Earth's atmosphere is in the form of charged particles.

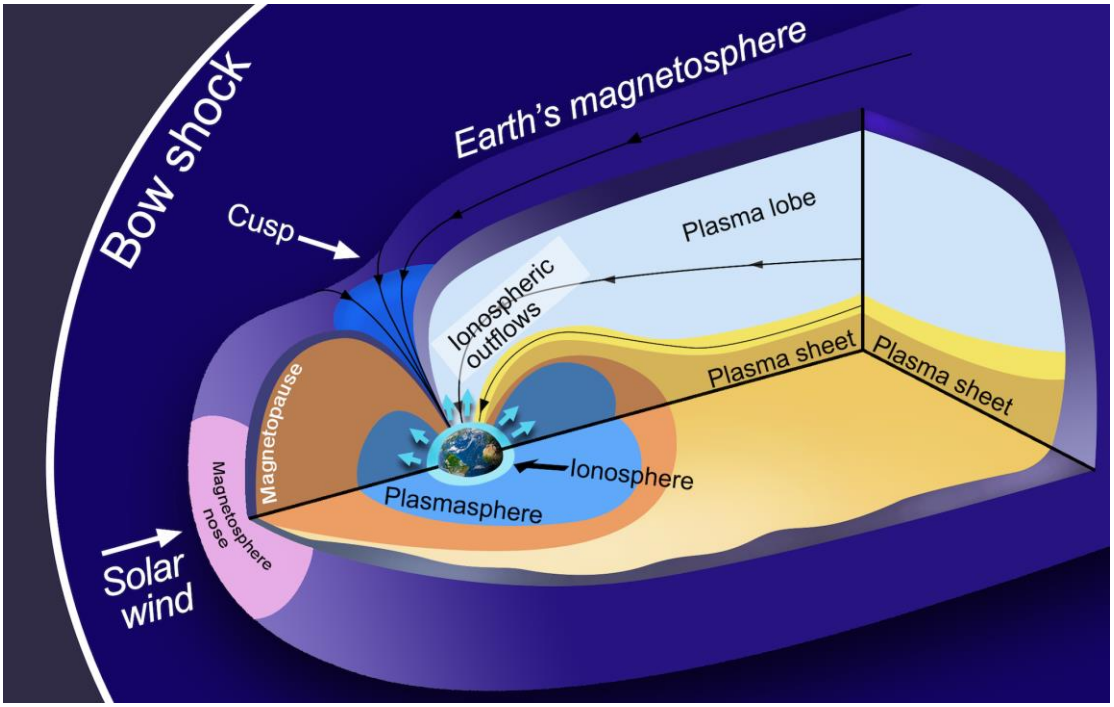

Figure 1. Main regions of the Earth's magnetosphere. Ionospheric ions are continuously escaping along magnetic field lines, and end up in different magnetospheric regions depending on their initial geomagnetic location. Credit: J. M. Domínguez, adapted from Pollock et al. (2003).

What happens to each individual ion depends strongly on their initial location (latitude and longitude) and the magnetospheric conditions at the time (e.g., Huddleston et al., 2005). Due to the configuration of the Earth´s magnetic field, it is convenient to separately discuss high latitudes and mid latitudes, i.e., roughly above or below the auroral zone (see Figure 2). At high latitudes (section 2.1.1), magnetic field lines are open, i.e. connected to the interplanetary magnetic field (IMF) originating from the Sun. The source region, i.e., the location where the ions leave the ionosphere, and their transport along the continuously changing open magnetic field, connected to the solar wind, determines where the ions go, how much they get energized, and where they contribute to the magnetospheric particle populations. At mid latitudes (section 2.1.2), where the geomagnetic field lines close back to Earth, the ionospheric ions accumulate and form the plasmasphere, see Figure 1.

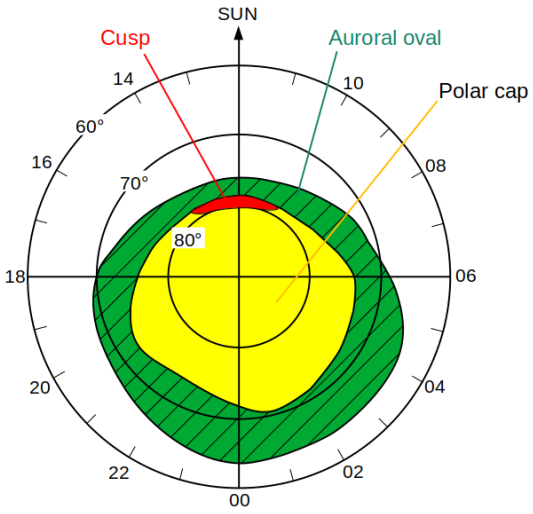

Figure 2. Top view of the Earth's ionosphere in geomagnetic latitude and local magnetic time coordinates, indicating typical locations of the auroral oval (green color), the cusp (red) and the polar cap (yellow). Poleward of the auroral oval, magnetic field lines are open, with the polar cap mapping to the tail lobes, and the cusp mapping to the dayside. Adapted from Akasofu (2015).

2.1.1 High-latitude outflow

In the polar cap region, where magnetic field lines are open and connected to the IMF (see Figures 1 and 2), an ambipolar electric field starts the upflow of ions, above ~800 km of altitude. This upflow is the basis for the aforementioned "classical" polar wind at high latitudes (Axford, 1968; Banks & Holzer, 1969). These ions can be further energized by centrifugal acceleration (due to the drift caused by a large-scale convection electric field in the curved geomagnetic field), the mirror force (e.g., Comfort, 1998) and waves. The ions are typically carried toward the magnetotail both by convection and a parallel velocity depending on the magnetic field direction. The classical polar wind, or simply polar wind, consists of the lighter H^+ and He^+ ions and electrons. A large fraction of these ions has low energies, less than tens of eV, up to altitudes of several Earth radii (R_E = 6371 km).

The auroral oval and the cusp constitute the regions at the boundary between open and closed magnetic field lines. As in the polar cap, ion upflow can be initiated by an ambipolar electric field within the dayside cusp and auroral oval. Here additional mechanisms like friction between the neutral atmosphere and charged particles affected by a convection electric field in the collisional ionosphere also initiate ion heating and upflow (e.g., Schunk 2007). In these regions upflowing ions typically reach higher energies than those ions originating from the polar cap. At higher altitudes, collisions are negligible, and electric fields in the form of waves or quasi-static structures can energize the ions. The energy required to energize the ions can come in the form of waves (often Alfvén waves) generated far away from the local upflowing ion population, or can be carried by particles locally producing waves (e. g., lower-hybrid waves). The mass composition and energy of the outflow depends highly on the ionospheric and magnetospheric conditions. Major ion species comprising ion outflow from the dayside cusp and nightside auroral oval are typically H^+, He^+ and O^+, but with contributions also from N^+, N^{++}, O^{++} and NO^+. These outflows are often referred as "energetic outflows" and were the first indicators of an ionospheric source of plasma in the magnetosphere (Shelley et al., 1972).

In the dayside cusp, energy often comes from waves or accelerated particles originating from magnetic reconnection or other processes at the dayside magnetopause. Wave-particle interactions seen in this

region of the ionosphere, particularly interaction with Alfvén waves, often results in ion heating in the direction perpendicular to the geomagnetic field. Together with ion motion in a diverging magnetic field, this interaction also provides a parallel velocity component, forming so-called conics in ion velocity space. These energetic outflows typically move across the polar cap and the lobes of the magnetotail via convection during southward IMF periods, with velocities depending on solar wind conditions. Sometimes these ions are hard to distinguish from ions originating in the polar cap. Many of these ions reach energies of at least one hundred eV at altitudes of several R_E.

In the nightside auroral region, energy can also come from waves or impinging particles originating at higher altitudes. Similar to the dayside cusp region, wave-particle interactions often cause outflowing ion conics. In addition, quasi-static parallel electric fields are common at altitudes of about one R_E, accelerating auroral electrons downward towards the Earth and ion beams upward. These energetic outflows are typically transported to the inner plasma sheet and the ring current region. Many of these outflowing ions reach keV energies at higher altitudes.

Ion energization and outflow mechanisms are discussed in several studies; for example, the polar wind is discussed by Barakat and Schunk (2006) and Yau et al. (2007), and the dayside cusp and nightside auroral region by, e.g., André and Yau (1997), Strangeway et al. (2005) and Moore and Horwitz (2007). For the purpose of this review, estimates of typical ion outflow rates are needed, as discussed in several papers (e.g., Yau and André, 1997; Su et al., 1998; Cully et al., 2003; Peterson et al., 2006; 2008; André et al., 2015; Slapak et al., 2017; Yau et al., 2017; André et al., 2020; Yau et al., 2020). Overall a typical outflow rate from the high-latitude region is 10^{26} ions/s, including H^+ and heavier ions such as O^+. Rates vary by at least one order of magnitude, typically increasing with higher solar EUV and geophysical activity. This trend is even more pronounced for heavier ions.

2.1.2 Mid-latitude outflow: the plasmasphere

The Earth's plasmasphere is a torus of cold (<1 eV), dense (10's to 100's cm^{-3}) plasma that occupies the inner magnetosphere, typically <3-6 R_E from the Earth, i.e., at magnetic latitudes up to ~60^o (up to L-shells 4-5), confined within the near-Earth closed geomagnetic field lines. It is composed primarily of H^+, with a substantial (1-10%) amount of He^+ and typically much less O^+ (Berube et al., 2005), in addition to electrons, originating from the low- to mid-latitude ionosphere. Mechanisms such as the ion outflows described above are applicable as the source of plasma escape from the ionosphere towards the plasmasphere. The low energy plasma of the plasmasphere approximately co-rotates around the Earth on closed plasma drift paths. The outer edge of the plasmasphere, known as the plasmapause, separates closed and open drift paths. Because of the interplay between the electric drift, which results from the cross-tail electric field set up by the motion of the solar wind past the Earth, and the magnetic gradient and curvature drifts due to the near dipolar magnetic field close to the Earth, plasma from the magnetotail convects inward and around the duskside or the dawnside depending on the charge and energy of the plasma (Figure 3). Ions with low energies, i.e., less than ~1 keV, convect dawnward on open drift paths and can encounter the magnetopause on the dawnside or duskside near noon local time. By contrast, higher energy ions convect to the duskside on open drift paths that may also encounter the magnetopause. At low energies, the convection paths set up a condition whereby the plasmasphere has an elongation or bulge on the duskside (e.g., Carpenter et al., 1993). The convection path in Figure 3 that separates open drift paths (dashed lines that intersect the magnetopause) from closed drift paths (solid lines in the plasmasphere) is called the plasmapause.

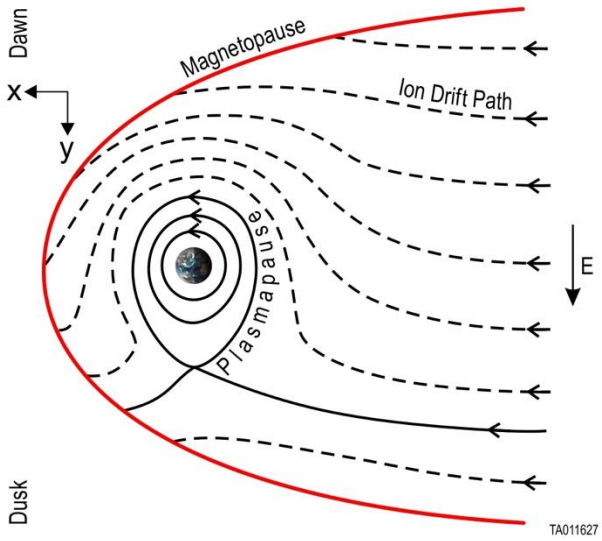

Figure 3. Schematic of the open and closed drift paths in the magnetosphere. The cross-tail electric field and the gradient and curvature drifts set up energy dependent, open drift paths to the dayside magnetopause. The plasmapause is the boundary that separates these open drift paths from closed drift paths in the plasmasphere. The Alfvén layer is the solid line that originates in the tail, connects to the plasmapause, and extends to the dayside magnetopause. This layer separates open drift paths around the dawnside from those on the duskside and indicates the location of the drainage region in the dayside magnetopause.

2.2 Transport of ionospheric plasma in the Earth's magnetosphere

2.2.1 Plasmaspheric erosion, trough, and wind (mid-latitude outflows)

The diagram in Figure 3 illustrates the conditions for relatively quiet and quasi-static magnetospheric conditions. These conditions rarely occur. Geomagnetic activity is typically either increasing or decreasing as the coupling changes between the Earth's magnetosphere and the highly variable solar wind. When geomagnetic activity increases, the plasmasphere contracts, a combined process that includes earthward flow on the nightside with erosion of the outer plasmasphere on the duskside. This is because, as it contracts, plasmaspheric plasma initially located on closed drift paths suddenly finds itself on open drift paths so that the plasma may drain along the newly open drift paths towards the magnetopause on the dayside. The plasma convects sunward approximately along the plasmapause boundary at a rate of the order of 20 km/s (e.g., Denton et al., 2019). This sunward convection carries the eroded plasmasphere material towards the dayside magnetopause. This erosion often produces high-density (> few cm^{-3}) clouds of plasma in the outer magnetosphere (Chappell, 1972), typically referred to as plasmaspheric plumes or simply plumes. The cross-section of this eroded plasma can be quite thin (< 1 R_E) or very thick (many R_E) (Borovsky and Denton, 2008). The thickness depends on the time history of the plasmaspheric erosion and the location and motion of the magnetopause. Typically the plasmaspheric plasma encounters the magnetopause on the duskside and late pre-noon sectors. This region is commonly referred as the plasmaspheric drainage region.

The original plasmaspheric composition does not change as the plasma convects to the magnetopause and observations at the magnetopause confirm the dominant H^+ component, with lower amounts of He^+ and O^+ number densities (Fuselier et al., 2017). However, as the exiting plasmaspheric material propagates toward the magnetopause, the magnetic flux tubes originating in and filled with plasma from the plasmasphere expand and their density decreases. The magnitude of the decrease in density

depends on the convection path and the location of the magnetopause. The plasmaspheric plasma is also heated as it expands in the magnetosphere (e.g., Genestreti et al., 2017), although the degree of heating is variable and there are certainly times when very cold plasmaspheric material is observed at the magnetopause. Finally, the density within the plasmaspheric material is quite variable. Detailed density measurements across plumes show variations of an order of magnitude (e.g., Chappell, 1974; Goldstein et al., 2004; Borovsky and Denton, 2008). These blobs, fingers and striations align along the line that separates drift paths around the dawnside from those on the duskside in Figure 3, i.e., the drainage region.

In addition to plasmasphere erosion by magnetospheric convection, there are other mechanisms that facilitate ion escape from the plasmasphere to the outer magnetosphere: the plasmaspheric trough (Chappell et al., 1971) and the plasmaspheric wind (Dandouras et al., 2013).

The plasmaspheric trough occurs at magnetic latitudes slightly above the plasmapause. The classical polar wind lifts light ions (H^+ and He^+) and electrons in the same way as inside the plasmasphere, but this plasma it located at open drift paths (see Figure 3), outside the corotating plasmasphere. Typical densities of the plasmaspheric trough are ~10 cm^{-3} at L-shell = 4 (Chappell, 1971), which drop to few tenths of cm^{-3} when they reach the magnetopause at L-shells of 10 – 12, due to radial expansion.

The plasmaspheric wind is believed to continuously eject material in the radially outward direction, from the plasmasphere to the outer magnetosphere, at all local times, as a consequence of diffusion occurring at the plasmapause due to the sharp density gradient. This continuous wind was predicted by Lemaire and Schunk (1992), and occurs as the result of instabilities at high latitudes that drive plasma outwards. However, there is no evidence that that the contribution of the plasmaspheric wind to plasmasphere erosion is significant.

2.2.2 Convection of high-latitude outflows and filter effects

When outflowing ions from the ionosphere at high latitudes escape the gravity potential of the Earth and reach altitudes above the exobase, collisions are no longer relevant. Plasma is tied to magnetic field lines, but can move freely along these lines. Additional magnetic field-aligned (upward) acceleration above the exobase takes place as a result of external forces, such as the magnetic mirror force (e.g., Comfort, 1998) or centrifugal acceleration (Cladis et al., 2000; Huddleston et al., 2005, Nilsson et al., 2008, 2010). In addition, waves and parallel electric fields accelerate plasma to keV energies in the auroral and cusp regions (e.g., André and Yau, 1997).

At the same time, the magnetic flux tubes connected to high latitudes move across the polar cap from the dayside to the nightside plasma sheet, due to the interaction between the solar wind and the magnetosphere at the dayside magnetopause, as described in the Dungey cycle (Dungey, 1963). The effective transport of outflowing ions to the magnetosphere is thus the result of the combination of magnetic field-aligned outflow and convection. For northward IMF, i.e., when magnetospheric convection becomes negligible, escaping ions from the dayside ionosphere travel along reconnected field lines directly to the dayside boundary layer (e.g., Fuselier et al., 1989, 2019b; Fuselier, 2020), while outflows that originate on the nightside ionosphere will travel towards the magnetotail, following the quasi-stagnant magnetic field lines. When magnetospheric convection is at work (typically for southward IMF), both dayside and nightside ionospheric outflows are convected towards the magnetotail. In situ observations have shown that the O^+ content of the ring current increases during geomagnetic storms (e.g., Hamilton et al., 1988, Moore et al., 2001, Grande et al., 2003). Kistler (2020) shows that the ionospheric contribution to the near-Earth plasma sheet increases strongly when *Dst* drops during the storm main phase.

For the same amount of parallel energization, lighter ions have larger parallel velocities than heavy ions. On the other hand, magnetospheric convection acts in the same way for all species. As a consequence, a mass filter effect arises when magnetospheric convection is non-negligible: lighter ions escaping the polar cap region or nightside auroral zone travel further along the magnetic field line before reaching the plasma sheet in the magnetotail than heavier ions (Figure 4). A velocity filter effect also applies within a single species: the slowest, i.e., less energetic, ions being deposited close to Earth, and faster, i.e., more energetic, ions further tailward. Some of the fast ions from this region will escape directly into the solar wind and plasma mantle (Slapak et al., 2015, 2017; Schillings et al., 2019; Krcelic et al., 2020) and do not contribute to the ionospheric plasma supply of the Earth's magnetosphere.

A fraction of escaping ions is able to travel very far down the magnetotail, beyond the distant neutral line at around 100 R_E downstream from Earth (Birn et al., 1992, Daly 1986, Nishida et al., 1996), before the containing flux tube closes via magnetic reconnection near the neutral line, resulting in the plasma being lost downtail (Haaland et al., 2012a). Other ions starting from the same location, but with a lower parallel velocity, will not reach as far before the flux tube is convected to the equatorial plasma sheet, resulting in the ions being deposited in the magnetotail closer to the Earth, where magnetotail magnetic reconnection can take place.

During quiet conditions, typically associated with a northward IMF, escaping ions from the nightside travel along open field lines that are more or less stagnant (e.g., Lavraud et al., 2002), due to the low magnetospheric convection. These ions are more likely to be lost in the distant magnetotail region or escape directly into the solar wind than during disturbed conditions. Interestingly, this scenario means that ions from the high latitude ionosphere are deposited far downtail during quiet conditions, and therefore will spend more time in the plasma sheet, where additional heating and acceleration can take place.

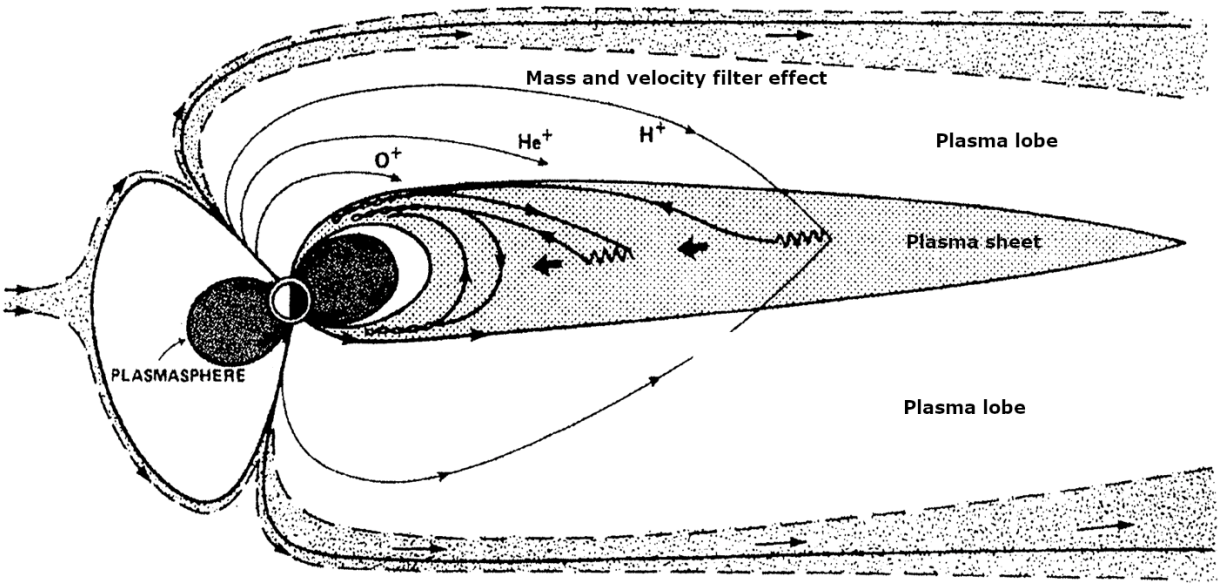

Figure 4. Schematic illustration of transport paths for ions escaping from the polar cap regions. Owing to magnetospheric convection, outflowing ions with the same energy will follow distinct paths depending on their mass. In a similar way, outflowing ions of the same species will follow different paths depending on their parallel velocity (energy). This is known as a velocity filter effect. Adapted from Chappell et al. (1987).

In summary, the upward flowing ions from the high-latitude regions are subject to energization along their individual trajectories. These trajectories depend on the magnetic latitude and local time of their initial escape from the ionosphere, their initial energy and pitch angle, i.e., angle between their velocity and the magnetic field direction, and any energization along their path of travel. The energization along the trajectory depends on waves and parallel electric fields the particles may encounter, on the changing shape of the magnetosphere, as well as the variable cross tail convection electric field that is caused by coupling to the solar wind (Huddleston et al., 2005).

2.2.3 Warm plasma cloak

In the early conceptual understanding of the magnetospheric particle populations in the 1960's, there were three energy ranges of plasma to consider. The first measured was the radiation belts which had MeV energies and were trapped in two donut shaped regions in the inner magnetosphere, the Van Allen radiation belts. A second region of plasma, the plasmasphere, was roughly co-located with the radiation belts but with energies of only a few eV that were directly relatable to the ionospheric ions at lower altitudes. The third, inter-related regions of the plasma sheet and ring current, with energies of 1's to 10's keV, were thought to be of solar wind origin.

As the instrumentation capability improved, an additional category of magnetospheric plasma emerged. Satellite observations made in the 1970's through 2000's (e.g., the ISEE, DE, Polar, and Cluster missions) measured the characteristics of a plasma population extending from the nightside through dawn up to the noon sector outside of the plasmasphere that appeared unrelated to the known magnetospheric plasma populations in the radiation belts, plasmasphere, magnetotail plasma sheet, and inner magnetospheric ring current. This plasma population had energies of 10's of eV to a few keV and was made up of both H^+ and O^+, suggesting an ionospheric source (e.g., Jahn et al., 2017). These high energies indicated that this population was not a direct ionospheric upflow originated by classical polar wind. Because the cross tail convection electric field causes particles to flow from the tail in a sunward direction, and because lower energy ions drift dawnward, the new region comprising this plasma population was called the warm plasma cloak (WPC), as the plasma was being "blown" sunward through the dawn sector to the magnetopause (Chappell et al. 2008).

Extensive modeling of ion trajectories has been done by e.g., Delcourt et al. (1989, 1993) and Huddleston et al. (2005). This modeling shows how the original low energy ionospheric origin ions can move through the various regions of the Earth's magnetosphere, having their energy and pitch angle changed as they travel. The energization may be caused by centrifugal acceleration in the polar cap, initially, followed by the energy-changing effects of curvature and gradient drift in the presence of the cross-tail convection electric field, which have values of 50 to 100 kV across the magnetospheric tail. The results of doing statistical trajectory calculations suggest that these up-flowing ions are energized to 100 eV, 1 keV, 20 keV as they move through the different regions. The study did not include acceleration by waves and parallel electric fields, which would add more energization to ions originating from the cusps and auroral regions. The net effect of the combination of these different up-flowing ions is to create both densities and energies that are actually observed in these different regions, indicating that the ion outflows constitute a primary source of plasma for the Earth's magnetosphere, see figure 5. It was shown that the source of the warm plasma cloak was indeed the ionosphere. However, unlike the ionospheric supply to the plasmasphere, where ionospheric ions with energies of a few eV move directly up the magnetic field line to fill flux tubes, the warm plasma cloak ions come from the ionosphere as polar wind and polar cusp outflows but follow different trajectories across the polar cap and into the near-Earth dawnside of the magnetotail where the ions are energized from 10's eV up to a few keV (Chappell et al, 2008). It was also shown that the ultimate energy of an ionospheric particle that flows

up into the magnetosphere is determined by where it enters the center plane of the magnetotail. The farther a particle travels down the tail, the more the magnetic field lines are distended in the center plane of the tail and the more curvature drift the particle will encounter when it enters this region. Particles which become the warm plasma cloak enter the tail earthward of those which become the plasma sheet and subsequently the ring current.

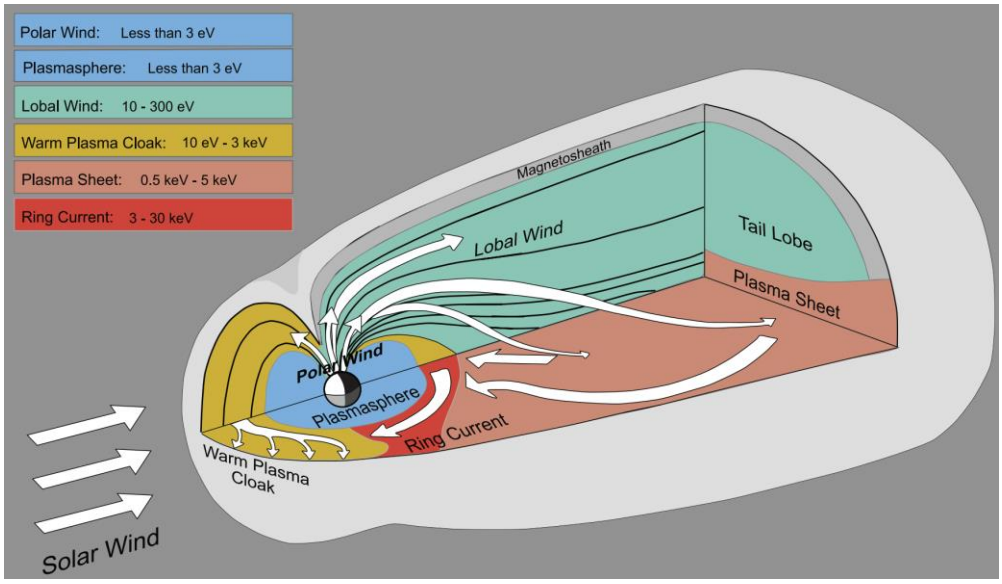

Figure 5. Schematic summarizing the particle tracing results from Delcourt et al. (1993) and Huddleston et al. (2005). The ions of ionospheric origin are energized as they travel in the Earth's magnetosphere. Adapted from Chappell et al. (2008).

Of direct significance to this review is the fact that the warm plasma cloak particles are convected past dawn to the post-noon magnetopause where they enter the reconnection region at the nose of the magnetosphere, changing the plasma characteristics both by energy and mass and thus affecting the rate of reconnection on the dayside, see sections 3 and 4. A corollary to this, of course, is that the entry of the ionospheric ions into the centerline of the magnetotail also affects the reconnection process there. As the polar/lobal wind particles (10's to 100's of eV) enter the distended field lines of this region, they will begin to be accelerated, thereby influencing the conditions conducive for magnetic reconnection in the magnetotail.

In summary, the flow of ionization from the ionosphere through the lobes to the central plane of the magnetosphere affects two different areas of reconnection, initially the neutral sheet area of the tail and potentially, through the sunward flow of the warm plasma cloak to the dayside magnetopause.

2.3 The ionospheric plasma source from a global modelling perspective

While the magnetosphere is known to have two sources of plasma, the solar wind and the ionosphere, global magnetospheric models have for many years only included the solar wind source. The first models to include an explicit source of ionospheric plasma appeared more than 20 years ago (e.g., Winglee 1998), but the regular inclusion of ionospheric outflows into global models is a relatively recent innovation. There are multiple approaches to modeling the source and impacts of ionospheric plasma in the magnetosphere implemented in different studies, but these disparate approaches all demonstrate that ion outflows can have a profound effect on the near-Earth space environment.

Tracking ionospheric plasma as it flows through the magnetosphere requires two critical components: 1) a model capable of following disparate plasma populations, and 2) a specification of the ionospheric source of plasma. One method of tracking the flow of ionospheric plasma through the magnetosphere involves tracking large numbers of test particles, launched from the ionosphere, through either static or dynamic fields using MHD (e.g., Peroomian et al., 2007, Moore et al., 2005). Such an approach has the advantage of allowing for kinetic effects and non-Maxwellian particle distributions as the full equation of motion is evolved for many particles. This test-particle method has the disadvantage is that the particles and fields do not evolve self-consistently. An alternative approach that has been more actively pursued in recent years is to track each source of plasma separately in its own fluid in a multi-fluid MHD model of the magnetosphere (e.g., Winglee et al., 2002, Glocer et al. 2009, 2018, 2020, Wiltberger et al., 2010). While this methodology does not allow for non-Maxwellian distributions, it does allow for the self-consistent evolution of both plasma and electromagnetic fields.

In terms of specification of the ionospheric source, three methods are commonly used. The simplest method is to specify an ionospheric boundary density which acts as a reservoir from which diffusion and MHD forces effectively pull ionospheric plasma into the magnetospheric simulation domain. This approach was studied extensively by Welling and Liemohn (2014) and found to roughly approximate the observed statistical pattern of ionospheric outflow. A more causally regulated method for representing the outflow is to apply a statistical relationship connecting magnetospheric energy inputs with escaping plasma developed from the FAST (Strangeway et al., 2005) or Polar (Zheng et al., 2005) spacecraft mission data. This approach has been applied in both test particle and multi-fluid MHD models (e.g., Brambles et al., 2010, Moore et al., 2005). The applicability and uncertainties inherent in the underlying statistical models of outflow has led in recent years to the incorporation of physics-based first principles models of ion escape in to magnetospheric models to represent the ionospheric source (Glocer et al., 2009; Varney et al., 2016a; Welling et al., 2016).

Although the approaches to studying the influence of ionospheric plasma on magnetosphere dynamics differ, they have demonstrated that ion outflow has wide ranging influences on the broader space environment. Moore and Delcourt (1995) introduced the concept of the geopause as boundary inside of which the plasma is primarily of ionospheric origin. The location of the geopause is found to depend heavily on the solar wind IMF orientation (Winglee, 1998) and may have significant North-South asymmetries (Li et al., 2000). The different transport paths to the magnetosphere taken by disparate plasma sources are found to have a major influence on the ring current. For example, polar wind protons and solar wind protons contribute similarly to the ring current during a geomagnetic storm, but the solar wind-originating protons have a higher mean energy due to a longer inward travel path from the tail (Moore et al., 2005). The different plasma trajectories through the magnetosphere also result in local time-dependent injections of plasma of different species into the ring current (Welling et al., 2011).

In simulations, ion outflows are also found to have large scale consequences for the magnetosphere. Indeed, simulations that include outflow often have a lower cross polar cap potential, and hence reduced global convection (Glocer et al., 2009; Wiltberger et al., 2010; Welling & Zaharia, 2012). Simulations that include ionospheric outflow with self-consistent feedback between the particles and fields are better able to reproduce observed magnetic fields (Glocer et al., 2009). Intriguingly, simulations by Brambles et al. (2010) suggest a potential connection between the escape of ionospheric outflow and periodic sawtooth oscillations (one particular manifestation of geomagnetic activity). These simulations were later reproduced with a more physically realistic simulation (Varney et al., 2016b), but the proposed mechanism remains an actively debated topic in the magnetospheric and ionospheric communities (e.g., Liao et al., 2014; Lund et al., 2018). In addition to sawtooth events, O^+ from the ionosphere is found to have a significant influence on dynamics in the magnetotail, such as bursty bulk

flows (Garcia et al., 2010, Garcia-Sage et al., 2015). Glocer et al. (2020) modeled separate H^+ fluids from the ionosphere and the solar wind and showed a significant contribution of ionospheric H^+ to both the plasma sheet and the ring current regions during times of southward IMF. The model also showed that the ring current contains both ionospheric O^+ and H^+ making the ionospheric contribution dominant over the solar wind H^+ and He^{++}.

2.4 Final considerations on the role of the ionosphere as a source of magnetospheric plasma

In the early years of magnetospheric physics, an important role for the ionosphere was recognized, but mainly as a region that was responding to the inflow of particle and wave energy from the energetic particle populations above. While the link between the plasma sheet and ring current regions to the auroral oval with particles, electromagnetic fields, and currents was accepted and studied, the role of the ionosphere as a source of the more energetic particles was neither fully realized nor understood (Chappell, 2015).

Advances in instrumentation that could measure the low (eV), medium (100 eV -1's keV) and higher energy (10 keV -100 keV) particles combined with the ability to separate masses were a critical new contribution. In the 1970's, 80's and 90's this improved instrumentation enabled the observation of a significant up-flow of ions from the ionosphere out into the magnetosphere (ISEE, Akebono, DE, Cluster, Polar). Early estimates of the contributions of these initially low energy particles showed that they were sufficient in terms of density to create the major observed plasma regions of the magnetosphere (Chappell et al., 1987). Later ion trajectory studies of these up-flowing cold ions showed that they not only moved through the different magnetospheric regions, but in so doing were energized to match the observed energies in these regions (plasmasphere, plasma sheet, warm plasma cloak, and ring current) (Delcourt el al., 1993, Huddleston et al., 2005). In addition, more recent studies show that the changing low energy plasma of the inner magnetosphere can have a significant effect on changing wave generation and propagation which can affect the creation and loss of the very energetic radiation belt electrons and ions (e.g., Thorne, 2010).

As discussed above, for the outflowing ions in the polar cap and lobes, the distance that they travel down the tail is controlled continuously by the changing solar wind magnetic field and velocity (Haaland et al., 2012b; Liemohn et al., 2007). The entry point of the ions from the lobe into the central plane of the magnetotail determines their subsequent trajectories and how much they will be energized (see also Figure 4). Huddleston et al. (2005) used a combination of data from the Thermal Plasma Dynamics Experiment (TIDE) on the Polar spacecraft combined with ion trajectories based on the work of Delcourt et al. (1993). Using TIDE measurement of the outflowing ions (2 eV - 400 eV) above the ionosphere as input to the trajectory models, Huddleston et al. (2005) showed that the sum of the outflowing ionospheric-originating ions, combined with the outflowing polar cusp ions and some nightside auroral zone upflowing ions, give enough flux to fill the plasma sheet to the densities that are observed.

One further consideration is the timing required for the two sources, solar wind and ionosphere, to add plasma to the plasma sheet. Sorathia et al. (2019) used particle tracing from the solar wind at the bow shock into the magnetosphere during northward IMF, which is the favorable condition to convect solar wind ions into the plasma sheet region by the Kelvin-Helmholtz instability between the magnetosheath and the flank magnetosphere. The solar wind ion access takes about 3 hours to move from the bow shock to the outer plasma sheet and add the particles. In contrast, when the IMF shifts to southward, the outflowing ions already in the tail lobes can be convected into the center of the plasma sheet in a matter of tens of minutes to an hour depending on their location in the lobe.

Finally, we want to emphasize an important consideration about basic nomenclature. For up-flowing ionospheric ions, cold plasma and ionospheric plasma are not necessarily synonymous. There are instances, particularly in the plasmasphere region where the outflowing ionospheric ions are not energized as they fill up the dipolar flux tubes that are corotating, hence cold and ionospheric are the same. At higher L-shells, however, where the ions are carried back into the tail, their energies can be significantly changed by their particular trajectories, hence the ions are still from an ionospheric source but can have total energies >1000 eV (bulk acceleration plus thermalization). The extension of this realization is that in the reconnection region of the magnetotail, there can be instances where lower energy cold ions can enter the reconnection region, but it is also the case that the hotter plasmas that are involved in the reconnection process are often ionospheric-originated.

3 Quantification of ionospheric plasma near the reconnecting regions

As described in Section 2, the escape and transport of ionospheric ions into the various regions of the magnetosphere depends on multiple interrelated processes, including for instance energy deposition in the ionosphere and magnetospheric convection. This section compiles all the statistical work that has quantified the contributions of the ionospheric plasma source to the regions where magnetic reconnection, the primary mechanism for coupling with the solar wind and driving energy in the Earth's magnetosphere, occurs.

There have been recent global modelling efforts including the ionospheric source, which clearly indicate their relevance for populating the Earth's magnetosphere, as discussed in section 2.3. The main drawback of these models is that they need to couple many different physical processes occurring at very different spatial scales and plasma regimes, from the highly collisional ionosphere, including chemical processes to assess the plasma density and composition, to the collisionless magnetosphere and convection of the magnetic field lines.

In the following subsections, we first describe the techniques for detecting cold ions (up to ~10 eV), corresponding to the initial energy of ionospheric ions when they escape to the magnetosphere. Then, we review all the available statistical in-situ and remote observations near the two main reconnection regions in the Earth's magnetosphere: the dayside magnetopause and the magnetotail. We describe and put together the statistics of observations of cold ionospheric-originating ions in these two key regions. As mentioned in section 2, not all ions of ionospheric origin are cold when they reach the reconnection regions. However, from an observational perspective, it is not possible to distinguish the origin of hot (keV) protons. The cold ions discussed in this section correspond to the young ionospheric plasma supply, in the sense that they did not yet have time to be energized significantly, and correspond unequivocally to the ionospheric source.

3.1 Techniques for cold ion measurements

While ionospheric-originating ions are very important for understanding magnetospheric dynamics and the coupling of the solar wind and magnetosphere to the ionosphere and underlying atmosphere, ions with energies of less than ~10 eV, such as those directly originating from ionospheric outflow and the plasmasphere, are often hard to detect in space plasmas. A main source of this difficulty arises from the fact that a sunlit spacecraft in a low-density plasma becomes positively charged up to tens of volts (Grard, 1973; Garrett, 1981; Whipple, 1981). Hence, positively charged ions at very low energies will not reach the spacecraft and cannot directly be detected. Various techniques have been developed to overcome this challenge (André and Cully, 2012).

Remote sensing can be used to detect plasmas of both low and high energy. For example, actively transmitting ground-based ionosondes and top-side sounding from a spacecraft has been used to

determine the plasma density at a specific altitude (Benson, 2010). With ground-based radars and incoherent scatter radars, several plasma parameters of the ionospheric plasma populations can be estimated (Ogawa et al., 2009). In the magnetosphere, passive remote sensing with instruments on spacecraft detect EUV solar photons resonantly scattered from He^+ ions (Spasojevic and Sandel, 2010). Also, energetic neutral atoms (ENAs) produced by charge-exchange between magnetospheric ions and hydrogen atoms in the exosphere travel in line-of-sight paths to a spacecraft and are detected at energies at least down to tens of eV (Sandel et al., 2003; Fuselier et al., 2020a), allowing for inference of the low-energy plasma populations in certain regions.

Observing plasma in situ with detectors onboard a spacecraft allows for direct measurements of local plasma properties, but adds uncertainties in the observations caused by interaction of the spacecraft itself with the plasma. In the source region of ionospheric outflow, the plasma density can be so high that the spacecraft potential becomes zero or slightly negative, due to many impacting electrons on the spacecraft surface, allowing for low-energy populations to be measured. At altitudes of a few hundred km ion detectors are used to study positive ions at low energies (Shen et al., 2018). Additionally, Langmuir probes are used to determine electron density and temperature in dense plasmas (Brace, 2013; Knudsen et al., 2017).

At higher altitudes in a low-density plasma, low-energy ions are still able to be observed in situ, for instance when a satellite is in eclipse (i.e., in the Earth's shadow) during short periods, and hence become negatively charged (Seki et al., 2003). When a spacecraft is positively charged, an indirect method for measuring the cold ion density is to estimate the total plasma density from observations of electromagnetic wave emission at the electron plasma frequency or upper hybrid frequency, and subtract the ion density deduced from particle detectors (Sauvaud et al., 2001; Lee et al. 2012; Jahn et al., 2020; Fuselier et al., 2020b). In addition, the total plasma density is estimated from the spacecraft potential. This potential depends on the density and the electron temperature but can in many magnetospheric plasmas be calibrated and used to estimate the total density (e.g, Grard, 1973; Laakso and Pedersen, 1998; Lybekk et al., 2012; Jahn et al., 2020). To obtain particle distribution functions in velocity space, the positive charging of the spacecraft that repels the positive ions must be reduced. One method is to use a negatively charged aperture plane around the ion detector entrance, as was used for the RIMS instrument on Dynamics Explorer (Chappell et al. 1980). An alternative approach is to negatively bias the entire instrument or a large part of the spacecraft as done for the Magnetospheric Plasma Analyzers (MPAs) on certain geosynchronous spacecraft (Borovsky et al., 1998). Yet another alternative approach used by some missions is to reduce the charging of the whole spacecraft by emitting a plasma cloud (Moore et al., 1997; Su et al., 1998) or a beam of positive ions (Torkar et al., 2016), but often a spacecraft potential of a few volts remains. We note that several studies concentrate on initially cold ions that have been heated (i.e., larger thermal velocity than expected given the plasmaspheric or ionospheric source) or are drifting, e.g., due to **E** x **B** motion, i.e., large enough bulk velocity to overcome the spacecraft charging (e.g., Lee and Angelopoulos, 2014). In these situations ion detectors on a positively charged spacecraft are still effective (e.g., Sauvaud et al., 2001; Lavraud et al., 2005), and accurate estimations of the densities of these cold populations requires moment calculations that properly account for the spacecraft potential (e.g., Lavraud & Larson, 2016).

An alternative method for determining the presence and properties of a cold ion population utilizes the fact that a supersonic flow of cold positive ions can create a large enhanced wake behind a positively charged spacecraft. The wake will be filled with electrons with a thermal energy that is higher than the ram kinetic energy, in contrast to that of the ions. This creates a local electric field which can be observed and then used to detect the presence of cold ions. Using multiple instruments to measure the geophysical electric field, magnetic field, and spacecraft potential in order to estimate the total plasma

density, the cold ion flux can be deduced (Engwall et al., 2009). This method requires one technique to determine the local electric field, such as detecting the potential difference between probes on wire booms in the spin-plane of a spinning spacecraft, and another to characterize the essentially unperturbed geophysical electric field, such as detecting the drift of artificially emitted keV electrons gyrating back to the spacecraft, as is done with an instrument onboard the Cluster and Magnetospheric Multiscale (MMS) missions. Such observations from the Cluster satellites have been used for statistical studies covering a major part of solar cycle (André et al., 2015). In addition, observations from the MMS spacecraft have been used to show that charging of the individual wire booms affects observations, but can also be used to obtain information on cold ions (Toledo-Redondo et al., 2019).

3.2 Quantification of ionospheric-originating ions at the dayside magnetopause

In this subsection, we summarize the findings of the statistical studies found in the literature which attempted to infer the properties of ions of ionospheric origin present at the dayside magnetopause, i.e., the region where the magnetosphere couples to the solar wind via magnetic reconnection. Most of these studies are based on in-situ observations, which are local in nature and orbit dependent. Inferring the global properties of the ionospheric component at the dayside magnetosphere by means of in-situ observations can only be done from a statistical perspective, using from months to years of spacecraft observations. Different missions have different orbits, including equatorial versus polar orbits, and different or even varying apogee and perigee distances. In addition, the dayside magnetopause location is dynamic, most of the time being located between 8 – 12 R_E from Earth. Another important difference between studies is the instruments and associated techniques they use for inferring the plasma properties, in particular density, composition and temperature. We decided to group the studies by the main technique they use for cold ion detection. Since the studies reviewed in this section use different spacecraft, different techniques, and even different definitions of ionospheric plasma, one needs to be careful when comparing their results. We tried to enunciate the main points to consider for each of these studies when discussed together. At the end of this sub-section, we provide a table with the main findings, compare the results of each of these studies and draw conclusions from putting all these observations together.

3.2.1 Studies based on in-situ ion detectors

The most straightforward technique to infer the properties of cold ions in space plasmas is by using the low-energy range (up to few tens or few hundred eV) of ion detectors onboard spacecraft. The main problem of this approach is that any ion with total energy (bulk drift energy plus thermal energy) lower than the spacecraft potential will not be detected, cf. Section 3.1. While this is not a problem for detecting the WPC (typical thermal energies of few hundred eV), it poses a serious challenge for detecting plasmaspheric material (typical thermal energies in the eV range).

Chappell (1974) performed a statistical analysis of the plasmaspheric plume properties using OGO 5 satellite (equatorial orbit). He reported 73 cases (orbits) of observations of exiting plasmasphere material in the dayside magnetosphere, at L-shells > 4. He reports only peak densities and found an average peak density of ~65 cm^{-3}, and the observations being concentrated in 9:00 – 21:00 Local Time (LT) sector, i.e., mainly in the drainage region.

Chen and Moore (2006) used 3.5 years (January 2000 - June 2003) of the Polar spacecraft (polar orbit) data to infer the statistical probability of observing thermal ions (cold ions, i.e., eV temperature but any drift velocity) as a function of local time in the dayside magnetosphere. This method allowed for detection of the plasmaspheric material but disregarded WPC events, which are often not so cold. Thermal ions were detected 50% of the time near the dusk side magnetopause, while the occurrence

near the dawn-side magnetopause was 30% (see Figure 6), considering as detection any flux above the noise level of the instrument at the low energy range. Their occurrence probabilities are higher for larger L-shells, and this is because the ion detector requires that the bulk plasma velocity has higher energies than the equivalent spacecraft potential (typically few to several V). This occurs preferentially near the magnetopause, where local motions of the boundary and ULF waves accelerate the cold plasma to energies above the spacecraft potential. The dawn-dusk asymmetry is explained by the location of the drainage region, which is predominantly in the dusk sector. Finally, they also compared the statistical occurrence of thermal ions with the orientation of the solar wind magnetic field, or Interplanetary Magnetic Field (IMF). They found a larger occurrence probability of thermal ions during southward IMF periods, consistent with the picture of enhanced magnetic reconnection and magnetospheric convection that facilitates erosion of the plasmasphere, including plume formation.

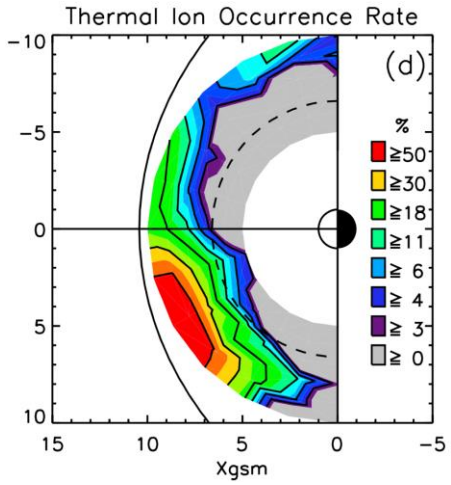

Figure 6. Occurrence probability of thermal ions, based on 3.5 years of POLAR spacecraft observations. Adapted from Chen and Moore (2006).

Borovsky and Denton (2008) used 210 plasmaspheric plume events during geomagnetic storms, observed at geosynchronous orbit (6.6 R_E) by the MPA onboard Los Alamos satellites (equatorial orbit). They found that plasmaspheric plumes are a persistent feature of geomagnetic storms, and that they last for ~4 days. Their typical flow velocities are ~15 km/s towards dayside magnetopause. The average mass flux is ~2 x 10^{26} ions/s, and the average mass released per event is ~2 x 10^{31} ions. These numbers indicate that plumes constitute a primary escaping path of plasma. The plume plasma density, flow velocity and width all decrease with the plume age. However, these observations are taken far away from the Earth's magnetopause, which is typically situated at ~10 R_E. Assuming an effective area of the drainage plume region at the magnetopause of ~9 x 12 R_E, as in André and Cully (2012), and an average outflow velocity of ~15 km/s (Borovsky and Denton, 2008), the resulting ionospheric average density at the magnetopause in the drainage region corresponds to ~3 cm^{-3} during storm times.

The previous studies discussed the presence of plasmaspheric material in the outer, dayside magnetosphere. Another important population that brings ionospheric-originating ions to the dayside magnetopause is the WPC (cf. section 2.2.3). Nagai et al. (1983) analyzed ISEE-1(equatorial orbit, 30^0 inclination) data (June 1978 – December 1980) and searched for field-aligned bidirectional ion jets in the energy range 10 – 100 eV, and found occurrences larger than 50% at the dawn side magnetopause (L-shells ~10, see Figure 7a). Their search criteria match with the properties of the WPC. Similar results are obtained by Chappell et al. (2008), who analyzed 1 year (March 2001 – March 2002) of Polar spacecraft data (polar orbit) searching for the WPC population. Their criteria were to find bidirectional, field aligned

ions in the energy range 10 – 400 eV within 1 L-shell portion of the orbit. They did not impose a minimum density threshold for the bidirectional jets. They found, for L-shells of 10 – 12, i.e., the region where the magnetopause is located, WPC detections of 30 – 50 % in the dusk side and > 70 % in the dawn side (see Figure 7b), with larger occurrence for latitudes < 30°.

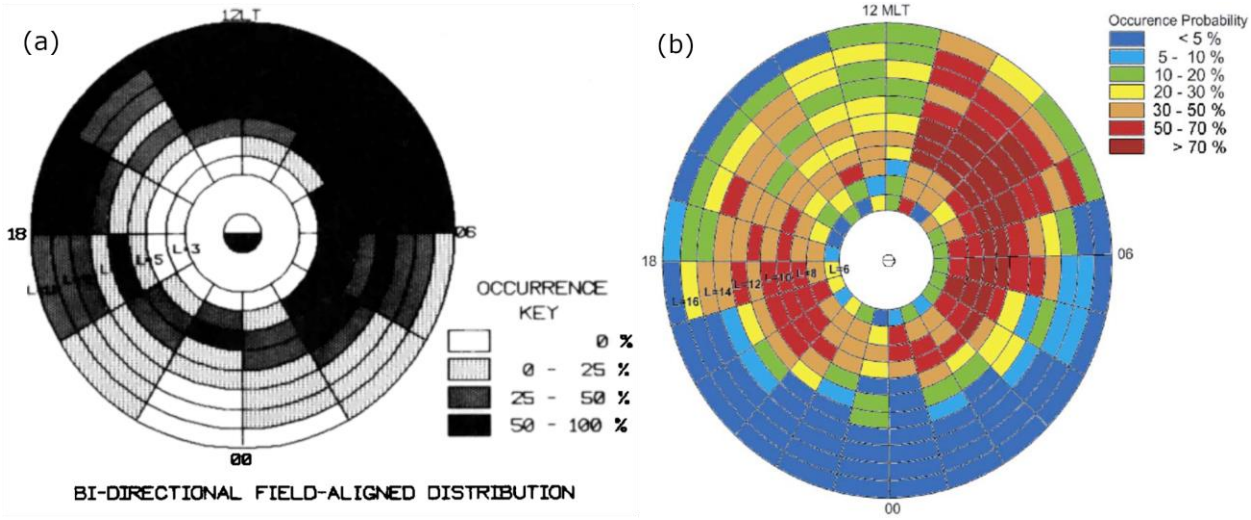

Figure 7. (a) Statistical occurrence of warm plasma cloak observed from ISEE-1, June 1978 – December 1980, in the 1 – 100 eV energy range. Adapted from Nagai et al. (1983). (b) Polar statistical (March 2001 – March 2002) observations of the warm plasma cloak (bidirectional field aligned ion jets of less than 400 eV).. The occurrence is larger than 70% in the dawn side, for L-Shells of 10 – 12, i.e., the region where the magnetopause is located. Adapted from Chappell et al. (2008).

Lee et al. (2016) used Cluster data in the 2007 – 2009 period, to infer the occurrence and density of both the plasmaspheric plume and the WPC near the magnetopause. They looked individually at each of the 442 magnetopause crossings of Cluster 3 spacecraft, and searched for fluxes >10^5 keV/(cm^2 s sr keV) lasting at least 2 min, in the energy range 10 – 1000 eV). Plasmaspheric material may be underestimated, as in Chen and Moore (2006), because it often has energies below 10 eV, the instrument threshold. They distinguish between the two populations based on the pitch angle of the ions. The WPC typically exhibits field-aligned bidirectional jets, while the plasmaspheric material is observed at pitch angles perpendicular to the magnetic field (owing to drift motion). Plasmaspheric material was found in the dusk sector near the magnetopause for 41 events out of 221 crossings, i.e., 19%. This number is lower than for other studies probably due to non-detections of cases with total energies below 10 eV. With regards to the WPC, they find for the dawn sector 17 events out 221 featuring bidirectional jets for more than 2 min, corresponding to 8% occurrence. This value is again lower than previous estimates by Nagai et al. (1983) and Chappell et al. (2008), and the reason is that their threshold requirements for density and duration for considering detection were more restrictive for this study. They estimate a median density of 5.4 cm^{-3} for plasmasphere-originating ions, and a median density of 5.2 cm^{-3} for the WPC, indicating that they captured only very dense events.

3.2.2 Studies based on in-situ, mass-resolving, ion detectors

Some ion detectors measure the time of flight inside the instrument, allowing to discriminate their mass. Fuselier et al. (2017, 2019a) statistically analyzed the properties of the plasmaspheric material and the WPC in the dayside magnetosphere, using roughly 5 months of MMS data between September 2015 and March 2015. In their approach, they looked for observations with H^+ density above 1.5 cm^{-3} in the

dayside magnetosphere (i.e., plasmaspheric plumes and dense WPC), at distances > 7 R_E, and within 1.5 h in time from the magnetopause crossing. They exclude the magnetosheath and the low-latitude boundary layer by imposing the requirement that no significant He^{++} is present. They distinguished the origin of the population depending on the relative amounts of heavy (He^+ and O^+) ions, which are measured by the Hot Plasma Composition Analyzer (Young et al., 2016). They found that WPC intervals have $n_{He+}/n_{O+} < 1$ and plume intervals have $n_{He+}/n_{O+} > 1$. Outflow from the high-latitude ionosphere is dominated by O^+ with much less He^+ (e.g., Collin et al., 1988); thus, it stands to reason that the WPC is distinguishable from the plume by its O^+ content. Since their observations rely on particle instruments, they cannot measure populations with total energy below the spacecraft potential (several eV to few tens of eV). Most of the plume observations occurred in the LLBL, where the convection flows are large and the cold plume can reach energies above the spacecraft potential and be observed by HPCA. Overall, they find that ionospheric H^+ with number density > 1.5 cm^{-3} was detected by HPCA ~14 % of the time in the magnetospheric side of the magnetopause, 10% for the WPC and 4% for the plume populations. This study shows the lowest occurrence percentages, with findings similar to those in Lee et al. (2016). Their lower occurrences may be explained by the threshold density imposed (WPC) and the hidden plume at energies below the spacecraft potential.

3.2.3 Studies using specific techniques aimed for cold ion detection

Walsh et al. (2013) examined all magnetopause crossings by the THEMIS constellation (equatorial orbit) during the years 2008 – 2010 and searched for dense plasmaspheric plumes on the magnetospheric side. Their criteria were that the total density was larger than twice the plasmasphere density expected from a plasmaspheric model (Sheeley et al. 2001) inside the magnetosphere. The threshold for considering plume detection at 10 R_E was 3.8 cm^{-3} and therefore looked only for high-density plumes. The density was inferred from the average spacecraft potential, during 2 min of observations in the magnetosphere adjacent to the crossing. In principle, inferring the density from the spacecraft potential has the advantage of accounting for typically 'hidden' low-energy ions, but this method has to be carefully calibrated by comparing with other observations (cf. Section 3.1). They found that 137 out of 520 crossings (26%) contained the high-density plasmaspheric plume adjacent to the magnetopause in the dusk sector, with most densities greater than 5 cm^{-3} and up to more than 100 cm^{-3}.

Lee and Angelopoulos (2014) used ~5 years of data (January 2008 – May 2013) from 3 spacecraft of the THEMIS constellation to infer the statistics of cold ions. Their observations are also based on the ion detector onboard the spacecraft, which cannot detect cold ions with total energy below the equivalent spacecraft potential (~10 eV). To account for that, they normalize their dwell times to the times when **E** x **B** energy exceeds the spacecraft potential, i.e. the times where the bulk drift energy exceeds the equivalent spacecraft potential. By using this normalization, they ensure that their occurrence rates are not biased by hidden, low-energy, plasmasphere material. They search for ions in the 5 – 120 eV range, and impose that the number density measured by the ion detector and using the spacecraft potential match within a factor of 2. They find that cold ions are most frequently seen in the late morning and afternoon sector, i.e. the drainage region, with relative occurrences of 60 – 90 %. They also found dependence with *Kp* index, an index that accounts for the level of geomagnetic disturbance at the magnetosphere, with cold ions being more spread along all Magnetic Local Times (MLT) for *Kp* < 1, and more concentrated in the late morning to afternoon sector for *Kp* > 1. Figure 8 shows the median density and temperature of H^+. The densities are typically >1 cm^{-3} in the drainage region and <1 cm^{-3} in the other dayside regions. Typical temperatures are always below 50 eV. The ion instrument onboard the THEMIS spacecraft cannot directly resolve the mass of ions. However, if the ions experience flows, it is possible, under certain assumptions, to gain information on the multiple ion populations. For He^+, they found that the median number density ratio $n_{He+}/n_{H+} < 0.1$ in the dusk sector, and ~0.5 in the dawn

sector. For O+, they found roughly the same median ratios in the dayside, i.e., $n_{O+}/n_{H+} < 0.1$ in the dusk sector, and ~0.5 in the dawn sector. In their heavy ion calculations, they exclude detections with total energies > 1 keV.

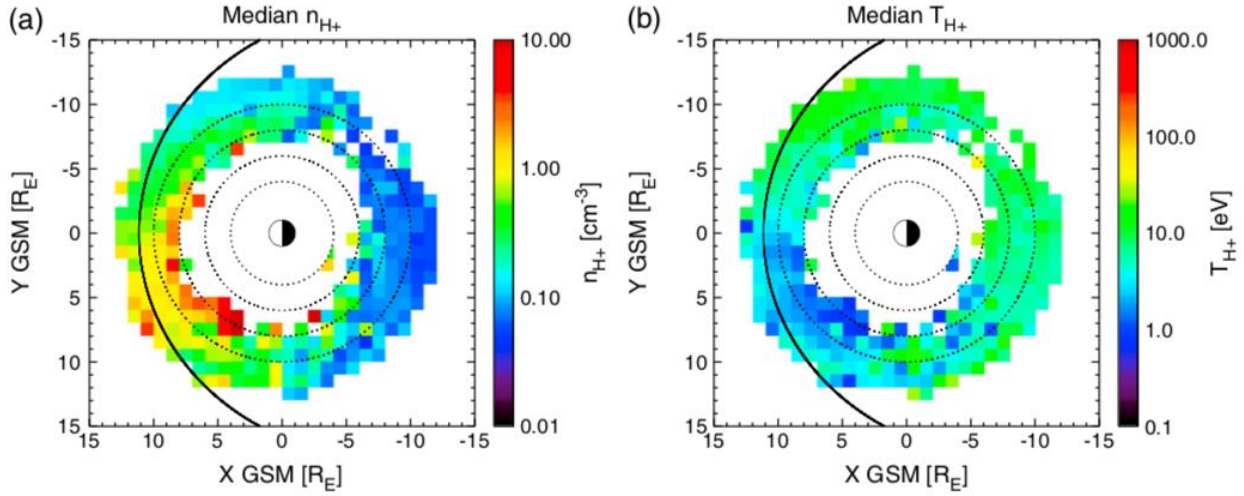

Figure 8. Median cold (< 120 eV) H^+ (a) density and (b) temperature, obtained from 5 years of THEMIS data using 3 spacecraft. Adapted from Lee and Angelopoulos (2014).

André and Cully (2012) studied the statistical occurrence and characteristics of the cold ion component (below a few tens of eV) in various regions of the Earth's magnetosphere using data from the Cluster spacecraft (polar orbit), obtained during the period November 2006 to July 2009. They combined various techniques for assessing the occurrence and density of the cold ions: direct measurements by the ion detectors, inferred from the plasma frequency, inferred from the spacecraft potential, and using the wake method, cf section 3.1 (Engwall et al. 2009). Figure 9 summarizes their statistics on cold ion detections at the magnetopause. Panel a shows the location in the YZ GSE plane and the respective cold ion density for each of the 370 Cluster 3 magnetopause crossings analyzed. The drainage region (red) corresponds to the region where the plasmaspheric plumes are most likely to hit the magnetopause. Figure 9b indicates that the inside the drainage region, ~20% of the crossings showed cold ion densities higher than 3 cm^{-3}. Outside the drainage region, typical cold ion densities are usually below 1 cm^{-3}. These densities are obtained by subtracting the observed density by the ion detector (corresponding to hot ions) to the total electron density (*n*) inferred from the cutoff plasma frequency ($\omega_p = ne^2/\varepsilon_0 m$), where *e* and *m* are the electron charge and mass, respectively. Finally, in Figure 9c a histogram of the relative occurrence of cold ions present in the magnetopause is shown. Cold ions contribute a significant fraction of the total number density (>40%) during more than 85% of the time inside the drainage region, and 50 - 70% of the time in other regions of the dayside magnetopause.

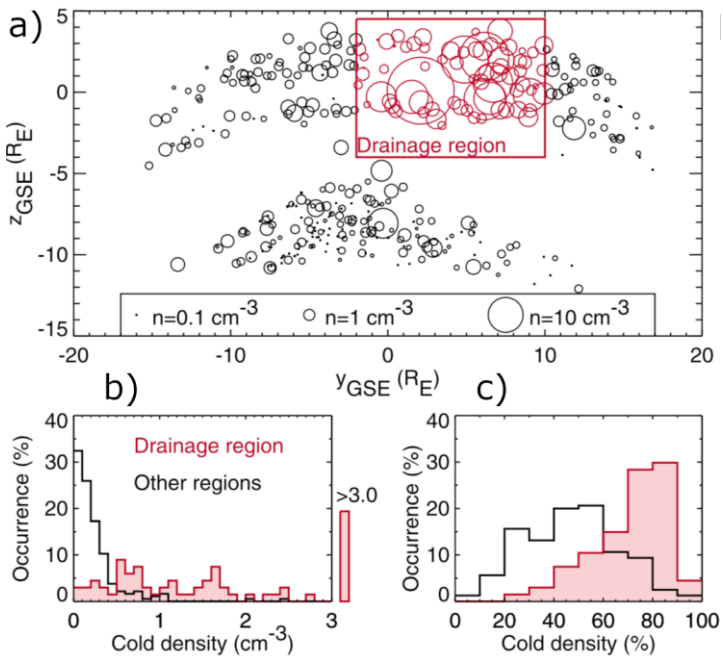

Figure 9. Statistics of cold ionospheric-originating ions at the magnetopause from Cluster data. (a) Cold ion density and location for each of the 370 magnetopause crossings identified during November 2006 to July 2009. The plasmaspheric drainage plume region is identified in red. (b) Histograms of cold ion density in the drainage region (red) and other regions (black) of the magnetopause. (c) Histograms of the fraction of the ion population not visible to the ion instrument in drainage (red) and other (black) regions. Low-energy ions contribute a significant fraction of the density nearly all of the time (>85%) in the drainage region, and 50–70% of the time outside of that region. Adapted from André and Cully (2012).

3.2.4 Remote imaging of He^+

Spasojevic and Sandel (2010) used a different technique to infer the total ion escape via plasmaspheric plumes. The used the Extreme Ultraviolet (EUV) imager instrument onboard the IMAGE mission (Sandel et al. 2003), which is capable of imaging (0.1 R_E resolution) the amount of He^+, by resolving its resonance line emission at 30.4 nm. They looked at 5 independent moderate disturbance events (Sym-H above -100 nT), and found that the average loss rate to the dayside magnetopause was of ~0.38 – 2.1 x 10^{27} ions/s during the events, i.e., somewhat higher than the results by Borovsky and Denton (2008). They assumed a number density ratio n_{He+}/n_{H+} ~ 0.05 – 0.15 (Craven et al. 1997) at L-shell distances 2 - 5, and that on average 65% of the depleted He^+ ions finally escape towards the dayside magnetopause. Assuming an effective area of the drainage plume region of ~9 x 12 R_E, and an average outflow velocity of ~15 km/s, the resulting ionospheric average density at the magnetopause in the drainage region corresponds to 6 – 32 cm^{-3} during the plume events according to the results by Spasojevic and Sandel (2010), i.e., a factor 2 – 10 larger than for the estimations of Borovsky and Denton (2008). This discrepancy may be explained by the fact that the imaging method requires a minimum amount of He^+ density in the integrated line of sight of the instrument, which would result in only detecting high-density plumes.

3.2.5 Comparison between studies

We summarize, in Table 1, the statistics provided by the works described above, at the subsolar-to-dusk magnetopause (drainage region) and the subsolar-to-dawn magnetopause. Comparing the statistical studies presented in this section is not an easy task, owing to their different orbits, methods and criteria for cold ion detection. Nonetheless, several conclusions are drawn from Table 1.

Near the dayside magnetopause there are cold to warm (eV to few hundred eV) ions of ionospheric origin most of the time. These ions have approximately the same density, i.e., a few times 0.1 cm^{-3}, as keV magnetospheric ions (originally from the solar wind and the ionosphere). Cold ions in the dusk sector (drainage region) are found more frequently than in the dawn sector, and their density is higher. This is because the plasmaspheric material usually reaches the magnetopause in the dusk sector. By contrast, the WPC can be found in both sectors (Lee et al., 2016, Fuselier et al. 2017, 2019a).

		Density threshold for selection (cm^{-3})	Relative occurrence (%)	Mean n_{H+} Observed (cm^{-3})	Energy range (eV)	Observed n_{He+}/n_{H+}	Observed n_{O+}/n_{H+}
Dusk-side magnetopause	Chappell (1974)	~6 at L = 9 (decreasing with distance)	Convection dependent	6 – 310 (peak values)	Few[(a)] - few tens	0.1	-
	Chen and Moore (2006)	-	> 50	-	Few[(a)] – 400	-	-
	Borovsky and Denton (2008)	-	Whenever storm occurs	~ 3 (extrapolated to 10 R_E)	-	-	-
	Lee et al (2016)	Flux >10^5 keV/cm^2s sr keV	19	5.4	$10^{(a)}$ – 1000	-	-
	Fuselier et al. (2017)	1.5	4	5	Few[(a)] - several thousands	0.015 (assumed at L = ~10)	< 0.015
	Walsh et al. (2013)	~5.7 at L = 9 (decreasing with distance)	26 (high-density plumes)	> 5 - 10	-	-	-
	Lee and Angelopoulos (2014)	-	70 - 95	> 1	$5^{(a)}$ - 120	< 0.1	< 0.1
	André and Cully (2012)	-	> 85 including 20	> 0.2 - 1 > 3	up to few tens	-	-
	Spasojevic and Sandel (2010)	-	Disturbed times considered	6 – 32 (extrapolated to 10 R_E)	-	0.05 – 0.15 (assumed at L = 2 - 5)	-
Dawn-side magnetopause	Nagai et al. (1983)	-	> 50	-	$10^{(a)}$ - 100	-	-
	Chappell et al. (2008)	-	>70	0.5 - 3	$10^{(a)}$ - 400	-	-
	Lee et al. (2016)	Flux >10^5 keV/cm^2s sr keV	8	5.2	$10^{(a)}$ – 1000	-	-
	Fuselier et al. (2017, 2019a)	1.5	10	3	Few[(a)] -several thousands	< 0.02	~0.02/0.004
	Lee and Angelopoulos (2014)	-	30 – 70	0.15 – 0.7	$5^{(a)}$ - 120	~0.5	~0.5
	André and Cully (2012)	-	50 - 70	0.1 - 1	up to few tens	-	-

Table 1. Studies of ionospheric-originating ions near the Earth's magnetopause. The dusk side corresponds roughly to 12 - 18 LT, and the dawn side roughly to 06 – 12 UT.

(a) The real lower energy threshold is defined by the spacecraft potential, which is variable depending on spacecraft and plasma conditions, in the range of few eV to tens of eV.

3.2.5.1 Dusk side

The reported percent of time that plasmaspheric material is observed at the magnetopause, has a large variability in the literature. Except for Fuselier et al. (2017), the studies suggest that this number is >20 – 25 % of the time, and some indicate that the percent is > 70 - 80%. This variation is mainly due to the following factors: the density threshold imposed for considering a detection, and the minimum energy that the method can detect. Different studies impose a more or less restrictive density threshold for considering detection of cold ions, which range from being above the noise of the method (typically less than 1 tenth cm^{-3}), e.g., André and Cully (2012), Lee and Angelopoulos (2014), to more than 5.7 cm^{-3} for Walsh et al (2013). The second important factor is that for most of the studies, the plasmaspheric material can go undetected for a significant fraction of the time, because their methods do not allow to detect cold ions with total energy below the spacecraft potential. Only three studies tackle this shortcoming. André and Cully (2012) uses various indirect techniques that can detect ions below V_{sc}. They find that cold ions are present > 85%, with n_{H+} ~ 0.2 - 1 cm^{-3}, including a smaller fraction of time (~20%) when the cold ion number density is > 3 cm^{-3} (plumes). Lee and Angelopoulos (2014) only consider times when the convection speed is larger than the spacecraft potential, and therefore the cold ions will be detected if they are present. They find occurrence times (70 – 95%) in accordance to André and Cully (2012), with similar density estimates (> 1 cm^{-3}). The other study that can detect ions below the spacecraft potential is Walsh et al. (2013), because it relies on estimating density from the spacecraft potential measurement rather than from particle measurements. However, they search only for high-density plumes, and impose density thresholds of ~5 cm^{-3} (varying with radial distance to Earth). They find an occurrence probability of 26% and average densities of 5 – 10 cm^{-3}. Based on these results, we note that studies relying on particle detectors cannot provide accurate occurrence probabilities, because the cold ions often do not reach the detectors due to the positive spacecraft potential.

We conclude that cold ions are present at the dusk magnetopause > 80% of the time, with average H^+ densities of at least a few times 0.1 cm^{-3}. This includes 20 – 25 % of the time when the density is > 3 cm^{-3}. Periods of high density in the dusk region are often due to parts of the bulge region of the plasmasphere exiting and being sunward convected to the magnetopause, i.e., the so-called plumes. Plumes occur predominantly during storm times and up to few days later, while the lower density cold ions can come from various mechanisms, including the WPC, high-latitude outflows, the plasmaspheric trough and plasmaspheric wind.

It is difficult to draw significant conclusions from the composition measurements of ionospheric-originating ions near the magnetopause. There are too few studies using composition to determine if, for example, there is a composition change in the plume with L-shell.

3.2.5.2 Dawn side

With respect to the dawn sector, which is mainly affected by the warm plasma cloak and high-latitude outflows, Table 1 reveals that the studies provide different results depending mainly on the density threshold they imposed for the definition of cold ions. Lee et al. (2016) and Fuselier et al. (2017) were more restrictive, and therefore their results reflect the statistics of the high-density events. The WPC can be identified by its field aligned, bi-directional ion flows. Furthermore, it is more easily detected by particle instruments than the plasmaspheric material, owing to its larger total energy, and hence the

825 better agreement between studies than for the dusk side. Chappell et al. (2008) finds somewhat larger
826 occurrences (>70%) and densities (0.5 – 3 cm^{-3}) than Nagai et al. (1983), Lee and Angelopoulos (2014),
827 and André and Cully (2012). This is probably related to the higher upper energy limit they use (400 eV).
828 The WPC can be often be found at energies >100 eV, and these events would be missed by the other
829 studies. In addition, the ion detector used by Chappell et al. (2008) has a larger geometrical factor,
830 because it was specifically designed to measure cold to warm ion populations (few eV – 400 eV).

831 For the dawn side, we conclude that the probability of finding the WPC at the magnetopause in the
832 dawn side is > 50% – 70%, with average H^+ densities of few tenths of cm^{-3} to few cm^{-3}. For ~10% of the
833 time, the average H^+ density is $\geq$ 3 cm^{-3}. Similar to the duskside studies, there are too few studies using
834 composition to investigate composition differences with L-shell or local time.

835 **3.2.6 Relative importance of ionospheric-originating ions at the dayside magnetopause**

836 The other population that is always present on the magnetospheric side of the Earth's magnetopause is
837 made of the plasma sheet ions, with energies in the keV to tens of keV range and densities of few tenths
838 of cm^{-3}. The origin of this population is both the solar wind and the ionosphere (e.g., Huddleston et al.,
839 2005). For the dusk-side magnetopause, more than 80% of the time the density of cold ions is of the
840 same order of magnitude as hot magnetospheric ions. The cold ion density is one order of magnitude
841 larger than hot magnetospheric ions 20% – 25% of the time. For the dawn-side magnetopause, the
842 density of cold ions is of the same order of magnitude as hot magnetospheric ions > 50% - 70% of the
843 time. For 10% of the time, the cold ion density is one order of magnitude larger than hot
844 magnetospheric ions. Finally, on average, the plume (20% - 25% of the time) and high-density WPC
845 events (10% of the time) have number densities which are still ~one order of magnitude lower than the
846 magnetosheath (shocked solar wind) density, which is found at the other side of the magnetopause.

847 **3.3 Quantification of ionospheric-originating ions in the Earth's magnetotail**

848 The other main region where magnetic reconnection takes place is the Earth's magnetotail, which is
849 divided into two main regions: the plasma sheet, a relatively thin layer (~6 R_E thick on average,
850 depending on distance from Earth) which lies in the geomagnetic equatorial plane, and the lobes, i.e.
851 the regions that fill the space above and below the plasma sheet (see Figure 1). The particle populations
852 in these regions of the magnetotail are quite different. As magnetotail reconnection onset occurs in the
853 plasma sheet, its properties are important for controlling the initiation of reconnection. But once all the
854 plasma sheet material has reconnected, the lobes field lines are also brought into the reconnection
855 region and become the inflow material of the reconnection process. Therefore, plasma conditions on
856 lobe field lines are also important. We now examine the ionospheric contributions to the plasma
857 composition of the plasma sheet and the lobes.

858 **3.3.1 Plasma Sheet**

859 The plasma sheet ion population is typically hot, and has temperatures in the range of few keV to few
860 tens of keV. The ionospheric contribution to the plasma sheet is best determined by its composition,
861 because ionospheric-originating ions have generally been energized and thermalized together with ions
862 of solar wind origin through various processes in the magnetotail. Since both the ionospheric outflows
863 and the solar wind contain significant H^+, they mix in the plasma sheet and their origin is thus difficult to
864 discern once energized. However, O^+ can only come from the ionosphere, and so is often used as a
865 tracer for the ionospheric source. He^{++} in the plasma sheet is dominantly of solar wind origin, and high
866 charge state CNO species, such as O^{+6} are definitely of solar wind origin, and so these can be used to
867 trace the solar wind component. Lennartsson and Sharp (1985) used the energy distributions of the He^{++}
868 and O^+, compared to the H^+ to estimate the fraction of H^+ from the ionosphere, and concluded that the

ionosphere may contribute 30%, even during quiet times. Gloeckler and Hamilton (1987) used measurements from the AMPTE mission to estimate the ionospheric contribution through comparisons of the plasma sheet composition with average solar wind composition, and concluded that the ionospheric contribution to the plasma sheet at 15 R_E was 36% during quiet times and 65% during active times. However, these averages do not capture the variability of the ionospheric contribution with both solar EUV and geomagnetic activity.

Statistical studies of the mid-tail (distances of 10 - 30 R_E) plasma sheet meant to capture this variability have been performed using data from the ISEE satellites, Geotail, AMPTE and Cluster. Lennartsson and Shelley (1986) and Lennartsson (1989) performed a statistical study of the plasma sheet ion composition using the Plasma Composition Experiment on ISEE 1, covering energies from 0.1 - 16 keV/e and radial distances from 10 - 23 R_E, during the rise of solar cycle 21, i.e., 1978 and 1979. They compared their observations to geomagnetic activity using the Auroral Electrojet (*AE*) index, which measures the perturbations of the magnetic field in the auroral regions typically associated to substorm activity. They found a strong increase in the O^+/H^+ density ratio with increasing *AE*, from 0.01 at low *AE* up to 0.6 at *AE* of 1000 nT. This increase was predominantly due to an increase in the O^+ density by a factor of 10, from 0.02 cm^{-3} to 0.2 cm^{-3}. They also showed a distinct increase with solar EUV, with an increase of the O^+ density from 0.02 cm^{-3} to 0.08 cm^{-3} when the solar radio flux at 10.7 cm wavelength (F10.7 index, an excellent proxy for solar activity), increase from 50 sfu to >200 sfu. Baumjohann et al. (1989) reported ion number densities for the plasma sheet at 9 – 14 R_E using AMPTE and found values consistent with Lennartson (1989). Nose et al. (2009) used 16 years of data from the STICS instrument on Geotail (Energy range 9 - 212 keV) to examine the solar cycle variability. Their dataset covered a wider range of distances, from 8 R_E to 100 R_E. They showed clearly the increase in the O^+/H^+ ratio from 0.01 to 0.06 as F10.7 increased from 70 sfu to 200 sfu. Mouikis et al. (2010) performed a statistical analysis of the densities of H^+ and O^+ inside the plasma sheet using a more limited range of radial distances, 15 – 19 R_E, using 5 years of data (2001 – 2005) from the CIS/CODIF instrument on the Cluster mission. The instrument operates in the range 40 eV – 40 keV. Comparing the O^+ density as a function of F10.7 from Cluster with the results of Lennartsson (1989), Mouikis et al. (2010) find a similar increase with F10.7, although Lennartsson (1989) observed overall higher densities (Figure 10a). This is likely because the radial range extended to lower radial distances, where the density is higher (as will be discussed). Figure 10b compares the O^+/H^+ density ratio from the Cluster study as a function of F10.7 with the Nose et al. (2009) results (blue). While the ratio level is about the same, Nose et al. (2009) found a steeper slope with F10.7. This may be due to the higher energy range of the Nose study, or may be because the Geotail data accounted for all geomagnetic activity levels, while the Cluster data used are just for quiet times. Figure 10c compares the activity dependence found by the Cluster study with the results of Lennartsson and Shelley (1986) (blue). Again, the dependence is similar, but the ratio is higher in the ISEE study that covered closer radial distances. Clearly, all these studies agree that the density of O^+ and the O^+/H^+ density ratio increase both with solar EUV (as characterized by the F10.7 proxy), and with geomagnetic activity (characterized by *Kp* or *AE* indices) with approximately equal contributions. The solar EUV sets a baseline ratio for a given phase of the solar cycle, and then activity increases the O^+ content from there.

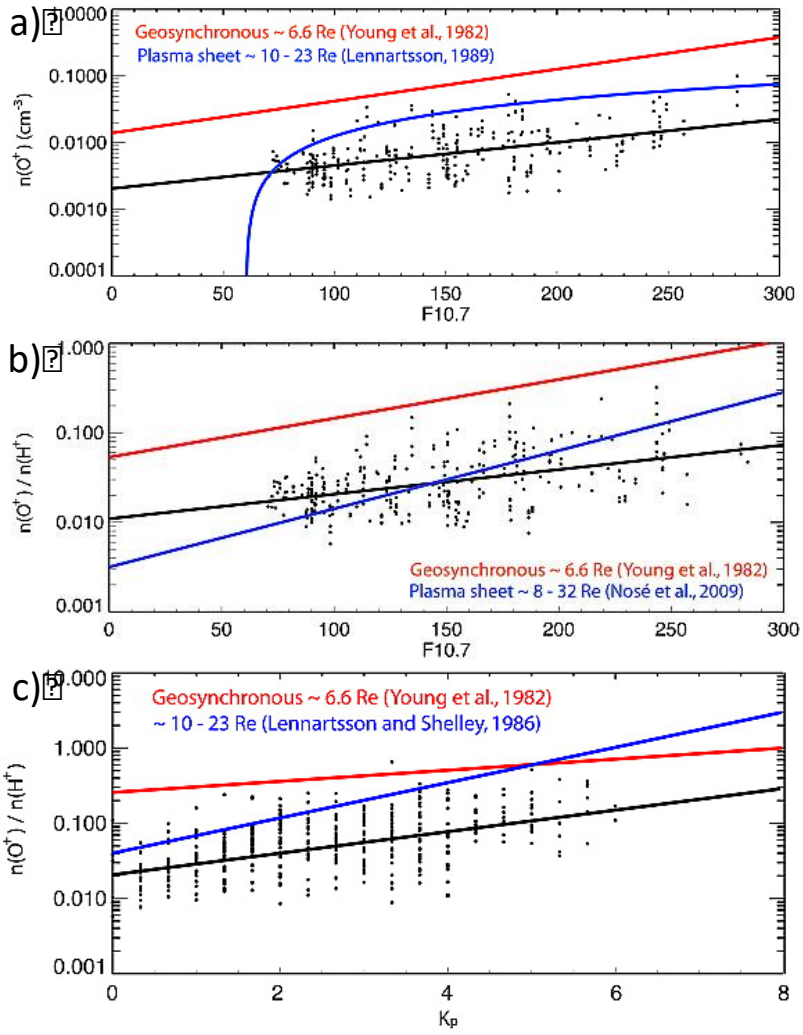

Figure 10. Variation in the O^+ and H^+ densities and the density ratio with a) and b) F10.7, and c) *Kp*. Adapted from Mouikis et al. (2010).

The plasma sheet densities closer to the Earth, at ~6 - 7, R_E were characterized by Young et al. (1982) and Kistler and Mouikis (2016). Both studies cover the "hot" population, with Young et al. (1982) covering the energy range from 0.9 - 17 keV using the GEOS data set (similar to the instrument on ISEE 1), and Kistler and Mouikis (2016) covering the energy range from 1 - 40 keV using Cluster/CODIF. While GEOS measurements were near-equatorial, the Cluster/CODIF measurements were taken at about ~30 degrees latitude for this L-range, so the distribution was mapped along the field line to the equator to obtain comparable results. The O^+ density and the O^+/H^+ ratio in this region is about a factor of 10 higher than in the 15 - 19 R_E region, as shown by the red lines in Figure 10abc, but show similar F10.7 and *Kp* dependencies. As was observed further out, EUV alone will increase the O^+/H^+ ratio by a factor of ~8, and then geomagnetic activity will increase it by another factor of 10.

Maggiolo and Kistler (2014) used the mapping technique to derive 2D maps of the H^+ and O^+ densities in the X-Y equatorial plane using the Cluster/CODIF data. Figure 11 shows the densities and density ratios as a function of the equatorial X position from this study. The O^+ density and the O^+/H^+ density ratios increase strongly inside L = -10, while the H^+ increases more gradually with decreasing distance. In the Y-direction, they did not observe a strong dawn-dusk asymmetry, but found the density and density ratios

to be relatively flat from dawn to dusk across the magnetotail at distances of 15 - 20 R_E. Closer to the Earth, the densities peak close to midnight during quiet times, with the peak shifting dawnward for higher activity. However, the O^+/H^+ density ratio remains relatively uniform.

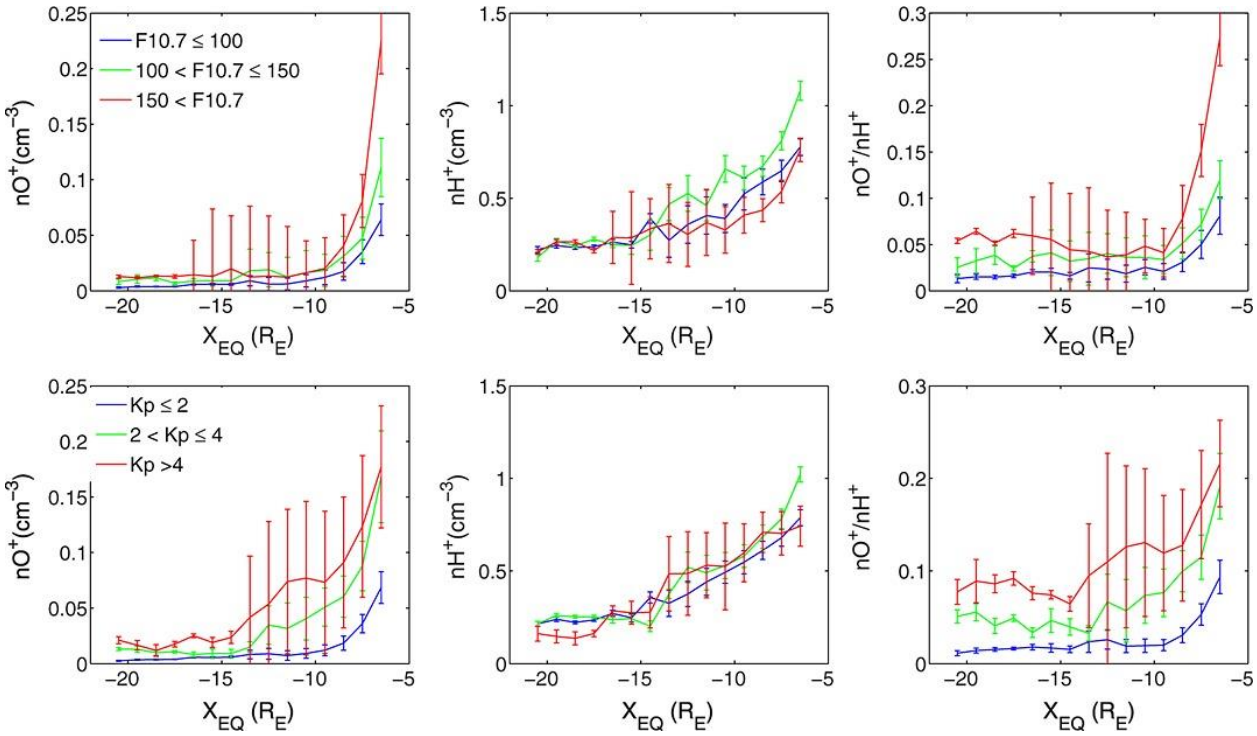

Figure 11. Radial dependence of the O^+ and H^+ densities in the plasma sheet, and their ratio. Adapted from Maggiolo and Kistler (2014).

Figure 12, from Kistler and Mouikis (2016), summarizes the *Kp* dependence found in the near-earth plasma sheet from these studies. A medium range of F10.7, 100 - 150, is shown, but results for other F10.7 values are similar. The black points are the L = 6 - 7 measurements from Kistler and Mouikis (2016), and the dark blue line is the fit to these points. The Maggiolo and Kistler (2014) fits for L = 7 - 8 are shown in green, while the Young et al. (1982) fits are in red, and the Moukis et al. (2010) results from 15 - 19 R_E are in light blue. The increase in O^+ and in the O^+/H^+ ratios with *Kp* agree very well between the three near-Earth studies, with the 15 - 19 R_E study showing lower values, as expected because of the radial dependence. Surprisingly, He^+ shows almost no variation with *Kp*, which leads to a decreasing He^+/H^+ ratio with *Kp*. The final panel shows the increase in the overall mass density with *Kp*. This also increases by a factor of 10 with geomagnetic activity.

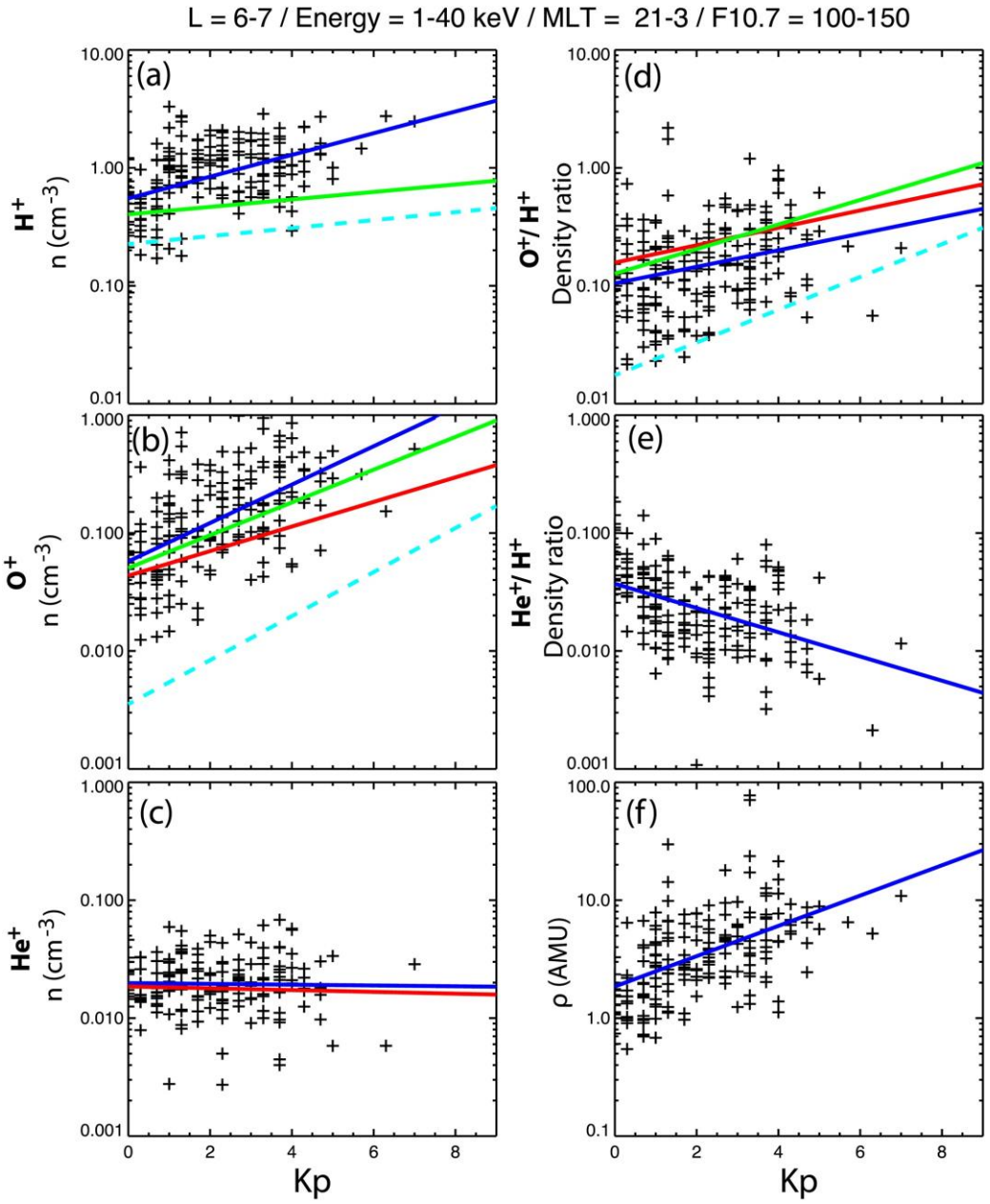

Figure 12. Ion composition as a function of *Kp*, comparing the studies of Kistler and Mouikis (points, and blue line fit), Maggiolo and Kistler (2014) (green) Young et al. (1982) (red) and Mouikis et al. (2010) (dashed light blue).

The studies described so far have analyzed the hot plasma sheet population, which is composed of a mixture of heated ions of both solar wind and ionospheric origin. There is also evidence of a cold, low-energy population of ionospheric origin in the plasma sheet, coexisting with the hot population. Seki et al. (2003) presented observations from time periods when the Geotail spacecraft was in eclipse, which causes the spacecraft to charge negatively. This negative potential attracts the positive cold ions, and brings them up to an energy where they can be observed. Observations during these eclipse time periods showed the existence of a cold population with density comparable to the hot population. This cold ion population becomes also detectable by particle detectors when the bulk drift energy is larger than the equivalent spacecraft potential but smaller than the thermal energy of the hot plasma sheet

population (e.g., Alm et al. 2018, 2019, Xu et al., 2019). André et al. (2015), using the wake method (cf. section 3.1), conducted a statistical survey in the magnetotail and found this cold population only ~10% of the time inside the plasma sheet. However, with their method it is difficult to detect cold ions in the plasma sheet because to detect an extended wake, indicating the presence of cold ions, requires the cold ion density to be at least about half of the total density, and the bulk drift energy to be less than the equivalent spacecraft charging, both of which may often be violated in the plasma sheet. In addition, to estimate also the cold ion flux, observations by the EDI instrument are needed, designed to operate in a reasonably steady and strong magnetic field, also conditions often violated in the plasma sheet. Lee and Angelopoulos (2014) also examined the number density of cold ions (energy below 1 keV) in the near tail (distances of 6 – 12 R_E), using THEMIS observations during ~5 years of data (January 2008 – May 2013). They found occurrence rates in the night sectors varying between 5 – 35 % depending on distance to Earth, with the largest occurrences at L = 4 – 6. They report average cold H^+ densities in the tail of ~0.05 – 0.1 cm^{-3} (see Figure 8), with average temperatures of ~10 eV. They also calculated the average He^+ and O^+ densities and temperatures of the cold ions (below 1 keV). Interestingly, they find higher number densities (~0.1 cm^{-3} for He^+ and ~0.2 cm^{-3} for O^+) than for H^+, and also larger temperatures (~50 eV for He^+ and ~200 eV for O^+).

3.3.2 Lobes

Magnetic reconnection in the magnetotail occurs first in the plasma sheet, where the stretched magnetic field lines from the North and South hemispheres form a thin current sheet. Magnetic reconnection then proceeds with lobes field lines, above and below the plasma sheet, which are filled only by high-latitude ionospheric outflows. These outflows either end up in the plasma sheet or are lost in the distant tail. As discussed in section 2.2.2, ion outflow from the cusp and polar cap are accelerated along the field line through centrifugal acceleration, and are dispersed by the velocity filter effect into the lobes. Thus, the populations normally observed in the lobes are cold, field-aligned streams of ions. Even if the source population has a broad energy range, the lobe population will have a narrow velocity distribution because only a particular velocity reaches a particular location. Ion species with the same velocity will have a different energy by their mass ratio. Thus in the 15 -20 R_E region, where these cold ions have been well-characterized by data from the Cluster mission, the lobe population consists of protons with energies of 10's of eV (Engwall et al. 2009, André et al. 2015) while the O^+ ions are in the 40 eV - 1 keV range (Liao et al. 2015). Svenes et al. (2008) inferred the electron number density indirectly from the Cluster spacecraft potential using 7 years of data from the waning part of solar cycle 23, and found that more than two thirds of the time the electron density, n_e, was between 0.007 cm^{-3} and 0.092 cm^{-3}, with a mode of 0.047 cm^{-3}. These averages were independent of solar wind and geomagnetic conditions, but for the high-density tail of the distribution (n_e > 0.2 cm^{-3}), a correlation with 10.7 cm solar radio flux was present. André et al. (2015) performed an extensive study of the lobe ion population over a solar cycle. Again the spacecraft potential was used to estimate the density and an extended spacecraft wake was used to detect streaming cold ions and to estimate the ion flux. They find that a cold population is present at least 64% of the time at distances of 5 - 20 R_E, with average densities of 0.2 - 0.4 cm^{-3}, and average field-aligned velocities of 25 - 30 km/s. The outflow flux increases by a factor ~2 with geomagnetic activity and with solar EUV over the solar cycle. The increase is mainly due to the density increasing, while the velocity distribution remains about the same.

The O^+ in the lobes was characterized by Liao et al. (2010, 2012, and 2015). During solar maximum, 2001 - 2002, the occurrence frequency of O^+ beams in the lobes is almost 100% during storms, but even during non-storm times, the occurrence frequency is ~50%. The location of the O^+ ions in the lobes shows a dawn-dusk asymmetry that depends on IMF By. When IMF By is positive, the O^+ in the northern lobe tends to be on the dawn side, while the O^+ in the southern lobe tends to be on the dusk side. For negative By, the asymmetry reverses, but not as strongly. If there are different amounts of outflow in

the northern and southern hemisphere, this could lead to dawn-dusk asymmetries in the plasma sheet, as well. The occurrence of the O^+ beams decreased significantly with solar cycle, with the decreases stronger in the tail lobes than in the polar cap. This decrease could be because the flux decreased below the threshold level for the instrument, or because the transport paths changed, due to changes during the minimum of the solar cycle, so the O^+ beams no longer reach the near-earth plasma sheet.

The H^+ and O^+ populations in the lobes are clearly related, but a focused study comparing the two has not been done. Backwards modeling indicates that the proton population comes from the full range of the polar cap (Li et al. 2013), while the more energetic O^+ is thought to come from the cusp. Liao et al. (2015) showed that during quiet times, the O^+ beam fluxes observed were consistent with the outflow fluxes from the cusp, while during more active times, some additional acceleration of the cusp outflow population was required. The densities and velocities of the two populations during the solar maximum time period are compared in Kronberg et al., (2014). The H^+ density is significantly higher than the O^+ (average 0.14 cm^{-3} for H^+, versus 0.009 - 0.02 cm^{-3} for O^+). But the velocity range is similar (average 40 km/s for H^+ versus 37.9 km/s for O^+). Similar velocities would be expected from the velocity filter effect.

3.3.3 Comparison between studies

We summarize, in Table 2, the statistical observations of the H^+ number density (n_{H+}), H^+ percent of ionospheric origin when available, and O^+/H^+ number density ratio (n_{O+}/n_{H+}), for the various studies presented in the near-Earth plasma sheet (< 10 R_E), distant plasma sheet (> 10 R_E) and tail lobes.

Table 2. Statistical studies of number density and plasma composition in the Earth's magnetotail.

		Distance to Earth (R_E)	n_{H+} of ionospheric origin (%)	Mean n_{H+} Observed (cm^{-3})	Energy range (keV/e)	Observed n_{O+}/n_{H+}
Near-Earth Plasma sheet	*Young et al. (1982)*	6 - 7	-	0.3 – 0.4[b] (Kp < 3) 0.4 – 0.5[b] (3 < Kp > 6) 0.5 – 0.6[b] (Kp > 6)	0.9 - 16	0.4 – 0.5[b] (Kp < 3) 0.5 – 0.9[b] (3 < Kp > 6) 0.9 – 1.4[b] (Kp > 6)
	Gloecker and Hamilton (1987)	8 – 9	47	-	1.5 - 315	0.11[a]
	Lennartson (1989)	< 10	-	0.8[b] (F10.7 < 100) 0.68[b] (100 < F10.7 < 150) 0.62[b] (150 < F10.7 < 200) 0.58[b] (F10.7 > 200)	0.1 - 16	0.1[b] (F10.7 < 100) - - -
	Lee and Angelopoulos (2014)	5 - 10	-	< 0.1[d]	< 1	> 1[d]
	Maggiolo and Kistler (2014)[c]	7 -8	-	0.4 – 0.5[b] (Kp < 3) 0.5 – 0.7[b] (3 < Kp < 6) 0.7 – 0.8[b] (Kp > 6)	1 – 40	0.2 – 0.3[b] (Kp < 3) 0.3 – 0.6[b] (3 < Kp < 6) 0.6 – 1.3[b] (Kp > 6)
	Kistler and Mouikis (2016)[c]	6 - 7	-	0.6 - 0.8[b] (Kp < 2) 0.8 -1.3[b] (2 < Kp < 4) >1.3[b] (Kp > 4)		0.1[b] (Kp < 2) 0.1 – 0.2[b] (2 < Kp < 4) 0.2 – 0.5[b] (Kp > 4)
Distant Plasma sheet	*Lennartson and Sharp (1985)*	10 - 23	20-30(AE <100)	-	0.1 - 16	< 0.1 (AE < 100 nT) 0.2 – 0.7 (AE > 300 nT)
	Lennartson and Shelley (1986)	10 - 23	-	0.5 – 1[b] (AE < 100) 0.2 – 0.3[b] (AE > 700)		0.01 – 0.08[b] (AE < 100 nT) 0.6[b] (AE > 700 nT)

	Gloecker and Hamilton (1987)	15	37 (quiet) 65 (disturbed)	-	28 - 226	0.09[a] (quiet) 0.17[a] (disturbed)
	Baumjohann et al. (1989)	9 - 14	-	0.5 (AE < 100) 0.4 (AE > 100)	0.02 - 40	-
	Lennartson (1989)	> 10	-	0.65[b] (F10.7 < 100) 0.55[b] (100 < F10.7 < 150) 0.4[b] (150 < F10.7 < 200) 0.48[b] (F10.7 > 200)	0.1 - 16	0.03[b] (F10.7 < 100) 0.05[b] (100 < F10.7 < 150) 0.15[b] (150 < F10.7 < 200) 0.15[b] (F10.7 > 200)
	Seki et al. (2003)	9 – 18	~50[d]	~0.2[d]	< 1	< 0.5[d]
	Mouikis et al. (2010)	15 – 19	-	0.2 – 0.3[b]	1 - 40	0.01 – 0.07[b]
	Maggiolo and Kistler (2014)[c]	15 – 20	-	~0.3[b]		0.01 – 0.05[b] (Kp < 3) 0.05 – 0.2[b] (3 < Kp < 6) 0.2 – 0.7[b] (Kp > 6)
Tail lobes	*Svenes et al. (2008)*	5 - 19	>90%[f]	0.047	N/A[e]	-
	André et al. (2015)	5 – 10		~0.25 (Kp < 3) 0.3 – 0.7 (Kp > 3)	Up to tens of eV	-
		10 – 15		0.1 – 0.2 (Kp < 3) 0.2 – 0.3 (Kp >3)		
		15 - 20		<0.1 (Kp < 3) 0.1 – 0.2 (Kp >3)		

[a] Considers n_{H+} of ionospheric origin only.

[b] Considers total n_{H+}, ionospheric plus solar wind origin.

[c] The values reported in the table consider F10.7 = 100 - 150 sfu.

[d] Accounts only for cold n_{H+}.

[e] The ion number density is inferred indirectly from the SC potential.

[f] Plasma in the lobes is almost entirely of ionospheric origin, although the studies presented do not attempt to quantify the origin.

3.3.3.1 Near-Earth Plasma Sheet (< 10 R_E)

The H^+ number density in the near-Earth plasma sheet (less than 10 R_E from Earth) depends mainly on the distance to Earth and geomagnetic activity, and to a lesser degree on solar EUV. It is estimated that roughly half of H^+ ions are of ionospheric origin (Gloecker and Hamilton, 1989). For ions with total energies above 1 keV, n_{H+} ~ 0.3 – 0.8 cm^{-3} for quiet magnetospheric conditions (Kp < 3), and n_{H+} ~ 0.4 – 1.3 cm^{-3} for disturbed conditions (Kp > 3). In addition, there is a cold ion component (total energy < 1 keV) with n_{H+} < 0.1 cm^{-3} (Lee and Angelopoulos, 2014), likely of ionospheric origin. The ratio of O^+/H^+ number densities strongly depends on geomagnetic activity, with n_{O+}/n_{H+} ~ 0.1 – 0.5 for quiet conditions (Kp < 3) and n_{O+}/n_{H+} 0.2 – 1.3 for disturbed conditions (Kp > 3). Both H^+ and O^+ number densities increase during disturbed conditions, but the increase in O^+ number density is larger. The number densities reported vary up to half order of magnitude depending on the study, and this is attributable to multiple factors including solar cycle, distance to Earth, other orbital biases (magnetic local time, latitude), and ion energy range considered by each study.

3.3.3.2 Distant Plasma Sheet (> 10 R_E)

In the distant tail, the total H^+ number density does not depend that much on geomagnetic activity (Mouikis et al., 2010, Maggiolo and Kistler, 2014) as in the near-Earth tail. Lennartson and Shelley (1986) found an anti-correlation between geomagnetic activity and H^+ number density, as opposed to the near-Earth plasma sheet. However, the relative contributions of the ionosphere and the solar wind do depend on geomagnetic activity, with around one third of the H^+ ions coming from the ionosphere during quiet times, and around two thirds coming from the ionosphere during disturbed times. Overall, at distances of 15 – 20 R_E, n_{H+} ~0.2 – 0.3 cm^{-3}, and is somewhat larger (n_{H+} ~0.5 cm^{-3}) when distances at 10 – 15 R_E are included in the study. The dependence of n_{H+} with solar EUV is also small. On the other hand, the amount of ionospheric O^+ in the distant plasma sheet depends largely on geomagnetic activity, as for the near-Earth plasma sheet. Typical O^+/H^+ density ratios are $n_{O+}/n_{H+} < 0.1$ for quiet times and n_{O+}/n_{H+} ~ 0.2 – 0.7 for disturbed times. In addition, Seki et al. (2003) reported the existence of a cold, hidden plasma population of ionospheric origin (up to few eV) that was only visible during spacecraft eclipses, with number densities of ~0.2 cm^{-3} and present < 50 % of the time.

3.3.3.3 Lobes

In the tail lobes, the main source of plasma is ionospheric outflows. The lobe populations are usually cold due to the cold nature of the classical polar wind and the velocity filter effect (cf. Section 2.2.2), and therefore they cannot be easily characterized using in-situ ion detectors. We report the results of two studies that used an indirect technique to infer the ion number density in the lobes using the Cluster spacecraft. The average densities reported (cf. Table 2) are roughly consistent but the estimates are somewhat larger in André et al. (2015) than in Svenes et al. (2008). This difference can be explained by the different datasets employed. Svenes et al. (2008) inferred the ion number density from the spacecraft potential, and found the most probable number density to be n = 0.047 cm^{-3}. André et al. (2015) selected data when the spacecraft wake showed that a majority of the ions were cold, and also used the spacecraft potential to estimate the density. Only events with an observed wake (drifting cold ions) and reliable EDI observations were included in the density statistics. In addition, to avoid large errors, only events with n > 0.01 cm-3 were included. These criteria select observations with mainly cold ions and exclude observations with low density, mainly at high altitudes. As a result, André et al. (2015) reported cold ion detections 64% of the time, and found n > 0.1 cm^{-3} for most radial distances and geomagnetic conditions. The two methods showed correlation with geomagnetic activity (solar cycle or *Kp* index) for the cases with large densities (above 0.2 cm^{-3}).

3.3.4 Relative importance of ionospheric-originating ions in the Earth's magnetotail

It is well known that O^+, and cold H^+ in the lobes and in the plasma sheet are of ionospheric origin. However, hot H^+ in the plasma sheet are from both the solar wind and the ionosphere. From inspection of Table 2, the conclusions are that the ionospheric source is the dominant H^+ source during disturbed magnetospheric conditions. During quiet times, the dominant H^+ source is the solar wind, and on average, i.e., quiet plus disturbed times, both H^+ sources are of the same order of magnitude. However, the number of statistical surveys that attempt to distinguish the two H^+ sources is small. In terms of mass density, the near-Earth plasma sheet is most of the time dominated by the ionospheric source, owing to the O^+ contributions. Various studies present the statistics as a function of geomagnetic activity or solar irradiance flux, but we also expect the correlation between plasma sheet parameters and IMF orientation to be large, because of increased convection of magnetic field lines from the lobes, favoring loading of the plasma sheet (e.g., Kistler, 2020).

4 Effects of ionospheric-originating ions on magnetic reconnection

Magnetic reconnection is one of the most important transport and energy conversion process in collisionless plasmas. It causes the transport of mass, momentum and energy across topologically distinct plasma regions, initially separated by a thin current sheet. Reconnection regulates solar eruptions, plays a key role in determining the shape and dynamics of planetary magnetospheres, and is involved in major disruptions in astrophysical systems, such as magnetar flares. Even on the ground, in the laboratory, reconnection is an important, albeit undesirable, process in fusion machines, as it can destroy magnetic field confinement. At the Earth's dayside magnetopause, it facilitates the entry of solar wind particles and magnetic energy into the magnetosphere. On the nightside, magnetic reconnection dissipates the accumulated magnetic energy, leading to substorms, storms and auroras, and powers the majority of the deleterious space environment effects collectively referred to as Space Weather.

Owing to its importance, magnetic reconnection has been studied for quite some time, see for instance the review by Yamada et al. (2010), and the review of observations of reconnection by Fuselier and Lewis (2011) and Cassak and Fuselier (2016). Decades of attempts to understand its inner machinery have recently culminated in breakthrough insights into how reconnection works, enabled by the combination of observations from the MMS spacecraft mission, theory and modeling. However, we still know very little about how it starts, and even less about how it stops.

Magnetic reconnection is enabled through a local decoupling between the particles and the magnetic field, which occurs at the smallest spatial scales of the plasma, i.e., the electron inertial length and gyroradius, in the so-called Electron Diffusion Region (EDR). The coupling between the magnetic flux transport and the flow of ions and electrons is described by the equation of the electric field. A general way of looking for regions where this coupling is violated is by analyzing the generalized Ohm's law (Vasyliunas, 1975):

$$\mathbf{E}+\mathbf{v}\times\mathbf{B}=\eta\mathbf{J}+\frac{m_e}{e^2n}\left[\frac{\partial\mathbf{J}}{\partial t}+\nabla\cdot(\mathbf{Jv}+\mathbf{vJ})\right]-\frac{\nabla\cdot\mathbf{P}_e}{en}+\frac{\mathbf{J}\times\mathbf{B}}{en} \quad (1)$$

The different terms on the right-hand side correspond to effects that violate the frozen-in condition ($\mathbf{E}+\mathbf{v}\times\mathbf{B}=0$), a condition where the magnetic field is carried together with the average plasma flow. For magnetic reconnection, such effects must be present to support the necessary electric field which allows the magnetic field to dissipate and merge, changing the topology of magnetic field lines.

The governing equation for ideal MHD ($\mathbf{E}+\mathbf{v}\times\mathbf{B}=0$) is scale invariant, meaning that it does not contain any spatial scales. However, the non-ideal terms (right-hand side terms of Equation 1) are characterized by characteristic time or spatial scales, related to the intrinsic properties of the plasma. Owing to the different mass of ions and electrons, they decouple at different scales. The largest of the characteristic scales in Equation 1 correspond to the Hall term**,** $\mathbf{J}\times\mathbf{B}/(en)$, which describes when the ion motion differs from the electron motion and two-fluid effects are in play. This occurs in the Ion Diffusion Region (IDR), with a characteristic spatial scale corresponding the ion inertial length.

The rest of the right-hand side terms of Equation 1 become non-negligible at electron scales, i.e., in the Electron Diffusion Region (EDR). Space plasmas are very dilute and collisions between particles are often negligible. Therefore, dissipation of the magnetic field (positive **J**·**E**) inside the EDR must occur in an unconventional way, since the collisional resistivity is too weak to explain the observations. One of the primary objectives of the MMS mission is to unravel which processes generate sufficient anomalous resistivity for the magnetic field to diffuse and reconfigure inside the EDR in collisionless plasmas. Wave-particle interactions are a strong candidate for the generation of anomalous resistivity (e.g., Graham et al., 2017b, Burch et al., 2018, Li et al., 2020).

The presence of additional plasma populations, e.g. ions of ionospheric origin, with different temperature or mass, has an impact on the different characteristic time and spatial scales associated with the diffusion regions, and affects how the process converts magnetic energy into thermal and kinetic particle energy. Understanding how different plasma populations couple to the reconnection process is what renders the physical process elusive and challenging. The characteristics of the plasma particle gyro orbits around the magnetic field lines can be quantified by the Larmor radius or gyroradius (R_{gs}) and the cyclotron frequency (ω_{cs})

$$R_{gs} = \frac{m_s v_{Ts}}{q_s B}, \qquad \omega_{cs} = \frac{q_s B}{m_s}, \tag{2}$$

where subscript *s* denotes the particle species, v_T is the thermal speed, *q* is the particle charge, *m* is the particle mass and *B* is the magnetic field magnitude. A colder plasma population will, for instance, have a smaller Larmor radius, while the cyclotron frequency remains unchanged, as it does not depend on the thermal speed. If the plasma contains a heavier plasma population (e.g. He^+, O^+), the cyclotron frequency will be smaller (assuming a comparable thermal speed), which has a profound influence on the time evolution of the reconnection process, as discussed in section 4.2.

The ion inertial length is, by definition, equal to the Larmor radius when $v_{Ti} = v_A$, i.e., the thermal velocity and Alfvén velocity ($v_A^2 = B^2/\mu_0\rho_i$) are equal. For a species *s*, the inertial length (d_s) and the plasma frequency (ω_{ps}) are defined as

$$d_s = \frac{c}{\omega_{ps}}, \quad \omega_{ps} = \left(\frac{n_s q_s^2}{\varepsilon_0 m_s}\right)^{1/2}, \tag{3}$$

where c is the speed of light, ε_0 is the vacuum dielectric permittivity, and n_s is the species number density. The height of the IDR and EDR are more precisely described by the particles bounce width, which involves the thermal velocity of the particles and therefore scales approximately as the Larmor radius.

Figure 13 shows a 2D particle-in-cell simulation of asymmetric magnetic reconnection (Dargent et al. 2017) that mimics the conditions of coupling between the solar wind (top) and the magnetosphere (bottom). The main regions, namely the EDR, IDR, inflow regions, outflow regions, and separatrices, are sketched. Once the magnetic field reconnects at the EDR, its new topology consists of highly bended magnetic field lines that accelerate to reduce their magnetic tension, generating the so-called reconnection jets, which accelerate and heat the particles, and can extend to spatial scales much larger than the EDR. The center of the EDR is known as the X-point in two dimensions, and extends out of the reconnection plane (XZ plane in Figure 13) forming an X-line in the Y direction in the realistic three-dimensional case. Magnetic reconnection initiates and is maintained at the EDR, but its consequences extend to meso- and system-scales. For instance, in the Earth's magnetosphere, it mediates solar wind plasma entry which drives the global magnetospheric convection cycle.

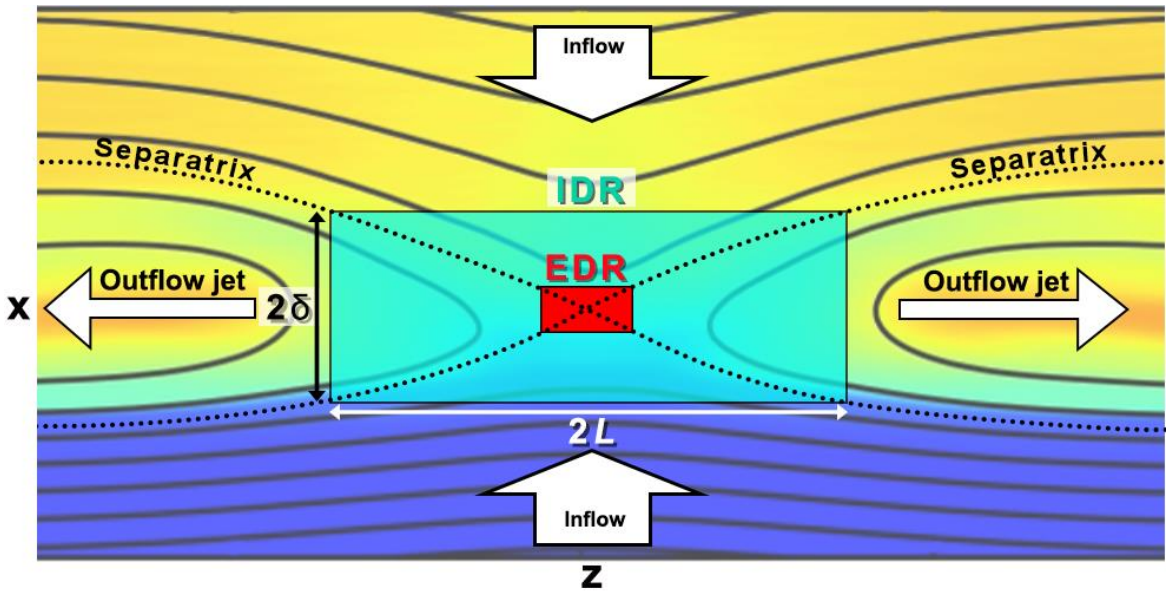

Figure 13. Particle-in-cell simulation of magnetic reconnection. The magnetic field lines (solid black lines) break and reconnect at the EDR, generating reconnection outflow jets. In this 2D simulation, the two topological regions that reconnect, have different magnetic field strength and electron density (color-coded), imitating solar wind (top region) – magnetosphere (bottom region) magnetic reconnection. Credit: J. M. Domínguez, adapted from Dargent et al. (2017).

As we have seen in section 3.2 and 3.3, plasma of ionospheric origin can dominate the mass density on the magnetospheric side of the magnetopause and in the tail. The system is mass-loaded and the characteristic Alfvén speed is modified, resulting into modified reconnection efficiency. This effect is investigated further in section 4.1. Additional plasma populations also modify the structure and dynamics of the reconnection region, owing to the introduction of multiple time and spatial scales. In section 4.2, we discuss recent modelling and observational works focusing on these effects. The energy conversion due to magnetic reconnection occurs on scales much larger than the tiny electron diffusion

region, involving the ion diffusion region, the separatrices and the exhausts, where the bulk of magnetic energy is converted to particle energy, including the energy of incoming cold ions. We review recent works on the energy balance of magnetic reconnection involving ionospheric-originating ions in section 4.3. In section 4.4, we discuss how the presence of heavy ions (mainly O^+) in the magnetotail changes its effective thickness and stability, and how this affects reconnection onset. Section 4.5 discusses about the capability of ionospheric populations to suppress magnetic reconnection at the dayside magnetopause.

4.1 Reconnection rate and mass-loading (macroscopic view)

Observations over the past decades have shown that the plasma composition in the magnetosphere is a function of both time and location, cf. Sections 2 and 3. The magnetospheric composition usually consists of ion species originating from the solar wind, from H to Fe, e.g., Haaland et al. (2020), and from the ionosphere, consisting of mainly H^+, He^+ and O^+.

To quantify the reconnection rate, i.e. the amount of magnetic flux that is reconnected per unit time, we proceed with a scaling analysis of the quantities involved in the reconnection process. This scaling analysis will allow us to quantify the rate based on quantities measured in the inflow region alone. The aspect ratio (δ/L) of the ion diffusion region (see Figure 13) follows from the mass continuity equation, and can be related to the rate at which magnetic reconnection proceeds, i.e., the amount of magnetic flux that is reconnected per unit time. Assuming the system is in steady-state, the evolutionary equation for mass is

$$\oint_S d\mathbf{S} \cdot (\rho \mathbf{v}) = 0, \tag{4}$$

where $\mathbf{v}$ is the flow velocity, ρ is the mass density and $d\mathbf{S}$ is the outward directed area element of the surface $\mathbf{S}$. By considering one quarter of the ion diffusion region in Figure 13, mass continuity relates the mass transport across in inflow surface and outflow surface:

$$\rho_{in} v_{in} L \sim \rho_{out} v_{out} \delta. \tag{5}$$

By evaluating the energy equation (assuming pressure does not contribute to the energy conversion), or by the momentum equation under the assumption that the outflow advection is driven by pressure (Sweet-Parker scheme), an expression for the outflow velocity is found:

$$v_{out}^2 = \frac{B_0^2}{\mu_0 \rho} = v_A^2, \tag{6}$$

where ρ is the average mass density flowing into the diffusion region from both sides, and B_0 is the magnetic field magnitude adjacent to the diffusion region, which is assumed to be approximately equal to B anywhere outside the field reversal region. Thus, the advection speed out of the diffusion region, and consequently the inflow speed, is approximately limited to the Alfvén speed just outside the diffusion region. For details, see Vasyliunas (1975).

The normalized reconnection rate is then readily defined as the ratio between the inflow and the outflow velocity, which can be related to the aspect ratio of the diffusion region

$$M_A = \frac{v_{in}}{v_A} \sim \frac{\delta}{L}, \tag{7}$$

where we have assumed an incompressible flow ($\nabla \cdot \mathbf{v} = 0$), and an outflow velocity equal to the Alfvén speed. The reconnection rate is directly related to the out of plane electric field in the diffusion region for 2D geometries (E_y in the coordinates of Figure 13, also known as reconnection electric field). We

assume that $\mathbf{E} = -\mathbf{v} \times \mathbf{B}$ holds at the edges of the diffusion region, i.e., the ions are frozen-in to the magnetic field outside the diffusion region, leading to $v_{in}B_x = v_{out}B_z$. Taking advantage of $\nabla \cdot \mathbf{B} = 0$, we find

$$E \sim v_A B_z = v_A B_x \frac{\delta}{L}. \quad (8)$$

In steady-state reconnection, the aspect ratio is typically δ/L ~ 0.1, found consistently in numerical simulations, spacecraft observations and laboratory experiments (e.g., Yamada et al., 2010, Cassak et al., 2017). As part of the Geospace Environment Modeling (GEM) challenge (Birn et al., 2001), different models of simulations were tested and all the models including the Hall term (multi-fluid, hybrid and full Particle-In-Cell) showed normalized reconnection rates comparable to the 0.1 value. Therefore, many concluded that the Hall term was the cause of the normalized reconnection rate having a rate of 0.1. However, subsequent works questioned this conclusion, see Cassak et al. (2017) and references therein. Liu et al. (2017), recently proposed that this specific value of the reconnection rate likely arises from MHD scale physics. They showed that by maximizing the reconnection rate within MHD-scale constraints, one obtains a maximum reconnection rate around 0.1 - 0.2. Furthermore, they showed that the weakening of the upstream reconnecting field as it extends towards the X-line is more important to the reconnection rate than the weakening of the outflow speed. This is another clue that the MHD-scale play a more important role in this problem compared to the kinetic scales, that were of prior importance in the previous assumption of a Hall term dependence. Liu et al. (2018) generalized those results for asymmetric magnetic reconnection, obtaining similar results.

The reconnection electric field value depends, therefore, on the plasma conditions (magnetic field and number density) upstream of the diffusion region. Varying plasma properties in the inflow region can directly be related to the reconnection electric field through the Alfvén velocity. As we have seen in sections 2 and 3, ionospheric plasma contributions to the mass density in the reconnection regions are often significant. The additional mass lowers the Alfvén speed, resulting in a reduced reconnection electric field and reconnection rate. This effect is termed the "mass-loading effect". Intuitively, additional mass means that the flux tubes have more inertia, making it harder to push the reconnected flux tubes out of the way in the outflow region.

In a symmetric configuration, where the mass-density and the magnetic field of the two inflow regions is equal, the relation between the reconnection electric field, Alfvén velocity and aspect ratio is straightforward and given in Equation 8. For asymmetric reconnection, where both the density and magnetic field strength are different between the two inflow regions, the scaling must include the appropriate contributions from the two inflow regions (1 and 2) to find the effective Alfvén speed (Cassak and Shay, 2007):

$$E \sim \left(\frac{\rho_{out} B_1 B_2}{\rho_1 B_1 + \rho_2 B_2}\right) v_{out} \frac{2\delta}{L}, \quad (9)$$

which reduces to Equation 8 if the density at both inflow regions are the same and equal to the outflow density ($\rho_1 = \rho_2 = \rho_{out}$), and the magnetic field is symmetric ($B_1 = B_2$).

4.1.1 Local, in-situ observations of the mass-loading effect of ionospheric plasma

Various works have attempted to measure the mass-loading effect on the reconnection rate at the dayside magnetopause, using local, in-situ spacecraft observations. Su et al. (2000) provided the first observational evidence of the plasmaspheric plume participating in dayside magnetic reconnection. Their observations were made from satellites at geosynchronous orbit (6.6 R_E), and therefore their magnetopause observations correspond to times when the magnetosphere is highly compressed by the

solar wind. They observed magnetosheath and plume plasma simultaneously in the same flux tube, concluding that the plume participated in reconnection instead of being convected towards the tail in closed field lines, indicating that the ionospheric-originating ions can potentially mass-load the reconnecting magnetopause.

Walsh et al. (2013), performed a statistical study of reconnecting magnetopause observations with and without a plasmaspheric plume using the THEMIS mission (cf. Section 3.2.2). They found that the outflow velocity resulting from magnetic reconnection was on average smaller for the events with the plume, and attributed this behavior to mass-loading of the magnetopause by plasmaspheric ions.

Wang et al. (2015) measured the reconnection electric field of 8 magnetopause crossings by the Cluster mission, and normalized them to the magnetosheath and magnetosphere upstream conditions, where some of them included cold protons and heavy ions (O^+) on the magnetospheric side. Comparing their measurements to the scaling law in Equation 9, the estimated an average aspect ratio of ~0.07. Slightly better correlation was obtained when using only magnetosheath upstream parameters, providing an aspect ratio of 0.09. Overall, the reconnection rate mainly depends on magnetosheath parameters, although significant changes (~20%) on the reconnection rate may be produced by ionospheric ion mass-loading. However, direct measures of the reconnection rate based on local in-situ measurements are challenging and require a number of assumptions and approximations. These include the dependence on distance to the X line, the ability to determine the reconnection plane, and the **E** field measurement itself, since the typical reconnection electric field values in the dayside magnetopause are of few mV/m (Genestreti et al., 2018).

Fuselier et al. (2017, 2019a), conducted a statistical survey using 5 months of MMS observations (phase 1a) and inferred the mass-loading capabilities of the ionospheric ions. More details on this study are found in section 3.2. In contrast to Walsh et al. (2013) and Wang et al. (2015), the reconnection *E* field is not directly measured, it is inferred from Equation 9. They concluded that, for nominal magnetospheric activity, the warm plasma cloak and the plasmaspheric plume can reduce the reconnection electric field by more than 20% only a few percent of the time. They also found that during geomagnetic storms the warm plasma cloak is rich in O^+, resulting in denser number density. During disturbed conditions, they found that the warm plasma cloak would reduce the reconnection electric field, due to mass-loading, by more than 20% about 25% of the time. By rewriting Equation 9 it is straight-forward to show that the reduction of the reconnection electric field due to magnetospheric mass-loading (ML) can be rewritten as:

$$R = \frac{E_{ML}}{E_S} = \frac{1}{\sqrt{1+\frac{n_m B_S}{n_S B_m}}} \quad (10)$$

where subscripts *m* and *s* correspond to magnetosphere and magnetosheath, respectively (Borovsky et al., 2013). If the magnetospheric number density $n_m = 0$, then $R = 1$ and there is no reduction due to magnetospheric mass-loading. On the other hand, if if $n_m >> n_s$, R ~ 0. Using typical values for magnetospheric and magnetosheath B field (B_m = 50 nT, B_s = 20 nT) and for magnetosheath number density (n_s = 20 cm^{-3}), one finds that the magnetosphere density has to be n_m = 28 cm^{-3} to produce a reduction of 20% in the reconnection rate due to magnetospheric mass-loading. Based on the results of section 3.2, this number density at the magnetopause has been reported but it is rare. Very dense plasmaspheric material, rich O^+ warm plasma cloak or a highly compressed magnetosphere (n_m ~ 30 cm^{-3} at L-shell = 5, Sheeley et al. (2001)) can lead to densities of ~28 cm^{-3} at the magnetopause. Such high-density magnetospheric plasma near the magnetopause occurs mainly during geomagnetic storms. For instance, Fuselier et al. (2020b) compiled a database of magnetopause crossings on the dayside with the highest He^+ densities. These events consisted of high density plasmaspheric plume material. These

extreme events showed that the magnetospheric mass density can reach values above 50 amu/cm^{-3}, which would cause a reduction of the reconnection rate of about 40%.

During periods of Northward IMF, O^+ escapes from high latitudes directly to the dayside magnetopause, where it can be accumulated until the IMF turns southward and reconnection initiates. Fuselier et al. (2019b), studied a case in such a situation and predicted a transient reduction of the reconnection rate by ionospheric O^+ of 32%.

4.1.2 Global measurements of the mass-loading effect of ionospheric plasma

The mass-loading effect of ionospheric plasma at the dayside magnetopause, and subsequent reduction of the reconnection rate, has also been studied by monitoring the magnetosphere activity using geomagnetic indices. The plasmaspheric drainage plume is a major source of cold plasma at the dayside magnetopause (cf. section 3.2). Borovsky and Denton (2006) used four decades of data from various sources to study the effect of the of the plume on geomagnetic activity. They found a statistically significant reduction of the geomagnetic indices when plasmaspheric plumes were detected in the magnetosphere, for *Kp* > 3. They parametrized the solar wind as a function of $-vB_z$. The coupling reduction is observed for $-vB_z$ > 3000 nT km/s, i.e., strong flows and/or large southward IMF. Borovsky (2008, 2013) derived an empirical formula relating the solar wind main parameters (magnetic field, velocity and pressure) to the global reconnection rate, inferred from geomagnetic indices. They found that ionospheric plasma starts influencing the reconnection rate (they use the term *plasmasphere effect*) when $\rho_m > M_A^{0.87}\rho_{sw}$, where ρ_m is the magnetospheric number density, M_A is the solar wind Alfvén Mach number, and ρ_{sw} is the solar wind number density. Coronal Mass Ejections (CMEs) have low M_A, and therefore the plasmasphere effect is more likely to play a role during the impact of CMEs at the magnetopause (Lavraud and Borovsky, 2008).

4.1.3 Local versus global control of the integrated reconnection rate

There has been some debate on whether the integrated dayside reconnection rate, i.e., total amount of magnetic flux merged per unit time, between the solar wind and the Earth's magnetosphere is set by local parameters near the X line, e.g., Borovsky and Birn (2014) (local control), or by the forcing exerted due to upstream conditions of the solar wind, e.g., Lopez (2016) (global control). The local control hypothesis is implied in the works described in section 4.1.2. The global control hypothesis argues that the merging magnetopause reconfigures itself to accommodate eventual magnetospheric mass-loading produced by ionospheric ions, and that there is no net effect over the integrated coupling across the magnetopause. Recent MHD multi-fluid modelling (Zhang 2016, 2017) suggests that for a moderate amount of mass-loading (plasmaspheric plumes with ρ_m < 8 cm^{-3}), the magnetosheath pressure remains unchanged and the integrated reconnection rate is not significantly affected (global control). On the other hand, for plumes impacting the magnetopause with $\rho_m \geq$ 16 cm^{-3}, the magnetosheath pressure in the inflow region increases owing to pile up of the plasma, leading to more solar wind flux diverted around the magnetosphere (local control). Based on these studies, the two hypotheses (local control versus global control) seem to be complementary.

4.2 Kinetic effects on magnetic reconnection (microscopic view)

The most studied effect of ionospheric-originating ions on magnetic reconnection is the mass loading effect (cf. section 4.1). This effect is considered as macroscopic, as its effect are based on fluid arguments. In this subsection, we focus on the kinetic consequences at the smallest scales of the plasma (microscopic view), and the modification of the plasma dynamics under the presence of cold or heavy ionospheric-originating ions. The behavior of the different plasma populations on kinetic scales depends on their characteristics, such as the Larmor radius and cyclotron frequencies (see Equations 2 and 3).

The corresponding characteristic temporal and spatial scales determine which electromagnetic field fluctuations can be followed by the plasma population. Compared to warm protons, a cold proton population will have a smaller Larmor radius, and hence, will decouple at smaller spatial scales, leading to a new scale length in the system. Heavy ions (e.g., He^+, O^+) have a larger Larmor radii, and smaller gyrofrequency, compared to protons with the same thermal velocity. This would lead to an additional larger scale length of the system. In addition, these heavier species require that the timescales of the reconnection process to be large enough so that the heavy ions can keep up with the evolution. The inclusion of additional scales results in a multi-scale reconnection process, where the properties of the different plasma populations introduce various competing dynamics.

4.2.1 Multiple ion scales

4.2.1.1 Multi-scale separatrices

Magnetic reconnection is initiated and maintained owing to magnetic field dissipation inside the EDR, with a characteristic spatial scale of a few electron inertial lengths. The EDR is surrounded by the IDR, where the ions become demagnetized. The IDR extends in the form of separatrices, i.e., the boundary that separates the inflow from the outflow regions (see Figure 13). Most of the particles involved in reconnection do not cross the EDR or the IDR, and their energization occurs in the separatrices and in the outflow jet. The separatrices are characterized by a Hall **E** field region of widths comparable to the ion scales, sustained mainly by the $\mathbf{J}\times\mathbf{B}/en$ term of the Ohm's law.

Wygant et al. (2005) investigated H^+ and O^+ ion energization across the normal electric field layer present in the separatrices of magnetotail reconnection. The observed normal electric field layer thickness was of a few to several H^+ Larmor radius, allowing the H^+ and electron populations to $\mathbf{E}\times\mathbf{B}$ drift inside the layer and not being significantly energized, while the O^+ was ballistically accelerated by the electric field, resulting into an O^+ energization consistent with the equivalent potential drop observed across the layer. Lindstedt et al. (2010) observed a similar situation at the magnetopause near the cusps, where the normal **E** field near the separatrix of magnetic reconnection accelerated H^+ and O^+ to different energy levels, and attributed it to the different degree of demagnetization of the H^+ and the O^+ inside the layer.

André et al. (2010) and Toledo-Redondo et al. (2015) used Cluster spacecraft measurements to study the behavior of cold ions in the separatrix region of dayside magnetic reconnection. Figure 14a illustrates a 2-spacecraft crossing of the separatrix region, where a 2D, laminar model of magnetic reconnection is assumed. They found that cold ions, owing to their smaller Larmor radius, were able to remain magnetized inside the separatrix region, $\mathbf{E}\times\mathbf{B}$ drifting together with electrons and therefore reducing the perpendicular currents associated to the Hall effect ($\mathbf{J}\times\mathbf{B}/en$ term). This situation is sketched in Figure 14b. They accounted for the reduction of the Hall effect by rewriting the steady state Ohm's law in a three-fluid form, including electrons (subscript e), cold ions (subscript c) and hot ions (subscript h):

$$\mathbf{E} = \frac{1}{en}\,\mathbf{J}\times\mathbf{B} - \frac{n_c}{n}\mathbf{v}_c \times\mathbf{B} - \frac{n_h}{n}\mathbf{v}_h\times\mathbf{B} - \frac{1}{en}\,\nabla\cdot\mathbf{P}_e \qquad (11)$$

where the electron inertia is neglected and $\mathbf{J} = q(n_h\mathbf{v}_h + n_c\mathbf{v}_c - n_e\mathbf{v}_e)$ is the current density.

More recently, several works have confirmed quantitatively, using high-resolution MMS measurements, the differential ion behavior between cold and hot ions in the separatrices of magnetic reconnection, both at the dayside magnetopause (André et al., 2016, Toledo-Redondo et al., 2018) and in the magnetotail (Alm et al., 2018, 2019). Figures 14c and 14d show MMS crossings of the separatrix region, without and with cold ions, respectively. One can see that the Hall term of the Ohm's law, $\mathbf{J}\times\mathbf{B}/en$ (red

curves in bottom panels of Figures 14c and 14d), is smaller in the case with cold ions, because they remain magnetized and **E**×**B** together with electrons (cyan curve in bottom panel of Figure 14d).

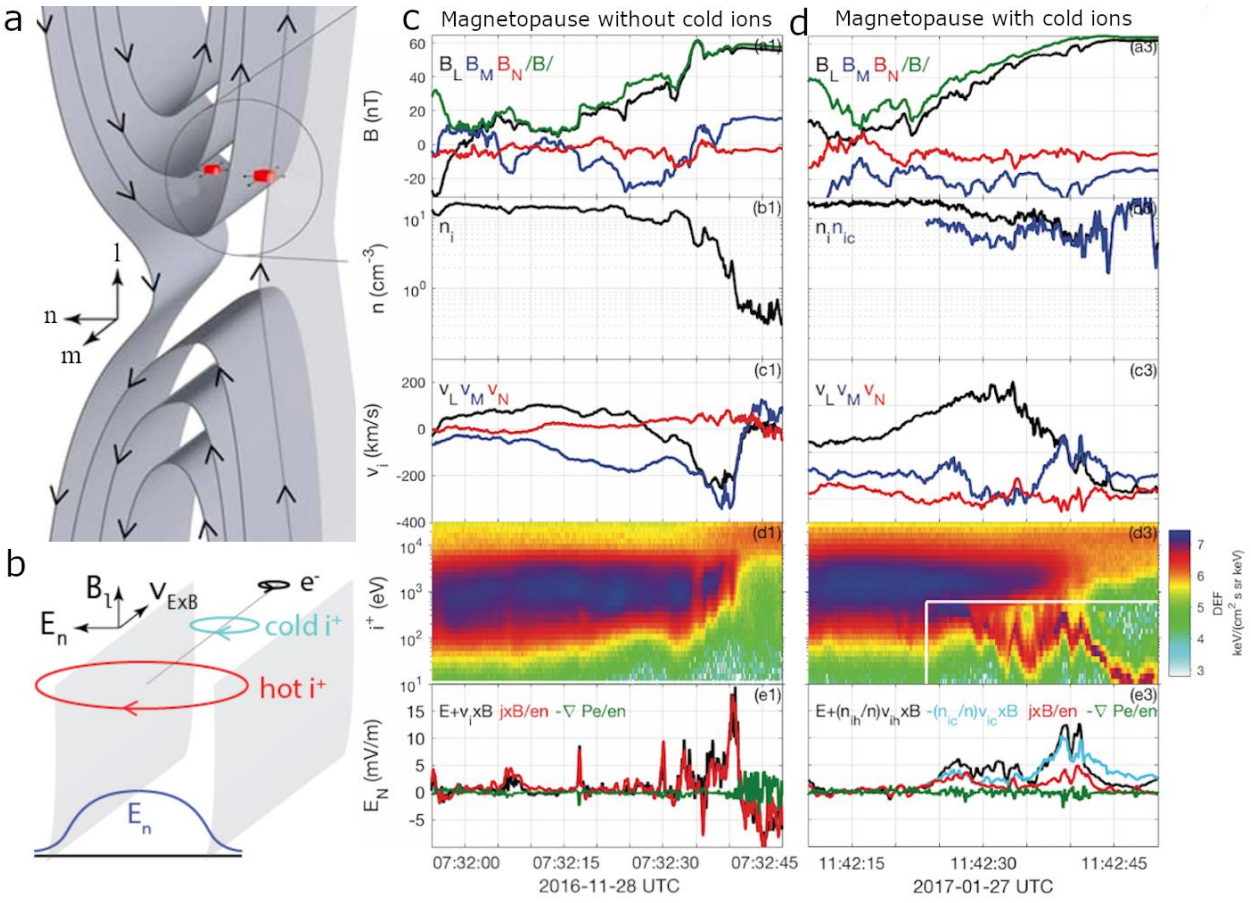

Figure 14. (a) Sketch of multiple spacecraft crossing the separatrix at the dayside magnetopause. Adapted from Toledo-Redondo et al. (2015). (b) Illustration comparing the width of the separatrix layer and its Hall electric field with the giroradii of electrons, cold ions and hot ions. Adapted from Toledo-Redondo et al. (2015). (c) MMS observations of the separatrix region without cold ions. (e) MMS observations of the separatrix region with cold ions. Adapted from Toledo-Redondo et al. (2018).

The Hall **E** field in the separatrices energizes the demagnetized ions that cross it, and therefore one could think that a reduction in the **J**×**B**/*en* term should end up in a reduction of the ion energization across the separatrices. Toledo-Redondo et al. (2018) investigated that, using PIC simulations. They ran two simulations, where one of them included both hot and cold ions in the magnetosphere side. The two simulations had identical asymptotic conditions, that is, magnetic field magnitude, and total particle density and temperature. They found that the maximum Hall **E** field (Figures 15a and 15d) was reduced in the separatrices for the simulations with cold ions, but that at the same time the Hall **E** field layer was wider (Figures 15b and 15e), resulting into very similar integrated potential drops across the separatrix (Figures 15c and 15f).

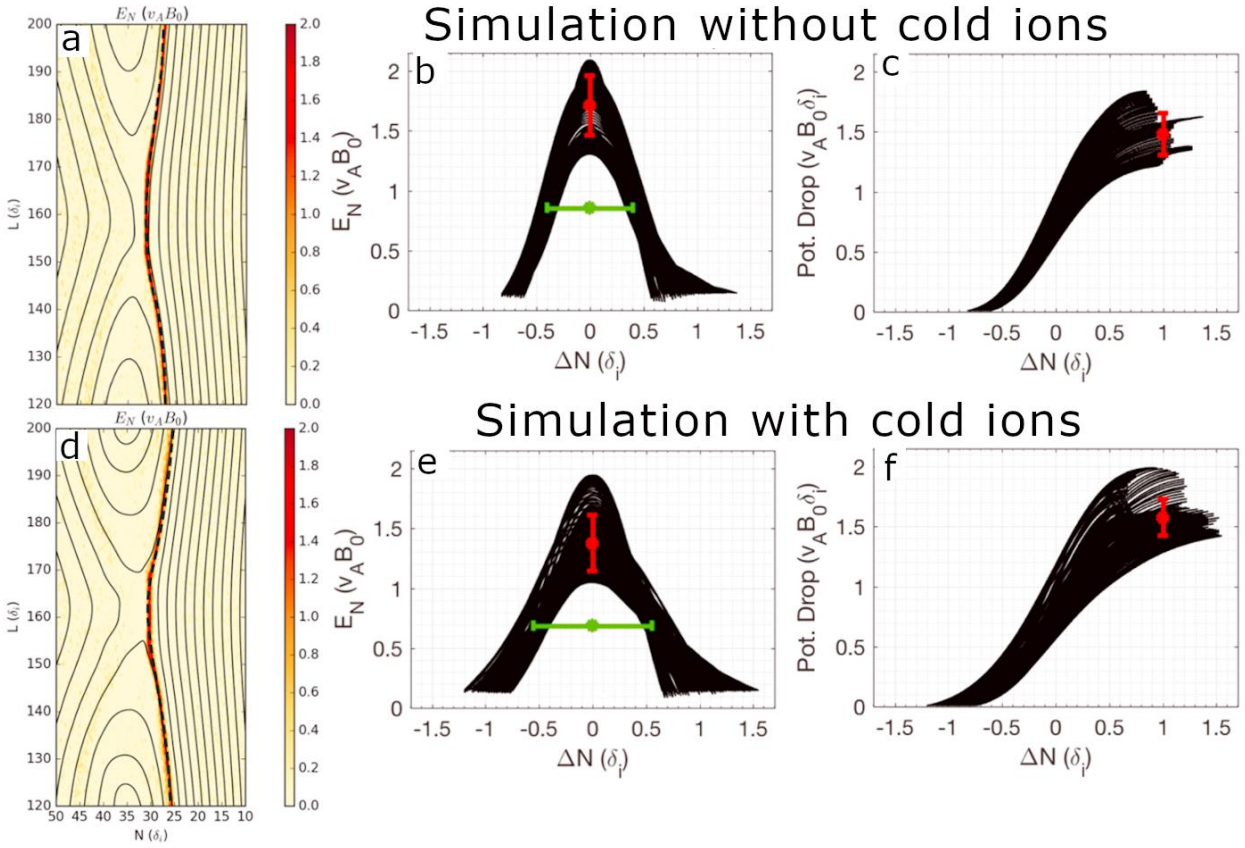

Figure 15. PIC simulations of dayside reconnection with and without cold ions. (a) Hall electric field for the run without cold ions. (b) Hall electric field statistics for the run without cold ions. (c) Potential drop statistics for the run without cold ions. (d-f) Same as a-c for the run with cold ions. Adapted from Toledo-Redondo et al. (2018).

Dargent et al. (2017) ran two kinetic simulations of magnetic reconnection, with and without cold ions, and noticed the presence of a new electric field layer along the magnetospheric separatrices, adjacent to the Hall **E** field layer, but weaker and wider, and with an opposite sign. They argue that this new field results from cold ions being frozen-in at scales where hot ions begin to demagnetize with the proximity of the asymmetric layer. This field is also observable in other simulations (e.g., Dargent et al., 2020), although its relevance for energy conversion from the fields to the particles by reconnection remains unexplored.

4.2.1.2 Multi-scale ion diffusion regions

The presence of multiple ion populations in magnetic reconnection also affects the topology of the IDR. Each ion population has its own characteristic spatial scales, namely the ion inertial length and the Larmor radius, which depend on the atomic mass and temperature of the population. Therefore, each ion population sets its own ion diffusion region, resulting in a multi-scale ion diffusion region (two or more layers). This behavior in magnetic reconnection has been observed both using PIC simulations and spacecraft observations at the Earth's magnetopause and in the magnetotail.

Liu et al. (2015) run 2.5D PIC simulations of symmetric magnetic reconnection, including electrons, H^+ and O^+. They found that, in the steady-state regime, the O^+ demagnetize at a larger scale than H^+, measured through the agyrotropy of the populations (Figure 16a). This results in a three-scale diffusion

region, one for each population, as sketched in Figure 16b. They compared the ion velocity distributions functions of their simulation to real observations made by Cluster in the Earth's magnetotail, and confirmed the multi-scale nature of the diffusion region when O^+ is present.

Divin et al. (2016) also run 2.5D PIC simulations of symmetric magnetic reconnection, and included cold H^+ in addition to hot H^+ and electrons. They also found a multi-scale diffusion region, where the cold ions remain magnetized down to smaller scales than the hot H^+, owing to their different Larmor radius. Figure 16c shows particle trajectories for hot H^+ (red), cold H^+ (pink), and electrons (blue) in the vicinity of the X line. Electrons remain frozen-in to the inflowing magnetic field and reach the inner part of the current sheet, while hot ions are demagnetized upstream in the inflow region and follow distinct trajectories. Cold ions are demagnetized at intermediate distances between the center of the current sheet and the region where the hot ions are demagnetized. Figure 16d corresponds to a diagram of the multi-scale diffusion region due to electrons, cold H^+ and hot H^+.

A multi-scale ion diffusion region created by cold and hot H^+ was also reported at the dayside magnetopause, using MMS observations (Toledo-Redondo et al., 2016a). MMS crossed near the EDR of magnetic reconnection, with both Northward and Southward ion jets observed in the vicinity of the magnetopause crossing. The spacecraft separation was of only ~15 km, i.e., comparable to the cold H^+ gyroradius and much shorter than the hot H^+ gyroradius (~200 km). One of the spacecraft observed the cold H^+ being accelerated parallel to **E** in a thin region of ~15 km width, while the other spacecraft observed that cold H^+ was $\mathbf{E}\times\mathbf{B}$ drifting, in a region where the hot ions were already demagnetized. These regions were identified as the cold IDR and the hot IDR, respectively. At the Earth's magnetopause, the cold ions are of ionospheric origin and can be present only in the magnetospheric inflow region. Therefore, the topology of the multi-scale IDR must be asymmetric. A subjacent question that arises from the observation of multi-scale diffusion regions, both symmetric and asymmetric, is whether this results into an effective modification of the aspect ratio, i.e., the normalized reconnection rate. This question is addressed in Section 4.2.2. Finally, it is known that cold plasma escaping from the ionosphere is composed of both cold electrons and cold ions. The effects of multiple electron populations (cold and hot) on magnetic reconnection have not been addressed in the literature, to our knowledge.

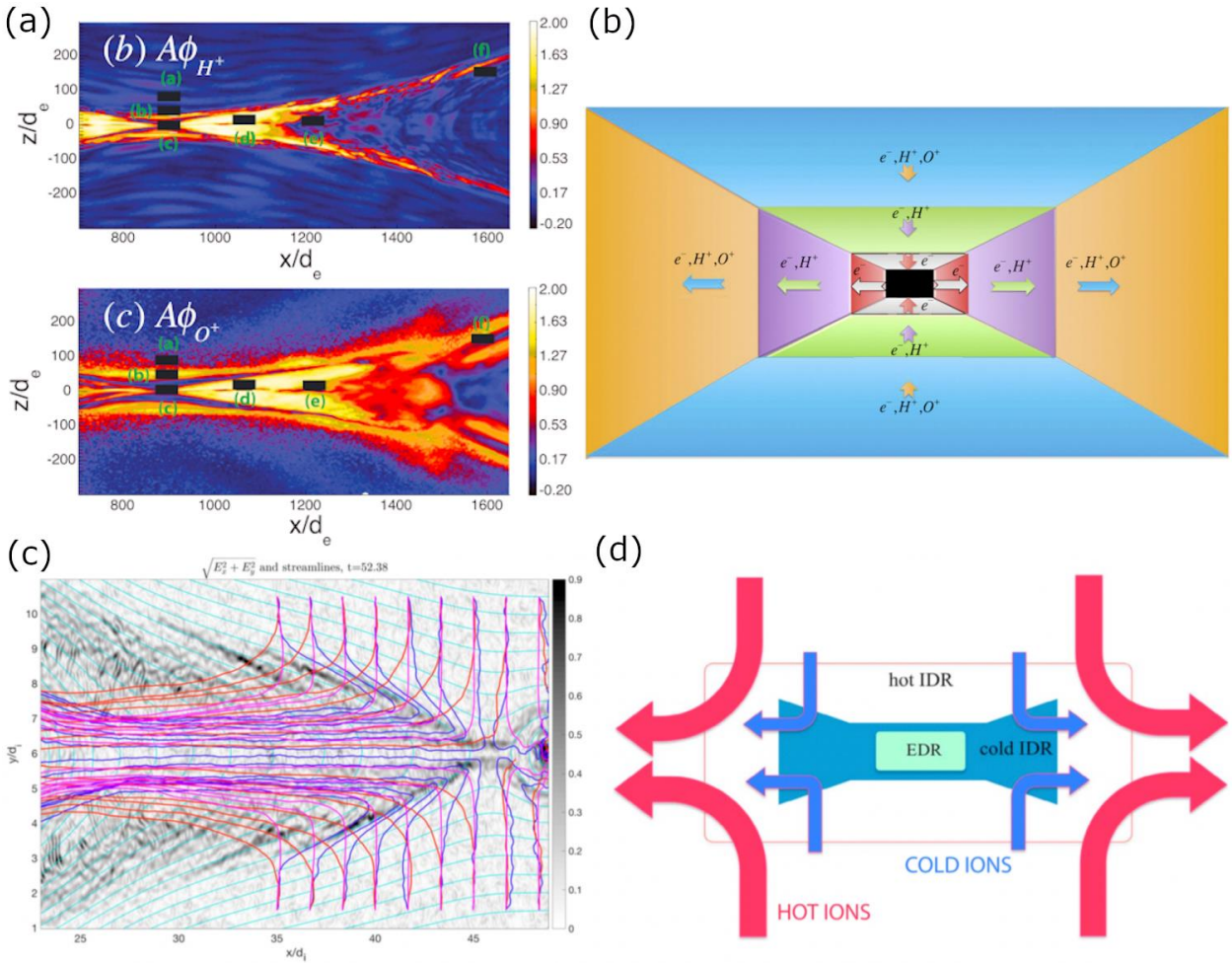

Figure 16. PIC simulations of symmetric magnetic reconnection including O^+ (top panels) and cold protons (bottom panels). (a) Agyrotropy of H^+ and O^+. Adapted from Liu et al. (2015). (b) Sketch of a multi-scale diffusion region including electrons, protons and oxygen. Adapted from Liu et al. (2015). (c) Trajectories of electrons (blue), cold ions (pink) and hot ions (red) inside the diffusion region of symmetric magnetic reconnection. Adapted from Divin et al. (2016). (d) Sketch of a multi-scale diffusion region including electrons, cold protons and hot protons. Adapted from Divin et al. (2016).

4.2.2 Kinetic effects on reconnection rate

4.2.2.1 Cold ions and reconnection rate

We have already seen in section 4.1 that ions of ionospheric origin have a mass loading effect on the magnetic reconnection rate. However, based on the scaling analysis (see Equations 8 and 9) there is no direct dependence on temperature. For instance, a cold plasma population should not affect the reconnection rate as long as the total mass density remains constant. However, a cold population introduces a new length-scale and therefore should lead to a reconfiguration of the diffusion region. In particular, a cold ion population is expected to reduce the average height of the ion diffusion region (δ). According to Equation 8 (Equation 9 for asymmetric magnetic reconnection), maintaining a constant reconnection rate would then imply that the diffusion region configures itself so that the length L is reduced in order to keep constant the aspect ratio δ/L.

Numerical simulations have shown that the inclusion of multiple ion populations with different temperatures has a negligible effect on the reconnection rate if the mass density is constant, both for symmetric reconnection (Divin et al., 2016, Tenfjord et al., 2020), and for asymmetric reconnection (Dargent et al., 2017, 2020).

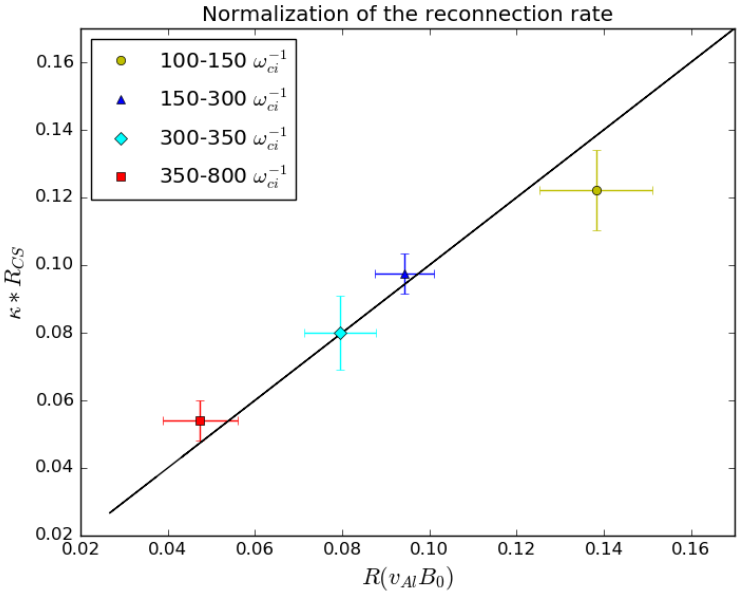

Figure 17. Scatter plot for all times of the observed reconnection rate versus the calculated one (i.e. Equation 9 assuming δ/L = 0.1). The factor κ = 0.127 is calculated such as $\kappa R_{CS}/R$ scales along a slope of 1. Each point corresponds to the mean value of the reconnection rate on a time interval and the bars associated with them provides one standard deviation. The given time intervals correspond to the different phases of the simulation: yellow, early unsteady magnetic reconnection; blue, steady magnetic reconnection without the plasmaspheric plume; light blue, transition phase with the impact of the plume; red, steady magnetic reconnection with the plasmaspheric plume. Adapted from Dargent et al. (2020).

All these works observe a ratio δ/L ~ 0.1, as expected by Liu et al. (2017,2018). In particular, Dargent et al. (2020) studied how the reconnection rate evolves during the impact of a dense, cold, plasmaspheric plume at the reconnecting magnetopause. Figure 17, shows the observed reconnection rate R versus the expected one, using for calculation Equation 9, assuming δ/L = 0.1. The yellow dot represents the average value of the measured versus the expected reconnection rate during the early stage of the

simulation. The observed reconnection rate is larger than the expected using Equation 9 and assuming δ/L = 0.1 in this early stage of the simulation. This is a well-known feature of PIC simulations, often called the overshoot period, that occurs before the simulation reaches steady state (Shay et al., 2007). The blue, cyan, and red dots correspond to the simulation time prior to the arrival of the plasmaspheric plume to the reconnection region (blue), the transition time during the impact of the plume (cyan), and the new steady state reached by magnetic reconnection under the presence of the plume in the magnetospheric inflow region (red). The observed reconnection rate diminishes owing to the mass-loading effect of the plume (cyan and red dots). However, for any of the three phases, the observed reconnection rate matches in average the calculated one using upstream conditions and assuming δ/L ~ 0.1. Despite the dynamic evolution of magnetic reconnection when the plume impacts the layer, this figure confirms that the aspect ratio remains roughly constant in average, with a value of δ/L ~ 0.1. A simulation study by Spinnangr et al. (2020) investigated how the reconnection process reorganizes itself on kinetic scales when cold protons get involved in the reconnection process. The authors found, as expected from arguments presented above, a significant reduction of δ. From our scaling arguments we would then expect L to be reduced by the same factor for the ratio to be kept at a constant δ/L ~ 0.1. However, the length (L) was found to decrease less, which corresponded to a small discrepancy between the rescaled reconnection rate in a simulation with cold ions, and a run without. This suggests that, on ion-scales, some of the assumptions made in the scaling do not always hold. The reorganization of the aspect ratio was found to be enabled by temporal inertia of the cold population during a transition period. This result suggests that the process indeed reconfigures itself to account for the inclusion of an additional ion population with a lower temperature, resulting in a lower reconnection efficiency.

4.2.2.2 Heavy ions and reconnection rate

The ion outflow from the high-latitude ionosphere is often composed of He^+ and O^+, in addition to H^+, and is believed to be a significant source of plasma for the terrestrial magnetosphere, and in particular for the tail, cf. Sections 2 and 3. This additional composition leads to an increased total mass density which affects fundamental plasma properties such as the Alfvén speed, plasma pressure and plasma beta. Under geomagnetically active times, O^+ can even dominate the number density in the magnetotail (e.g., Kistler et al., 2005, Wygant et al., 2005). Similar to cold protons, the presence of heavier species also leads to multiple scales in the reconnection process. Heavier ion populations will have a larger diffusion region compared to that of protons with the same thermal velocity. Additionally, the presence of heavy ions can lead to different Hall dynamics (see Section 4.2.1.1) and also influence the dynamics of dipolarization fronts (Liang et al., 2017, Markidis et al., 2011). Heavier species such as O^+ can also, if magnetized for the spatiotemporal scales of interest, lead to a significant mass-loading of the reconnection process (Hesse and Birn, 2004; Shay and Swisdak, 2004; Borovsky, 2013). Additional effects of heavier ion species also include an impact on the tearing growth rate (Karimabadi et al., 2011), induced charge separation effects, i.e., ambipolar electric fields (Liang et al., 2016) and may contribute to the generation of bifurcated current sheets (George and Jahn, 2020). Wang et al. (2014) investigated the role of O^+ and H^+ in a reconnection event using Cluster, and found that the O^+ energization depends on the location at which the O^+ enters the exhaust. If the O^+ enters close to the diffusion region they behave like pick-up ions (Drake, 2009b), whereas further downstream they retained their adiabatic motion and follow the rest of the plasma in the outlflow region (Drake, 2009a). Because of the significantly larger inertia of these heavy ions, they also introduce an additional time scale because of the cyclotron frequency dependence on ion mass. The evolutionary timescale of the system must evolve slowly enough for the heavy ions to remain magnetized.

Assuming a magnetic field of B_0 = 20 nT in the magnetotail lobes, the cyclotron period of H^+ is ~3 s, while for O^+ the cyclotron period is ~50 s (since the O^+ mass is 16 times that of H^+). Magnetic reconnection in

the tail occurs in the plasma sheet, which is emptied by reconnection jets and refilled by plasma in the lobes. If we assume that a reconnection event in the tail (e.g., a Bursty Bulk Flow) lasts for about 200 proton cyclotron periods, i.e., about 10 minutes, the heavy, sluggish O^+ has only had time to gyrate about the magnetic field 12 times. This affects the ability of the O^+ to stay magnetized, since in its frame of reference the evolutionary timescale of the reconnection process can be comparable or even faster than its own cyclotron period, preventing the real system to reach steady state (Markidis 2011, Tenfjord et al., 2018, 2019 , Kolstø et al., 2020). The effect is that in the frame of the O^+, the frozen-in approximation no longer holds, and they lose the ability to add inertia to the flux tube. The consequence being that the role of O^+ on the reconnection process can no longer adequately be described as a simple mass-loading process. Using PIC simulations, Tenfjord et al. (2018) investigated the behavior of O^+ as it was captured by reconnection in the tail. They found that O^+, as a consequence of being demagnetized, was ballistically accelerated, primarily by the Hall electric field. Simulations by Tenfjord et al., 2019 and Kolstø et al., 2020, show that both for symmetrically and asymmetrically distributed O^+, the reconnection rate is significantly reduced, but not as much as predicted by mass-loading. The authors describe a mechanism where the O^+ population (and the accompanying electrons) acts as an energy sink on the system, altering the energy partitioning. Even though O^+ ions do not directly influence the reconnection process through mass-loading, they do extract energy from the fields that would otherwise be available for accelerating protons and electrons. Based on a scaling analysis the authors find a scaling based on the energy extracted by the unmagnetized species which describes the reduced reconnection rate.

While measurements of the variations in the local rate of reconnection in the tail with heavy ions are still elusive, the global effects of the reconnection rate can be determined by studying the substorm unloading. After substorm onset, reconnection occurs in the magnetotail, reducing the magnetic flux that has built up in the tail lobes during the growth phase. Therefore, the rate of unloading is related to the tail reconnection rate. Liu et al. (2013) studied the global effect of heavy ions on the substorm unloading rate using data from the Cluster mission, by correlating the rate of unloading with the mass density and O^+/H^+ ratio in the tail prior to substorm onset. They found that unloading rate is in fact faster when the O^+ density and O^+/H^+ ratios are higher. This faster rate is contrary to the naïve expectation that increased O^+ should decrease the reconnection rate. Further, the faster rate indicates that other parameters, such as the generally higher activity that usually is associated with high O^+, or the width of the tail over which the reconnection is occurring may be playing a larger role in determining the unloading than the reconnection rate itself.

At the dayside magnetopause, magnetic reconnection is thought to occur more steadily, due to the dominant effect of the dense inflowing solar wind. In this scenario, the reconnection process can reach steady-state relative to the O^+ characteristic timescale. In this case, O^+ would have sufficient time to remain magnetized, and the reduction of the reconnection rate may be estimated based on mass-loading scaling (Fuselier et al., 2019a, Karimabadi et al., 2011; Kistler et al., 2005; Liu et al., 2015).

4.2.2.3 Effect of streaming ions (suppression of rate)

An additional effect beyond the previous described slowdown scenarios is the involvement of a moving cold ion population in the inflow region. Ions originating from the ionosphere stream parallel to the magnetic field (e.g., Bouhram et al., 2004; Fuselier et al., 2019b). The outward velocity is typically observed to be up to ~50 km/s (Haaland et al., 2012c; André et al., 2015). Consequently, this additional plasma population adds net, tailward directed momentum to the reconnection process. At the dayside magnetopause, as we move away from the subsolar point, the differential motion between the draped

solar wind and the magnetospheric convection also causes differential ion streams on both sides of the reconnection region.

As soon as streaming ions become involved, they contribute to the overall momentum balance, altering the reconnection dynamics. Tenfjord et al. (2020) investigated the effect of a streaming cold proton population on the reconnection process using PIC-simulations. In the magnetotail, this results in a tailward propagation of the reconnection X line. The inclusion of streaming particles influenced the initially symmetric outflow regions, producing asymmetries in outflow velocities and temperatures. In a similar study, Kolstø et al. (2020) investigated the effect of a streaming oxygen population. As already discussed, O^+ remains demagnetized because the cyclotron period is much longer than the evolutionary timescale of the reconnection process. Even though O^+ did not exhibit a magnetized behavior they still impart their tailward directed momentum through electrostatic coupling. In addition, the authors observe the formation of an oxygen wave (Tenfjord et al., 2018) which becomes significantly altered by the added momentum.

For cold protons, this additional momentum does not appear to cause any additional reduction of the reconnection rate, after correcting for the additional mass. For streaming O+, the reduced rate corresponds to the scaling described in Tenfjord et al. (2019). However, both in the magnetotail and on the dayside, streaming ions can cause drift of the reconnection X line into regions where the plasma conditions are different, which could result in an effective change or even suppression of the reconnection process.

4.2.3 Additional consequences of multiple ion populations

4.2.3.1 Cold ion crescents

In weak guide field configurations, the dynamics of the ion populations inside the diffusion region are deeply affected. The magnetic field reversal in the center of the reconnecting current sheet implies a large B field gradient over less than an ion inertial length, and that the direction of a particle gyration is changing through the layer. Thus, the particles will be bouncing between the magnetic field lines on either side of the X-line instead of gyrating around one magnetic field line. The bounce-width of a population is therefore where the local thermal Larmor radius is equal to the distance to the center of the layer (Hesse et al., 2011). This bounce motion produces crescent-shaped distribution functions along the boundary of the bounce width. Such a signature in electron distribution functions has been proven to be a signature of magnetic reconnection (Hesse et al., 2014, Burch et al., 2016, Bessho et al., 2016), and is also expected for ions (Shay et al., 2016, Dargent et al., 2017). Dargent et al. (2019) showed another mechanism than can lead to the formation of such crescent-shaped distribution functions for cold ions. Cold ion distribution functions take a crescent shape along the magnetospheric separatrices, without magnetic field reversal. In this case, the driver of the signature is the Hall electric field, which accelerates and then decelerates the cold ions during one Larmor gyration.

4.2.3.2 Cold ion beams and lower hybrid instabilities

In collisionless plasmas, waves play an important role in coupling the various particle populations. Graham et al. (2017a) showed, using both spacecraft observations and linear theory modelling, that the presence of cold ion beams (ionospheric origin) near the ion diffusion region of magnetic reconnection at the Earth's magnetopause can be a free source of energy for the lower hybrid instability, when the cold ion beam interacts via an ion-ion instability with the solar wind population. The generated lower hybrid waves near the ion diffusion region heat the cold ions, acting as a preconditioner of the population in the magnetospheric inflow region.

4.3 Cold ion energization and energy budget of magnetic reconnection

One of the most important consequences of magnetic reconnection is the efficient conversion of magnetic energy into kinetic and thermal energies. Ionospheric ions, like any other particle, are energized by magnetic reconnection, in the form of bulk drift acceleration to form the outflow jets plus thermalization. Bulk acceleration is believed to occur in a similar way to pickup processes (e.g., Drake et al. 2009b) when the ionospheric ions enter the outflow jet. From the fluid description given in section 4.1, one can see that the outflow velocity, i.e. the Alfvén velocity, scales with the mass density in the inflow regions, and the energy conversion rate from magnetic fields into bulk drift acceleration is balanced.

However, magnetic reconnection also produces heating of the particle populations. This heating is accomplished by reconnection by means of various mechanisms, including the reconnection electric field, the Hall electric fields, or wave-particle interactions. These mechanisms occur at kinetic scales of the particles, and the level of turbulence achieved in the outflow jet may condition the amount of net heating.

4.3.1 Cold ion energization at the Earth's magnetopause

The typical temperature of the magnetosheath ions is approximately 100 - 200 eV, while the typical temperature of ionospheric cold ions reaching the magnetopause ranges from few eV for plasmaspheric material to several hundred eV for the warm plasma cloak, in addition to the keV plasma sheet ions that can originate in the solar wind or in the ionosphere. Cold ions are accelerated and heated when entering the diffusion region, separatrices, and reconnection outflow region. In those regions, cold ions are mostly mixed together with the magnetosheath ions, and it becomes difficult to distinguish between the two populations. Li et al. (2017) presented an MMS study of a magnetopause crossing with high-density (10 - 60 cm^{-3}) cold ions and on-going reconnection. Near the magnetospheric edge of the ion jet, they observed a mixture of plasma sheet ions, magnetosheath ions and heated cold ions (Figure 18, black arrow). On the magnetosheath edge of the ion jet, two distinct ion populations were observed. One population with high parallel velocities (200-300 km/s) but rather low temperature (~90 eV) was identified to be a cold ion beam, while the other population was the magnetosheath ions. They separated the distribution functions of the cold ion beams from the entire distribution functions, and computed the partial moments of the cold ion beams. The cold ion beams are hotter than the cold ions in the inflow region, but are still ~30% colder than the hot magnetosheath ions. In the deHoffman-Teller frame, the field-aligned magnetosheath ions are nearly Alfvénic and move toward the jet region, while the field-aligned cold ions move toward the magnetosheath boundary layer, with much lower speeds. The results suggest that the cold ion beams are accelerated close to the X line (Figure 18, red arrow). The study illustrates that the cold ion heating by reconnection is not homogeneous along the separatrix and suggests it may be lower close to the X line.

Toledo-Redondo et al. (2016b, 2017) reported Cluster and MMS spacecraft observations of cold ion heating in the separatrix region of magnetic reconnection, and showed that both waves near the ion cyclotron frequency and gradients of the Hall electric field were consistent with the amount of heating observed. They estimated, for the four events investigated, that cold ion heating took 10 – 25 % of the energy that went into ion heating, while the other 75 – 90 % went into heating the more abundant magnetosheath ions. Graham et al. (2017a) showed MMS observations of lower hybrid drift waves inside the separatrix region, formed owing to the presence of a cold ion beam, cf section 4.2.3. All these findings indicate that the presence of cold ions modifies the energy partition that is converted from the fields into particle kinetic energy by magnetic reconnection, although quantification of the energy taken by cold ions in the form of bulk kinetic acceleration and heating from a statistical perspective remains unknown.

Vines et al. (2017) studied the energization mechanisms of ionospheric ions, including H^+, He^+ and O^+, at the separatrix of magnetopause reconnection, and concluded that the energization mechanisms at play act in a different way depending on the atomic mass unit of the population. They observed two different energization mechanisms. The first energization mechanism was observed inside the outflow jet, and corresponds to the pickup process by the jet, identified by the characteristic velocity-space ring distributions of the ions in the plasma frame. For cold H^+, the pickup process resulted mainly in bulk drift acceleration. However, they noted that for heavy ions (He^+ and O^+) the pickup process occurred non-adiabatically, due to their larger characteristic spatial and time scales (Larmor radius and gyrofrequency), leading to less well-organized ring distributions which included ion heating and velocity and temperature anisotropy. The second energization mechanism was observed near the magnetospheric separatrix region, where the cold H^+ was preferentially heated, and did not affect much the heavy ions. The H^+ heating in the separatrix region is associated with fluctuations generated by a two-stream instability and the lower-hybrid instability (cf. section 4.2.3).

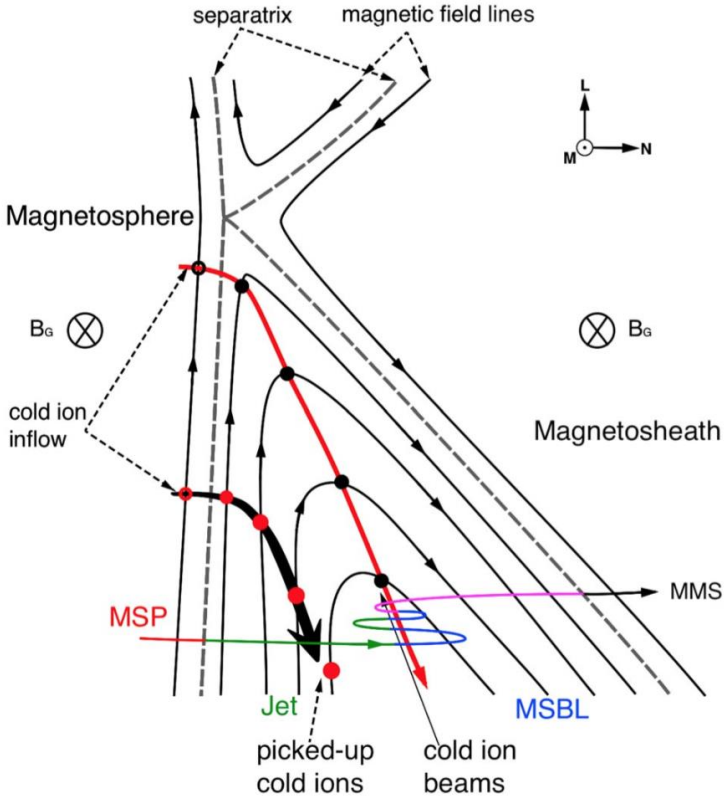

Figure 18. Diagram of the MMS observations during a magnetopause crossing with ongoing magnetic reconnection. Near the magnetospheric edge of the ion outflow jet, heated cold ions are observed (black arrow). Near the magnetosheath edge of the ion outflow jet, cold ions with lower temperature are observed, indicating that the amount of cold ion heating imparted by reconnection depends on the distance to the X line where the cold ions cross the magnetopause boundary. Adapted from Li et al. (2017).

4.3.2 Cold ion energization in the plasma sheet

The plasma sheet boundary layer (PSBL) and the lobe region always contain certain amounts of cold ions of ionospheric origin. The amount of ionospheric plasma present in the magnetotail is variable, depends

on magnetospheric activity (cf. section 3.3), and can affect magnetic reconnection in the magnetotail. One prominent feature is that cold ions can create highly structured ion distribution functions including ion beams that deviate from a Maxwellian distribution. Among these distributions, counter-streaming cold-ion beams along the direction normal to the current sheet were frequently observed in the ion diffusion region (e.g,, Nagai et al., 1998; Shay et al., 1998; Wygant et al., 2005, Divin et al., 2016). The counter-streaming cold ion beams are accelerated to several keV, but are still much colder than the plasma sheet hot ions. Using measurements from the Cluster spacecraft, Wygant et al. (2005) showed that the counter-streaming cold ions are accelerated by the large-amplitude Hall electric field in the ion diffusion region, and numerical simulations from Aunai et al. (2011) and Divin et al. (2016) showed a similar acceleration process of cold ions across the current sheet. Combining the THEMIS observations and the particle-in-cell simulations, Eastwood et al. (2015) illustrated that the ion beams originate from the thermal component of the preexisting plasma sheet hot ion, and are accelerated by the reconnection electric field and rotated from out-of-plane direction to the outflow direction by the Lorentz force. Some other studies argue that the Fermi effect is the main acceleration mechanism for the counter-streaming cold-ion beams (e.g., Runov et al., 2017, Birn et al., 2017; Xu et al., 2019). Quantitative and statistical analysis of the cold-ion beams are needed to assess the contribution from each acceleration mechanism.

4.4 Heavy ion effects on reconnection onset and efficiency

Baker et al. (1982) proposed that O^+ would enhance the linear ion tearing instability in the plasma sheet, and so decrease the stability of the tail to reconnection. Multiple studies since then have attempted to test this. One way to test it is to determine if O^+ is generally enhanced prior to substorm onset. Daglis et al. (1990) found that O^+ was enhanced in the near-earth plasma sheet, but studies further down the tail closer to the reconnection region did not find that O^+ is enhanced prior to onset except during storm-time sawtooth events (Lennartsson et al., 1993, Kistler et al., 2006, Liao et al., 2014). Another method to test this is to determine whether there are more substorm onsets when there is more O^+. Lennartsson et al. (1993) and Nose et al. (2009) performed long-term studies, and they both showed the well-known correlation between O^+/H^+ and F10.7, but found no correlation between O^+/H^+ ratio and the frequency of substorms over a solar cycle. A final method is to examine the effect of O^+ on loading during substorms. The amount of loading that occurs before substorm onset gives an indication of how unstable the tail is to reconnection onset. If the plasma sheet is more unstable, we would expect there to be less loading before reconnection is triggered. Liu et al., (2013) used Cluster data to determine the correlation between the amount of loading and the O^+ in tail. The amount of loading was positively correlated with the amount of O^+ in the tail, which would indicate that the O^+ in fact makes it harder to trigger substorm onset. They also found that, once reconnection was triggered, the magnetic flux was dissipated faster when O^+ was present, suggesting either an increased reconnection rate or an increased length of the X line in the dawn-dusk direction. Using observations and multi-fluid simulation, Winglee and Harnett (2011) found that O^+ can play a role in the development of substorms, as O^+-enriched reconnected flux tubes can influence the energy dissipation and modify the plasma distribution in the plasma sheet. Various numerical studies indicate that the ionospheric outflow favors the creation and enhancement of substorms, moves the X line earthward and may be responsible for sawtooth events (e.g., Wiltberger et al., 2010; Brambles et al., 2010, 2013; Zhang et al., 2020). On the contrary, the results by Lund et al. (2018), using cluster observations, seem to indicate that sawtooth events are not produced by the ionospheric outflow.

4.5 Change of plasma beta and reconnection suppression

For asymmetric reconnection, where the plasma density and temperature vary greatly across the reconnection region, the net diamagnetic drift of the plasma in the reconnection exhaust can influence, and even suppress, the progression and efficiency of reconnection (Swisdak et al., 2003, 2010, Phan et al. 2013, Cassak and Fuselier, 2016). Diamagnetic drift arises from a thermal plasma pressure gradient as the result of ions and electrons effectively gyrating in opposite directions about the magnetic field. An apparent flow is created if there is a gradient in temperature (gradient in average particle thermal speeds), density (gradient in the number of gyrocenters) or both. During magnetic reconnection this leads to the reconnection X-line moving along the direction of the electron diamagnetic drift due to the ability of electrons to remain magnetized down to smaller scales. When the diamagnetic drift velocity exceeds the Alfvén speed, reconnection can no longer continue, as the force due to the outflowing reconnected magnetic field is unable to overcome the force arising from the effective net plasma drift induced by the pressure gradient (Swisdak et al., 2003). The suppression mechanism may be altered when there is a gradient in temperature but no substantial density gradients present, as demonstrated by Liu et al. (2016) using PIC simulations.

The conditions that may suppress reconnection via diamagnetic drift can be expressed in terms of the difference in plasma β (the ratio of thermal plasma pressure to magnetic pressure) on either side of the current sheet ($\Delta\beta$) and the magnetic shear angle (θ), i.e., the change in magnetic field orientation across the reconnection site:

$$\Delta\beta > 2\left({}^{L}/_{d_i}\right)\tan(\theta/2), \tag{12}$$

where *L* is the current sheet width and d_i is the ion inertial length (Swisdak et al. 2010). For small values of $\Delta\beta$, where the plasma populations and magnetic field strength are similar on both sides of the reconnection site, the effect of diamagnetic drift is not substantial, and so reconnection can proceed for a wide range of magnetic field orientations. It is important to note, however, that Equation 12 is a necessary, but not sufficient condition for reconnection to proceed (e.g., Vernisse et al., 2020). As the difference in plasma beta increases, the locations of reconnection sites become increasingly confined to regions of anti-parallel magnetic fields (i.e., regions where magnetic shear angles are closer to 180°) (Swisdak et al., 2003; 2010; Cassak and Fuselier, 2016).

When ionospheric plasma is present on one side of the reconnection site, as is often the case for the Earth's magnetopause, the diamagnetic drift relationship can be altered locally. Through changes in $\Delta\beta$ due to the plasma temperature and density on one side of the reconnection region, the ionospheric-originating plasma reaching the magnetopause may affect reconnection beyond mass-loading the reconnection site, as discussed in sections 4.1 to 4.3. Taking, for instance, typical plasma conditions in the Earth's magnetosheath and normal magnetic field strengths in the magnetosheath and outer magnetosphere, listed in Table 3 and in Cassak and Fuselier (2016), the largest values of $\Delta\beta$ (and so the most restrictive conditions for reconnection to proceed with regards to the diamagnetic drift effect) occur when the magnetospheric population consists of the plasma sheet population alone, which is always present.

For dense and cold plasma reaching the magnetopause, as when the plume extends to the outer magnetosphere during geomagnetic storms, the resulting $\Delta\beta$ using typical magnetosheath conditions is very similar to the $\Delta\beta$ observed for nominal magnetospheric plasma conditions when no dense, cold populations are present, because the plume population does not contribute significantly to the plasma pressure. When the warm plasma cloak population reaches the magnetopause, it contributes to the magnetospheric plasma β (i.e., increasing the temperature and density), resulting in smaller $\Delta\beta$ across the magnetopause. Therefore, the presence of the warm plasma cloak or, equivalently, heated plasmaspheric material (e.g., Toledo-Redondo et al. 2017) can increase the range of magnetic field orientations across the magnetopause at which magnetic reconnection can proceed, relaxing the condition for the diamagnetic drift suppression mechanism.

The varying plasma conditions under which reconnection suppression due to diamagnetic drift occur hold implications for where reconnection regions at the magnetopause are expected to be located, both for Earth and for other planets like Jupiter and Saturn. The moons of Jupiter and Saturn produce very large amounts of cold, dense plasma, and the very fast rotation of those planets confines the plasma to low-latitudes (Bagenal and Delamere, 2011, Vasyliunas, 1983, Louarn et al., 2015 and references therein). Coupled with a much weaker interplanetary magnetic field in the outer solar system and a much stronger planetary magnetic field of these planets, reconnection is thought to be generally suppressed across most of the magnetopause at Jupiter and Saturn via this mechanism of diamagnetic drift (e.g., Desroche et al., 2013). While the diamagnetic drift-induced suppression is just one possible mechanism that may control the continuation after onset and efficiency of reconnection, the simple example above of how an inner plasma source may alter the plasma β at Earth's magnetopause, as well as observations of Saturn's magnetopause (Masters et al., 2012, Fuselier et al., 2014), show the complex effect that cold plasma populations can have on reconnection dynamics.

Unlike the magnetopause, in the Earth's magnetotail, the diamagnetic drift suppression mechanism is not expected to be important because the β magnitude in the plasma sheet is typically smaller than in the magnetosheath. In addition, reconnection in the magnetotail is typically symmetric and involves the

plasma sheet populations in both sides, and therefore no substantial $\Delta\beta$ is expected across the current sheet.

Table 3. Representative plasma conditions for different populations and effect on $\Delta\beta$ at the Earth's magnetopause

Plasma Population	**Density (cm^{-3})**	**Temperature (keV)**	**B[a] (nT)**	**β**	**$\Delta\beta = \lvert\beta_{sh} - \beta_{sp}\rvert$**	**Presence at Earth's Magnetopause**
Magnetosheath	~20	0.05 – 0.10	~20	0.80[b]	-	Always
Plasma sheet	< 1	10's	50	0.16	0.64	Always
Plasma sheet plus warm plasma cloak / heated plasmaspheric material	~1's	~0.1 – 1.0	50	0.016 – 0.16	0.48 – 0.62	50 – 70% of the time in the dawn sector
Plasma sheet plus plasmaspheric plume	~10's	~0.001 – 0.01	50	1.6×10^{-3}	0.64	20 - 25% of the time in the dusk sector
Plasma sheet plus detached plasmaspheric material	~ 1	~0.001 – 0.01	50	1.6×10^{-5}	0.64	> 80% of the time in the dusk sector

[a]Nominal magnetic field strength observed in the subsolar magnetosheath and in the Earth's outer magnetosphere near the subsolar magnetopause

[b]Most probable magnetosheath β given typical magnetosheath conditions (*Cassak and Fuselier*, 2016)

[c]For calculating β in the magnetosphere, 50 nT is used for the magnetic field strength. Values used for "cold", "warm", and "hot" temperatures are 1 eV, 100 eV to 1 keV, and 10 keV, respectively. Values used for "dense", "moderately dense", and "tenuous" densities are 10 cm^{-3}, 1 cm^{-3}, and 0.1 cm^{-3}, respectively.

4.6 Summary of cold and heavy ionospheric ions effects on magnetic reconnection

Plasma sheet ions (mainly H^+, with number densities < 1 cm^{-3} and temperatures of ones to tens of keV) are present both at the dayside magnetopause and in the magnetotail, and their origin is both the solar wind and the ionosphere, with variable contributions depending on solar and geomagnetic activity. The contribution of each source to the plasma sheet is still subject of debate and we discuss it in Section 5. In addition to plasma sheet ions, cold and heavy ionospheric outflows, detached plasmaspheric material and the WPC populations can also be present at the reconnection regions (cf. Sections 2.1 and 2.2). Section 4 has focused on reviewing the effects of these cold and heavy ionospheric-originating populations in magnetic reconnection.

Cold and heavy ionospheric ions are often present and have non-negligible contributions to the mass density in the two key reconnecting regions: the dayside magnetopause and the magnetotail. These ionospheric ions mass-load the reconnecting flux tubes, and locally reduce the reconnection efficiency. This reduction is estimated to be significant (>20 %) mainly during storm times, when the production of detached plasmasphere material and WPC is larger (Fuselier et al., 2017, 2019a, 2020b). There is also indirect evidence, using geomagnetic indices, of global reduction of the coupling to the solar wind when large amounts of ionospheric ions are present at the magnetopause, i.e., during storm times (Borovsky et al. 2013).

In addition, cold and heavy ionospheric ions introduce multiple spatial and time scales into the reconnection process, owing to the dependence of gyroradius and gyrofrequency on temperature and particle mass. A large set of microphysical effects, including multiple-scale IDRs, wave-particle interactions, etc. are enabled by these multiple ion populations. One then may think that the effective aspect ratio of the diffusion region and the energy conversion mechanisms are changed, resulting in modified reconnection efficiencies. However, according to recent PIC simulations, cold ions do not significantly modify the normalized reconnection rate once a steady state has been reached (Divin et al., 2016, Dargent et al. 2017, 2020). The reconnection rate, on average, may be set by MHD constraints, as suggested by Liu et al. (2017), when no other large-scale forcing acts over the process. A key question is when and for how long magnetic reconnection reaches steady state at the magnetopause. On the other hand, O^+ may not have time to reach steady state in magnetotail reconnection, resulting in a modified reconnection efficiency (Tenfjord et al. 2019). Another key question is to what extent the local properties (MHD and microphysics) of the reconnecting boundary can control the global efficiency of solar wind - magnetosphere coupling versus the global forcing driven by the solar wind (cf. Section 4.1.3).

There is direct evidence that cold and heavy ions are heated and accelerated by reconnection in the tail and the dayside magnetopause, and therefore they take a portion of the energy budget of reconnection. Toledo-Redondo et al. (2017), based on four case studies, found that cold ions take 10 – 25 % of the energy that goes into ion heating. However, statistical studies of the energy budget at the magnetopause and magnetotail accounting for ionospheric ions have not been conducted.

Along with effects on the local microphysics of magnetic reconnection, the presence of cold and heavy ionospheric-originating ions can affect dynamics on a more global scale in the magnetosphere. In the magnetotail, it was predicted that the tearing instability threshold should be reduced by the presence of O^+ (Baker et al., 1982), favoring the onset of magnetic reconnection. However, spacecraft observations have found that fewer substorms are observed when the magnetotail is loaded with O^+ (Liu et al., 2013).

For the dayside, ionospheric-originating ions can alter local, and possibly global, conditions required for reconnection to occur. The dayside magnetopause is typically asymmetric, with shocked solar wind on one side and magnetospheric plasma on the other. If $\Delta\beta$ is large across the reconnecting boundary, then magnetic reconnection can be suppressed by the diamagnetic drift. Based on theoretical computations using average magnetosheath conditions, it is expected that the WPC ions will facilitate magnetic reconnection to proceed at the dayside magnetopause at smaller IMF clock angles by reducing $\Delta\beta$. More work and observations are needed to further our understanding of the complex cross-scale dynamics resulting from the presence of ionospheric-originating ion populations at reconnection sites.

5 Remaining issues and open questions

We list below what we consider the most outstanding open questions inferred from this review work, related to ionospheric-originating ions in the magnetosphere and their effects on magnetic reconnection. Table 4 summarizes these open questions, grouped in two categories.

5.1 What is the relative contribution of solar wind versus ionospheric-originating H^+ to the magnetosphere?

The sources of magnetospheric plasma at all energies are the ionosphere and the solar wind. Because the dominant ion population in the magnetosphere is H^+, and H^+ comes from both the ionosphere and the solar wind, we cannot directly determine the origin of the H^+ in the magnetosphere: it all looks the same. Separating the sources can be done using the minor ion composition (e.g., Kistler, 2020), or using modeling (e.g., Glocer et al., 2020). It is well documented that the ionospheric source becomes

dominant during southward IMF periods associated with increased geomagnetic activity. Overall, the relative contributions of the ionosphere and the solar wind are estimated to be of the same order of magnitude, but precise quantitative knowledge of the relative contributions is missing. Global modelling is the most straightforward method to discriminate the origin of H^+, but these models are challenging because they need to account for many processes occurring at very different scales.

5.2 How is the plasma sheet formed?

The plasma sheet boundary layer is a key transition region in which the inflowing lobe ions from the ionosphere enter the plasma sheet region and are energized to become part of it. The lobe ions (eV to hundreds of eV) are energized to the 1 - 10 keV energies typically observed in the plasma sheet, which contains remnants of solar wind and energized polar wind ions from earlier time periods, as well as from more distant places down the magnetotail. It is this changing mix that sets the stage for the reconnection that is observed. MMS measurements across the plasma sheet boundary layer between the lobes and the neutral sheet can show us how this takes place. Model trajectories combined with differential measurement capabilities can show how the plasma sheet is created.

5.3 Does the variable magnetospheric density affect the global coupling with the solar wind efficiency?

Solar wind - magnetosphere coupling via magnetic reconnection depends mostly on solar wind parameters, in particular the orientation of the IMF, but mass density and magnetic field magnitude also affect the efficiency of the coupling. The magnetospheric mass density at the magnetopause depends on the time history of the magnetosphere. It is not clear to what extent the magnetospheric forcing in general, and the ionospheric source in particular, can exert control of the efficiency of the coupling. Recent modelling (cf. Section 4.1.3) suggests that for a moderate variation of magnetospheric conditions at the magnetopause the system can respond and the efficiency is defined by solar wind parameters. On the other hand, for large mass density changes on the magnetospheric side of the magnetopause, the coupled system efficiency can be modified. Further modelling in this direction, in connection with large statistical surveys of available space and ground datasets may help improving our understanding of what controls the reconnection efficiency between the solar wind and the magnetosphere.

5.4 How do the microphysics introduced by multiple ion populations change magnetic reconnection at MHD scales?

Recent spacecraft observations have shown that several changes are produced at kinetic scales of magnetic reconnection when multiple ion populations are present. These changes include for instance the generation of ion-ion instabilities or modification of the ion diffusion region. However, recent simulations indicate that these changes by themselves seem not to affect the reconnection efficiency, once a steady-state is reached. How magnetic reconnection self-arranges at fluid scales and how the information of the processes at kinetic scales is transferred to these fluid scales remains a mystery. PIC models of magnetic reconnection are a very powerful tool to improve our understanding on how the system self-arranges at system scales under the presence of multiple ion populations..

5.5 Does the WPC alter the suppression of magnetic reconnection?

As discussed in Section 4.5, the warm plasma cloak can reduce the difference in plasma beta between the two sides of the dayside magnetopause, and this may facilitate magnetic reconnection to proceed under smaller **B** field clock angles. This reasoning comes from the current understanding of analytical theory of magnetic reconnection, but this hypothetical effect of the WPC has not been shown. Global modelling of the magnetosphere including the WPC population can be used to test this effect. In

addition, performing statistics of local observations of the flank magnetopause, where this effect should be more pronounced, in the SW parameter space can also help understanding the relative importance of the WPC in altering the suppression of reconnection.

5.6 Which portion of the reconnection energy is taken by cold and heavy ions?

When cold and heavy ions of ionospheric origin are present in the reconnection region, they are both accelerated and heated. Therefore they take a portion of the converted magnetic energy by reconnection, although there exists no quantification on how the available magnetic energy is partitioned among the various ion and electron populations. The heating mechanisms and their relative importance are not well understood, and hence is difficult to include them in modelling. On the other hand, performing statistics on spacecraft observations of heated cold ions at the magnetopause is achievable with current datasets.

5.7 What are the effects of cold electrons in magnetic reconnection?

There is observational evidence that the cold ion populations in the magnetosphere are accompanied by cold electrons. The possible effects of this cold electron population to magnetic reconnection or the magnetospheric dynamics has not been widely addressed. However, these electrons are challenging to measure, because they are often intermixed with spacecraft-originating photoelectrons, and new instrumentation capable of adequately resolving the velocity distribution function of cold electrons may be required.

5.8 How ionospheric ions in the plasma sheet condition the onset of magnetic reconnection?

During disturbed times, the mass density of the magnetotail is usually dominated by O^+. The presence of such heavy ions should reduce the tearing instability threshold and therefore facilitate the onset of magnetic reconnection. However, various observational studies seem to indicate the contrary, i.e. that reconnection becomes more difficult to trigger reconnection when O^+ is present (cf. Section 4.4). How ionospheric ions modify the onset of reconnection and therefore affect the driving storms and substorms remains not well understood. More reconnection modelling including multiple ion populations can help understanding the role of the ionospheric source.

Table 4. Summary of open questions in the role of ionospheric ions and magnetic reconnection in the magnetosphere

Global magnetospheric dynamics	What is the relative contribution of solar wind versus ionospheric-originating H^+ to the magnetosphere?
	How is the plasma sheet formed?
	Does the variable magnetospheric density affect the global coupling with the solar wind efficiency?
Kinetic physics of magnetic reconnection	How do the microphysics introduced by multiple ion populations change reconnection at MHD scales?
	Does the WPC alter the suppression of magnetic reconnection?
	Which portion of the reconnection energy is taken by cold and heavy ions?
	What are the effects of cold electrons in magnetic reconnection?
	How ionospheric ions in the plasma sheet condition the onset of magnetic reconnection?

6 Summary and concluding remarks

The ionosphere is a prime source of particles for the magnetosphere. The polar wind is constantly outflowing at mid and high latitudes, creating low-energy (eV to tens of eV), light ion populations (H^+ and He^+). At high latitudes, additional energy sources such as waves in the cusp and auroral oval, create more energetic (hundreds of eV) outflows, that include O^+ in addition to light ions. These outflowing ions travel along the magnetic field lines and are convected together with them. Depending on the solar wind IMF orientation, which drives the convection, the initial parallel velocity of the outflowing ions, and their starting latitude and longitude location in the ionosphere, they will end up in the magnetotail, in the outer dayside magnetosphere, or will be trapped in the inner plasmasphere. Each of these paths may result in various energization levels, and the outflows will become part of the plasma sheet, the ring current, the plasmasphere, or the warm plasma cloak. Most of these ions do not return to the ionosphere, and escape the magnetosphere at an average rate of ~10^{26} ions/s.

Magnetic reconnection takes place at the dayside magnetopause and in the magnetotail, is responsible for the coupling of the magnetosphere to the solar wind, drives storms and substorms, as well as magnetospheric convection, and supplies magnetic energy that is converted to kinetic and thermal energies of the particle populations. Near the magnetopause, the magnetospheric mass density is composed of plasma sheet ions (keV to tens of keV) of both solar wind and ionospheric origin, plus various colder populations (eV to hundreds of eV) of ionospheric origin. The magnetospheric mass density near the magnetopause is variable and dominated by the ionospheric source, although this density is usually smaller than the solar wind density on the other side of the magnetopause. In the tail, the near-Earth plasma sheet mass density is dominated by the ionospheric source all the time. In the distant tail, the ionospheric source becomes dominant during active magnetospheric times. During periods of southward IMF, which are associated to increased geomagnetic activity, more ionospheric-originating ions are found at the magnetopause and in the plasma sheet. These variable contributions to the plasma in the reconnecting regions modulate how reconnection proceeds. Additional mass reduces the rate of magnetic energy conversion at the dayside. In addition, a number of kinetic effects are introduced by the different masses and temperatures of the ionospheric-originating ion populations. For instance, waves are generated by ion-ion instabilities in the reconnection regions, which heat the ions. Cold ions have smaller intrinsic spatial scales (gyroradius), and therefore set different ion diffusion regions. In addition, they can remain magnetized inside the separatrices of reconnection, modifying the

perpendicular currents associated with this region. Heavy ions have larger intrinsic time scales (gyrofrequency), and may not be able to follow the intermittent and bursty evolution of magnetic reconnection in the tail.

The complexity of the magnetospheric system and its dynamics is enormous. Our knowledge has been growing significantly since satellite missions enabled in-situ and remote measurements of it, and with the aid of computer simulations. We now understand that the ionospheric source is a major supplier of plasma and that the variability of this source affects magnetic reconnection in various ways. However, there still remain open questions, in particular about how the system responds to this variability in a global sense.

Acknowledgments, Samples, and Data

The discoverer of energetic O^+ and He^+ of ionospheric origin in the magnetosphere, Dr. Edward G. Shelley, passed away in 2020. This review paper is dedicated to his enduring legacy. We are grateful to the International Space Science Institute (ISSI), who made possible this review by funding the international team *Cold plasma of ionospheric origin in the Earth's magnetosphere*. Data were not used, nor created for this research.

References

Akasofu, S. I. (2015). Paradigm transitions in solar–terrestrial physics from 1900: my personal view. *History of Geo-and Space Sciences*, *6*(1), 23-43.

Alm, L., M. André, D. B. Graham, Y. V. Khotyaintsev, A. Vaivads, C. R. Chappell, et al. (2019). MMS Observations of Multiscale Hall Physics in the Magnetotail. *Geophysical Research Letters*, pp. 1–10, doi:10.1029/2019gl084137.

Alm, L., M. André, A. Vaivads, Y. V. Khotyaintsev, R. B. Torbert, J. L. Burch, et al. (2018). Magnetotail hall physics in the presence of cold ions. *Geophysical Research Letters*, 45(20), 10,941–10,950, doi:10.1029/2018GL079857.

André, M., and C. M. Cully (2012). Low-energy ions: A previously hidden solar system particle population. *Geophysical Research Letters*, 39(3), doi:10.1029/2011GL050242.

André, M., K. Li, and A. I. Eriksson (2015). Outflow of low-energy ions and the solar cycle. Journal of *Geophysical Research: Space Physics*, 120(2), 1072–1085, doi:10.1002/2014JA020714.

André, M., W. Li, S. Toledo-Redondo, Y. V. Khotyaintsev, A. Vaivads, D. B.Graham, et al. (2016). Magnetic reconnection and modification of the Hall physics due to cold ions at the magnetopause. *Geophysical Research Letters*, 43(13), 6705–6712, doi:10.1002/2016GL069665.

André, M., S. Toledo-Redondo and A. W. Yau (2020). Cold ionospheric ions in the magnetosphere, Space Physics and Aeronomy Collection Volume 2: Magnetospheres in the Solar System, Geophysical Monograph 259, First Edition. Published 2021 by John Wiley & Sons. DOI: 10.1002/9781119507512

André, M., and A. Yau (1997). Theories and Observations of Ion Energization and Outflow in the High Latitude Magnetosphere, *Space Science Reviews*, 80, 27–48, doi: 10.1023/A:1004921619885.

André, M., Vaivads, A., Khotyaintsev, Y. V., Laitinen, T., Nilsson, H., Stenberg, G., et al. (2010). Magnetic reconnection and cold plasma at the magnetopause. *Geophysical research letters*, *37*(22).

Aunai, N., Belmont, G., & Smets, R. (2011). Proton acceleration in antiparallel collisionless magnetic reconnection: Kinetic mechanisms behind the fluid dynamics. *Journal of Geophysical Research: Space Physics*, 116 (A9). doi: 10.1029/2011ja016688.

2031 Axford, W. I. (1968). The polar wind and the terrestrial helium budget. *Journal of Geophysical*
2032 *Research*, *73*(21), 6855-6859.
2033 Bagenal, F., P. A. and Delamere (2011). Flow of mass and energy in the magnetospheres of Jupiter and
2034 Saturn. Journal of *Geophysical Research*, *116*, A05209, doi:10.1029/2010JA016294.
2035 Baker, D. N., Hones Jr, E. W., Young, D. T., & Birn, J. (1982). The possible role of ionospheric oxygen in
2036 the initiation and development of plasma sheet instabilities. *Geophysical Research Letters*, *9*(12),
2037 1337-1340.
2038 Banks, P. M., and Holzer, T. E. (1968). The polar wind. *Journal of Geophysical Research*, *73*(21), 6846-
2039 6854.
2040 Banks, P. M., Nagy, A. F., & Axford, W. I. (1971). Dynamical behavior of thermal protons in the mid-
2041 latitude ionosphere and magnetosphere, *Planetary and Space Science*, *19*(9), 1053-1067.
2042 Barakat, A. R., and Schunk, R. W. (2006). A three-dimensional model of the generalized polar
2043 wind. *Journal of Geophysical Research: Space Physics*, *111*(A12).
2044 Baumjohann, W., G. Paschmann, and C. A. Cattell (1989). Average plasma properties in the central
2045 plasma sheet. Journal of *Geophysical Research: Space Physics*, *94*(A6), 6597-6606.
2046 Benson, R. F. (2010). Four decades of space-born radio sounding, *Radio Science Bulletin*, 333(13), 6705–
2047 6712, doi:10.1002/2016GL069665.
2048 Berube, D., M. B. Moldwin, S. F. Fung, and J. L. Green (2005). A plasmaspheric mass density model and
2049 constraints on its heavy ion concentration. Journal of *Geophysical Research*, 110, A04212,
2050 doi:10.1029/2004JA010684.
2051 Bessho, N., L.-J. Chen, and M. Hesse (2016). Electron distribution functions in the diffusion region of
2052 asymmetric magnetic reconnection. *Geophysical Research Letters*, 43(5), 1828–1836,
2053 doi:10.1002/2016GL067886,2016GL067886.
2054 Birn, J., Runov, A., & Zhou, X.-Z. (2017). Ion velocity distributions in dipolarization events: Distributions in
2055 the central plasma sheet. *Journal of Geophysical Research: Space Physics*, 122 (8), 8014-8025,
2056 doi:10.1002/2017ja024230.
2057 Birn, J., G. Yur, H. U. Rahman, and S. Minami (1992). On the termination of the closed field line region of
2058 the magnetotail. Journal of *Geophysical Research*, 97, 14,833, doi:10.1029/92JA01145
2059 Birn, J., Drake, J. F., Shay, M. A., Rogers, B. N., Denton, R. E., Hesse, M., et al. (2001). Geospace
2060 Environmental Modeling (GEM) magnetic reconnection challenge. *Journal of Geophysical*
2061 *Research: Space Physics*, *106*(A3), 3715-3719.
2062 Borovsky, J. E. (2008). The rudiments of a theory of solar wind/magnetosphere coupling derived from
2063 first principles. *Journal of Geophysical Research: Space Physics*, *113*(A8).
2064 Borovsky, J. E. (2013). Physical improvements to the solar wind reconnection control function for the
2065 Earth's magnetosphere. *Journal of Geophysical Research: Space Physics*, *118*(5), 2113-2121.
2066 Borovsky, J. E., and Birn, J. (2014). The solar wind electric field does not control the dayside
2067 reconnection rate. *Journal of Geophysical Research: Space Physics*, *119*(2), 751-760.
2068 Borovsky, J. E., and M. H. Denton (2006). Differences between CME-driven storms and CIR-driven
2069 storms. Journal of *Geophysical Research*,111(A7),A07S08, doi:10.1029/2005JA011447.7
2070 Borovsky, J. E., and M. H. Denton (2008). A statistical look at plasmaspheric drainage plumes. Journal of
2071 *Geophysical Research*, 113, A09221, doi:10.1029/2007JA012994.
2072 Borovsky, J. E., Denton, M. H., Denton, R. E., Jordanova, V. K., & Krall, J. (2013). Estimating the effects of
2073 ionospheric plasma on solar wind/magnetosphere coupling via mass loading of dayside

reconnection: Ion-plasma-sheet oxygen, plasmaspheric drainage plumes, and the plasma cloak. *Journal of Geophysical Research: Space Physics*, *118*, 5695–5719. doi:10.1002/jgra.50527

Borovsky, J. E., Thomsen, M. F., McComas, D. J., Cayton, T. E., and Knipp, D. J. (1998). Magnetospheric dynamics and mass flow during the November 1993 storm. *Journal of Geophysical Research: Space Physics*, 103, A11, 26,373-26,394.

Bouhram, M., Klecker, B., Miyake, W., Reme, H., Sauvaud, J. A., Malingre, M., et al., (2004). On the altitude dependence of transversely heated O+ distributions in the cusp/cleft. In *Annales Geophysicae*, 22(5), 1787-1798.

Brace, L. H. (2013). Langmuir Probe Measurements in the Ionosphere, pp. 23–35, American Geophysical Union (AGU), doi:10.1029/GM102p0023.

Brambles, O. J., Lotko, W., Damiano, P. A., Zhang, 1., Wiltberger, M. and Lyon, J. (2010). Effects of causally driven cusp O+ outflow on the storm time magnetosphere-ionosphere system using a multifluid global simulation. Journal of *Geophysical Research: Space Physics*, *115*(A9).

Brambles, O. J., Lotko, W., Zhang, B., Ouellette, J., Lyon, J., and Wiltberger, M. (2013). The effects of ionospheric outflow on ICME and SIR driven sawtooth events. *Journal of Geophysical. Research: Space Physics*, 118, 6026– 6041, doi:10.1002/jgra.50522.

Burch, J. L., Ergun, R. E., Cassak, P. A., Webster, J. M., Torbert, R. B., Giles, B. L., et al. (2018). Localized oscillatory energy conversion in magnetopause reconnection. *Geophysical Research Letters*, 45, 1237–1245

Burch, J. L., R. B. Torbert, T. D. Phan, L.-J. Chen, T. E. Moore, R. E.Ergun, et al. (2016). Electron-scale measurements of magnetic reconnection in space, *Science*, doi:10.1126/science.aaf2939.

Carpenter, D. L., Giles, B. L., Chappell, C. R., Decreau, P. M. E., Anderson, R. R., Persoon, A. M. et al. (1993). Plasmasphere dynamics in the duskside bulge region: A new look at an old topic. Journal of *Geophysical Research,* 98, 19253-19271.

Cassak, P.A., and S. A. Fuselier (2016). Reconnection at Earth's Dayside Magnetopause, in *Magnetic Reconnection*, Astrophysics and Space Science Library, **427**, edited by W. Gonzalez and E. Parker, Springer, Cham, Switzerland, doi:10.1007/978-3-319-26432-5_6.

Cassak, P. a., and M. a. Shay (2007). Scaling of asymmetric magnetic reconnection: General theory and collisional simulations, *Physics of Plasmas*, 14(10), 102,114, doi:10.1063/1.2795630.

Cassak, P. A., Liu, Y. H., and Shay, M. A. (2017). A review of the 0.1 reconnection rate problem. *Journal of Plasma Physics*, *83*(5).

Chappell, C. R. (1972). Recent satellite measurements of the morphology and dynamics of the plasmasphere. *Reviews of Geophysics*, *10*(4), 951-979.

Chappell, C. R. (1974). Detached plasma regions in the magnetosphere. *Journal of Geophysical Research*, *79*(13), 1861-1870.

Chappell, C. R. (1988). The terrestrial plasma source: A new perspective in solar-terrestrial processes from Dynamics Explorer. *Reviews of Geophysics*, *26*(2), 229-248.

Chappell, C. R. (2015). The role of the ionosphere in providing plasma to the terrestrial magnetosphere—an historical overview. *Space Science Reviews*, 192, 5-25.

Chappell, C. R., C. R. Baugher, and J. L. Horwitz (1980). *New advances in thermal plasma research*.

Chappell, C. R., Harris, K. K., & Sharp, G. W. (1971). The dayside of the plasmasphere. *Journal of Geophysical Research*, *76*(31), 7632-7647.

2116 Chappell, C. R., Huddleston, M. M., Moore, T. E., Giles, B. L., & Delcourt, D. C. (2008). Observations of
2117 the warm plasma cloak and an explanation of its formation in the magnetosphere. *Journal of*
2118 *Geophysical Research: Space Physics*, *113*(A9).

2119 Chappell, C. R., Moore, T. E., & Waite Jr, J. H. (1987). The ionosphere as a fully adequate source of
2120 plasma for the Earth's magnetosphere. *Journal of Geophysical Research: Space Physics*, *92*(A6),
2121 5896-5910.

2122 Chen, S. H., and Moore, T. E. (2006). Magnetospheric convection and thermal ions in the dayside outer
2123 magnetosphere. *Journal of Geophysical Research: Space Physics*, *111*(A3).

2124 Cladis, J. B., H. L. Collin, O. W. Lennartsson, T. E. Moore, W. K. Peterson, and C. T. Russel (2000).
2125 Observations of centrifugal acceleration during compression of magnetosphere. *Geophysical*
2126 *Research Letters*, 27, 915, doi:10.1029/1999GL010737

2127 Craven, P. D., Gallagher, D. L., & Comfort, R. H. (1997). Relative concentration of He+ in the inner
2128 magnetosphere as observed by the DE 1 retarding ion mass spectrometer. *Journal of Geophysical*
2129 *Research: Space Physics*, *102*(A2), 2279-2289.

2130 Cohen, C. S., A. B. Galvinl, F. M. Ipavich, Y. Kol, A. T. Y. Lui, R. A.Lundgrenl, R. W. Mcentire, and D. J.
2131 Williams (1998). Concurrent obser-vations of solar wind oxygen by Geotail in the magnetosphere
2132 and Windin interplanetary space. *Geophysical Research Letters*, 25(15), 2987–2990.

2133 Collin, H. L., Peterson, W. K., Lennartsson, O. W., & Drake, J. F. (1998). The seasonal variation of auroral
2134 ion beams. *Geophysical research letters*, *25*(21), 4071-4074.

2135 Comfort, R. H. (1998): The Magnetic Mirror Force in Plasma Fluid Models, in Modeling Magnetospheric
2136 Plasma, Volume 44, AGU Geophysical Monograph Series, eds T. E. Moore, J. H. Waite Jr., T. W.
2137 Moorehead, W. B. Hanson, doi:10.1029/GM044p0051

2138 Comisso, L., and A. Bhattacharjee (2016). On the value of thereconnection rate*, Journal of Plasma*
2139 *Physics*, 82(6), 1–10, doi:10.1017/S002237781600101X.

2140 Cully, C. M., E. F. Donovan, A. W. Yau, and G. G. Arkos (2003). Akebono/Suprathermal Mass
2141 Spectrometer observations of low-energy ion outflow: Dependence on magnetic activity and solar
2142 wind conditions. *Journal of Geophysical Research:(Space Physics*, 108, 1093,
2143 doi:10.1029/2001JA009200.

2144 Daglis, I. A., Sarris, E. T., & Kremser, G. (1990). Indications for ionospheric participation in the substorm
2145 process from AMPTE/CCE observations. *Geophysical research letters*, *17*(1), 57-60.

2146 Daly, P. W. (1986). Structure of the distant terrestrial magnetotail, Adv. Space Res., 6, 245.
2147 doi:10.1016/0273-1177(86)90041-4

2148 Dandouras, I. (2013). Detection of a plasmaspheric wind in the Earth's magnetosphere by the Cluster
2149 spacecraft. *Annales Geophysicae, 0992768)*, *31*(7).

2150 Dargent, J., N. Aunai, B. Lavraud, S. Toledo-Redondo, and F. Califano(2019). Signatures of Cold Ions in a
2151 Kinetic Simulation of the Reconnecting Magnetopause. Journal of *Geophysical Research: Space*
2152 *Physics*, 124(4), 2497–2514, doi:10.1029/2018JA026343.

2153 Dargent, J., N. Aunai, B. Lavraud, S. Toledo-Redondo, and F. Califano (2020). Simulation of plasmaspheric
2154 plume impact on dayside magnetic reconnection. *Geophysical Research Letters*,
2155 doi:10.1029/2019GL086546.8

2156 Dargent, J., N. Aunai, B. Lavraud, S. Toledo-Redondo, M. A. Shay, P. A.Cassak, and K. Malakit (2017).
2157 Kinetic simulation of asymmetric magnetic reconnection with cold ions, *Journal of Geophysical*
2158 *Research: SpacePhysics*, 122(5), 5290–5306, doi:10.1002/2016JA023831.

2159 Delcourt, D. C., Chappell, C. R., Moore, T. E., & Waite Jr, J. H. (1989). A three-dimensional numerical
2160 model of ionospheric plasma in the magnetosphere. *Journal of Geophysical Research: Space*
2161 *Physics*, *94*(A9), 11893-11920.

2162 Delcourt, D. C., J. A. Sauvaud, T. E. Moore (1993). Polar wind ion dynamics in the magnetotail. Journal of
2163 *Geophysical Research: Space Physics*, *98*(A6), 9155-9169.

2164 Denton, M. H., M. G. Henderson, N. Maruyama, and S. A. Fuselier (2019). The cold ion population at
2165 geosynchronous orbit and transport to the dayside magnetopause: September 2015 to February
2166 2016. *Journal of Geophysical Research, 124,* 8685-8694, doi:10.1029/2019JA026973.

2167 Desroche, M., F. Bagenal, P. A. Delamere, and N. Erkaev (2013). Conditions at the magnetopause of
2168 Saturn and implications for the solar wind interaction. Journal of *Geophysical Research: Space*
2169 *Physics*, *118*, 3087– 3095, doi:10.1002/jgra.50294.

2170 Divin, A., Khotyaintsev, Y. V., Vaivads, A., André, M., Toledo-Redondo, S., Markidis, S., & Lapenta, G.
2171 (2016). Three-scale structure of diusion region in the presence of cold ions. *Journal of Geophysical*
2172 *Research: Space Physics*, 121 (12), 12001-12013. doi:10.1002/2016JA023606.

2173 Drake, J. F., Cassak, P. A., Shay, M. A., Swisdak, M., & Quataert, E. (2009a). A magnetic reconnection
2174 mechanism for ion acceleration and abundance enhancements in impulsive flares. *The*
2175 *Astrophysical Journal Letters*, *700*(1), L16.

2176 Drake, J. F., Swisdak, M., Phan, T. D., Cassak, P. A., Shay, M. A., Lepri, et al. (2009b). Ion heating resulting
2177 from pickup in magnetic reconnection exhausts. *Journal of Geophysical Research: Space*
2178 *Physics*, *114*(A5).

2179 Dungey, J.W. (1963). Interactions of solar plasma with the geomagnetic field, Planetary and Space
2180 *Science*, 10, 233-237, doi:10.1016/0032-0633(63)90020-5

2181 Eastwood, J. P., Goldman, M. V., Hietala, H., Newman, D. L., Mistry, R., & Lapenta, G. (2015). Ion
2182 reflection and acceleration near magnetotail dipolarization fronts associated with magnetic
2183 reconnection. *Journal of Geophysical Research: Space Physics*, *120*(1), 511-525.

2184 Engwall, E., A. I. Eriksson, C. M. Cully, M. André, R. Torbert, and H. Vaith (2009). Earth's ionospheric
2185 outflow dominated by hidden cold plasma, *Nature Geoscience*, 2, 24–27, doi:10.1038/ngeo387.

2186 Frank, L. A., K. L. Ackerson, and D. M. Yeager (1977). Observations of Atomic Oxygen (O+) in the Earth's
2187 Magnetotail, *Journal of GeophysicalResearch*, 82(1).

2188 Fuselier, S. A. (2020). Ionospheric Oxygen ions in the dayside magnetosphere. *Journal of Atmospheric*
2189 *and Solar-Terrestrial Physics*, *210*, 105448.

2190 Fuselier, S. A., Burch, J. L., Mukherjee, J., Genestreti, K. J., Vines, S. K., Gomez, R., et al. (2017).
2191 Magnetospheric ion influence at the dayside magnetopause. Journal of *Geophysical Research:*
2192 *Space Physics*, 122, 8617–8631, doi:10.1002/2017JA024515.

Fuselier, S. A., Dayeh, M. A., Galli, A., Funsten, H. O., Schwadron, N. A., Petrinec, S. M., et al. (2020a). Neutral atom imaging of the solar wind-magnetosphere-exosphere interaction near the subsolar magnetopause. *Geophysical Research Letters*, *47*(19), e2020GL089362.

Fuselier, S. A., R. Frahm, R., W. S. Lewis, A. Masters, J. Mukherjee, S. M. Petrinec, and I. J. Sillanpaa, (2014). The location of magnetic reconnection at Saturn's magnetopause: A comparison with Earth. Journal of *Geophysical Research: Space Physics*, *119*, 2563– 2578, doi:10.1002/2013JA019684.

Fuselier, S. A., Haaland, S., Tenfjord, P., Paschmann, G., Toledo-Redondo, S., Malaspina, D., et al. (2020b). High-density magnetospheric He+ at the dayside magnetopause and its effect on magnetic reconnection. *Journal of Geophysical Research: Space Physics*, in press.

Fuselier, S. A., Klumpar, D. M., Peterson, W. K., & Shelley, E. G. (1989). Direct injection of ionospheric O+ into the dayside low latitude boundary layer. *Geophysical Research Letters*, *16*(10), 1121-1124.

Fuselier, S. A., and Lewis, W. S. (2011). Properties of near-Earth magnetic reconnection from in-situ observations. *Space science reviews*, *160*(1-4), 95.

Fuselier, S. A., Mukherjee, J., Denton, M. H., Petrinec, S. M., Trattner, K. J., Toledo-Redondo, S., et al. (2019a). High-density O^+ in Earth's outer magnetosphere and its effect on dayside magnetopause magnetic reconnection. *Journal of Geophysical Research: Space Physics*, *124*. doi:10.1029/ 2019JA027396

Fuselier, S., K. Trattner, S. Petrinec, M. Denton, S. Toledo-Redondo, M. André, et al. (2019b). Mass-loading the Earth's dayside magnetopause boundary layer and its effect on magnetic reconnection. *Geophysical Research Letters*, 3, 6204-6213, doi:10.1029/2019gl082384.

Garcia, K.S., Merkin, V.G. and Hughes, W.J., 2010. Effects of nightside O+ outflow on magnetospheric dynamics: Results of multifluid MHD modeling. *Journal of Geophysical Research: Space Physics*, *115*(A12).

Garcia-Sage, K., Moore, T.E., Pembroke, A., Merkin, V.G. and Hughes, W.J., 2015. Modeling the effects of ionospheric oxygen outflow on bursty magnetotail flows. *Journal of Geophysical Research: Space Physics*, *120*(10), pp.8723-8737.

Garrett, H. B. (1981). The charging of spacecraft surfaces, *Reviews of Geophysics*, 19(4), 577–616, doi:10.1029/RG019i004p00577

Genestreti, K. J., Goldstein, J., Corley, G. D., Farner, W., Kistler, L. M., Larsen, B. A., et al. (2017). Temperature of the plasmasphere from Van Allen Probes HOPE. *Journal of Geophysical Research: Space Physics*, *122*(1), 310-323.

Genestreti, K. J., Nakamura, T. K. M., Nakamura, R., Denton, R. E., Torbert, R. B., Burch, J. L., et al. (2018). How accurately can we measure the reconnection rate EM for the MMS diffusion region event of 11 July 2017?. *Journal of Geophysical Research: Space Physics*, *123*(11), 9130-9149.

George, D. E., & Jahn, J. M. (2020). Energized oxygen in the magnetotail: Current sheet bifurcation from speiser motion. *Journal of Geophysical Research: Space Physics*, *125*(2), e2019JA027339.

Glocer, A., Toth, G. and Fok, M.C., (2018). Including kinetic ion effects in the coupled global ionospheric outflow solution. *Journal of Geophysical Research: Space Physics*, *123*(4), pp.2851-2871.

Glocer, A., Tóth, G., Ma, Y., Gombosi, T., Zhang, J.C. and Kistler, L.M., (2009). Multifluid block-adaptive-tree solar wind roe-type upwind scheme: Magnetospheric composition and dynamics during geomagnetic storms—Initial results. *Journal of Geophysical Research: Space Physics*, *114*(A12).

Glocer, A., Welling, D., Chappell, C. R., Toth, G., Fok, M. C., Komar, C., et al (2020). A case study on the origin of near-Earth plasma. *Journal of Geophysical Research: Space Physics*, e2020JA028205.

Gloeckler, G., & Hamilton, D. C. (1987). AMPTE ion composition results. *Physica Scripta*, *1987*(T18), 73.

Goldstein, J., Sandel, B. R., Thomsen, M. F., Spasojević, M., & Reiff, P. H. (2004). Simultaneous remote sensing and in situ observations of plasmaspheric drainage plumes. *Journal of Geophysical Research: Space Physics*, *109*(A3).

Graham, D. B., Khotyaintsev, Y. V., Norgren, C., Vaivads, A., André, M., Toledo-Redondo, S., et al. (2017a). Lower hybrid waves in the ion diffusion and magnetospheric inflow regions. *Journal of Geophysical Research: Space Physics*, *122*(1), 517-533.

Graham, D. B., Khotyaintsev, Yu. V., Vaivads, A., Norgren, C., André, M., Webster, J. M., et al. (2017b). Instability of agyrotropic electron beams near the electron diffusion region. *Physical Review Letters*, 119(2), 025101.

Grande, M., Perry, C. H., Hall, A., Fennell, J., Nakamura, R., & Kamide, Y. (2003). What is the effect of substorms on the ring current ion population during a geomagnetic storm?. *GMS*, *142*, 75.

Grard, R. J. L. (1973). Properties of the satellite photoelectron sheath derived from photoemission laboratory measurements. Journal of *Geophysical Research,* 78(16), 2885–2906, doi:10.1029/JA078i016p02885

Haaland, S., A. Eriksson, E. Engwall, B. Lybekk, H. Nilsson, A. Pedersen, et al. (2012a): Estimating the capture and loss of cold plasma from ionospheric outflow. *Journal of Geophysical Research*, Vol 117, A7. doi:10.1029/2012JA017679

Haaland, S. E., K. Li, A. Eriksson, M. André, E. Engwall, M. Forster, et al. (2012b). Cold ion outflow as a source of plasma for the magnetosphere, *Geophysical Monograph Series*, 199, 341–353, doi:10.1029/2012GM001317.

Haaland, S. E., K. Svenes, B. Lybekk, and A. Pedersen (2012c). A survey of the polar cap density based on Cluster EFW probe measurements: Solar wind and solar irradiation dependence, doi:10.1029/2011JA017250.

Haaland, S., Paschmann, G., Øieroset, M., Phan, T., Hasegawa, H., Fuselier, S. A., et al, (2020). Characteristics of the flank magnetopause: MMS results. *Journal of Geophysical Research: Space Physics*, *125*(3), e2019JA027623.

Hamilton, D. C., Gloeckler, G., Ipavich, F. M., Wilken, B., & Stuedemann, W. (1988). Ring current development during the great geomagnetic storm of February 1986. *Journal of Geophysical Research*, *93*, 14343–14355, doi:10.1029/JA093iA12p14343

Hesse, M., N. Aunai, D. Sibeck, and J. Birn (2014). On the electron diffusion region in planar, asymmetric, systems. *Geophysical Research Letters*, 41, 8673–8680, doi:10.1002/2014GL061586.

Hesse, M., T. Neukirch, K. Schindler, M. Kuznetsova, and S. Zenitani (2011),The diffusion region in collisionless magnetic reconnection. *Space Science Reviews*, 160(1-4), 3–23, doi:10.1007/s11214-010-9740-1.

Huddleston, M. M., C. R. Chappell, D. C. Delcourt, T. E. Moore, B. L. Giles and M. O. Chandler (2005). An examination of the process and magnitude of ionospheric plasma supply to the magnetosphere. *Journal of Geophysical Research: Space Physics*, *110*(A12).

Jahn, J. M., Goldstein, J., Reeves, G. D., Fernandes, P. A., Skoug, R. M., Larsen, B. A., & Spence, H. E. (2017). The warm plasma composition in the inner magnetosphere during 2012–2015. *Journal of Geophysical Research: Space Physics*, *122*(11), 11-018.

Jahn, J. M., Goldstein, J., Kurth, W. S., Thaller, S., De Pascuale, S., Wygant, J., et al. (2020). Determining Plasmaspheric Density From the Upper Hybrid Resonance and From the Spacecraft Potential: How Do They Compare?. *Journal of Geophysical Research: Space Physics*, *125*(3), e2019JA026860.

2281 Karimabadi, H., V. Roytershteyn, C. G. Mouikis, L. M. Kistler, and W. Daughton (2011). Flushing effect in
2282 reconnection: Effects of minor-ity species of oxygen ions. *Planetary and Space Science*, 59(7),
2283 526–536,doi:10.1016/j.pss.2010.07.014.
2284 Kasahara, S., H. Hasegawa, K. Keika, Y. Miyashita, M. N. Nishino,T. Sotirelis, Y. Saito, and T. Mukai (2008).
2285 Escape of high-energy oxygen ions through magnetopause reconnection under northward IMF,
2286 *Annales Geophysicae*, 26, 3955–3966.9
2287 Kelley, M. C. (2009). *The Earth's ionosphere: plasma physics and electrodynamics*. Academic press.
2288 Kistler, L. M. (2016). The impact of O+ on magnetotail dynamics, In Magnetosphere-ionosphere coupling
2289 in the solar system, doi:10.1002/9781119066880.ch6
2290 Kistler, L. M. (2020). Ionospheric and solar wind contributions to the storm-time near-earth plasma
2291 sheet. *Geophysical Research Letters*, 47, doi :10.1029/2020GL090235
2292 Kistler, L. M., and C. G. Mouikis (2016). The inner magnetosphere ion composition and local time
2293 distribution over a solar cycle. Journal of *Geophysical Research: Space Physics*,121(3), 2009–2032,
2294 doi:10.1002/2015JA021883.
2295 Kistler, L. M., C. Mouikis, E. Moebius, B. Klecker, J. A. Sauvaud, H. Reme, et al. (2005), Contribution of
2296 nonadiabatic ions to the cross-tail current in an O^+ dominated thin current sheet. *Journal of*
2297 *Geophysical Research: Space Physics*,110(A6), doi:10.1029/2004JA010653.
2298 Kistler, L. M., Mouikis, C. G., Spence, H. E., Menz, A. M., Skoug, R. M., Funsten, H. O., et al.(2016). The
2299 source of O+ in the storm time ring current. *Journal of Geophysical Research: Space*
2300 *Physics*, *121*(6), 5333-5349.
2301 Knudsen, D. J., J. K. Burchill, S. C. Buchert, A. I. Eriksson, R. Gill, J.-E. Wahlund, L. Ahlen, M. Smith, and B.
2302 Moffat (2017). Thermal ion imagers and Langmuir probes in the Swarm electric field instruments.
2303 Journal of *Geophysical Research: Space Physics*, 122(2), 2655-2673, doi:10.1002/2016JA022571.
2304 Kolstø, H. M., M. Hesse, C. Norgren, P. Tenfjord, S. F. Spinnangr, and N. Kwagala (2020). Collisionless
2305 Magnetic Reconnection in an Asymmetric Oxygen Density Configuration. *Geophysical Research*
2306 *Letters,*47(1), doi:10.1029/2019gl085359.
2307 Krcelic, P., S. Haaland, L. Maes, R. Slapak, and A. Schillings (2019) Estimating the fate of oxygen ion
2308 outflow from the high altitude cusp. *Annales Geophysicae*, doi:10.5194/angeo-37-125-2019
2309 Kronberg, E. A., Ashour-Abdalla, M., Dandouras, I., Delcourt, D. C., Grigorenko, E. E., Kistler, L. M., et al.
2310 (2014). Circulation of heavy ions and their dynamical effects in the magnetosphere: Recent
2311 observations and models. *Space Science Reviews*, *184*(1-4), 173-235.
2312 Laakso, H., and Pedersen, A. (1998). Ambient electron density derived from differential potential
2313 measurements. *GEOPHYSICAL MONOGRAPH-AMERICAN GEOPHYSICAL UNION*, *102*, 49-54.
2314 Lavraud, B., Dunlop, M. W., Phan, T. D., Reme, H., Bosqued, J. M., Dandouras, et al. (2002). Cluster
2315 observations of the exterior cusp and its surrounding boundaries under northward
2316 IMF. *Geophysical research letters*, *29*(20), 56-1.
2317 Lavraud, B., & Larson, D. E. (2016). Correcting moments of in situ particle distribution functions for
2318 spacecraft electrostatic charging. *Journal of Geophysical Research: Space Physics*, *121*(9), 8462-
2319 8474.
2320 Lavraud, B., H. Rème, M. W. Dunlop, J. M. Bosqued, I. Dandouras, J.-A. Sauvaud, et al. (2005). Cluster
2321 observes the high-altitude cusp region, *Surveys in. Geophysics*, 26, No. 1-3, 135-175,
2322 doi:10.1007/s10712-005-1875-3
2323 Lavraud, B., & Borovsky, J. E. (2008). Altered solar wind-magnetosphere interaction at low Mach
2324 numbers: Coronal mass ejections. *Journal of Geophysical Research: Space Physics*, *113*(A9).

2325 Lee, J. H., Chen, L., Angelopoulos, V., and Thorne, R. M. (2012). THEMIS observations and modeling of
2326 multiple ion species and EMIC waves: Implications for a vanishing He+ stop band. *Journal of*
2327 *Geophysical Research: Space Physics*, *117*(A6).

2328 Lee, J. H., and Angelopoulos, V. (2014). On the presence and properties of cold ions near Earth's
2329 equatorial magnetosphere. *Journal of Geophysical Research: Space Physics*, *119*(3), 1749-1770.

2330 Lee, S. H., Zhang, H., Zong, Q. G., Otto, A., Rème, H., & Liebert, E. (2016). A statistical study of
2331 plasmaspheric plumes and ionospheric outflows observed at the dayside magnetopause. *Journal*
2332 *of Geophysical Research: Space Physics*, *121*(1), 492-506.

2333 Lemaire, J., & Schunk, R. W. (1992). Plasmaspheric wind. *Journal of atmospheric and terrestrial*
2334 *physics*, *54*(3-4), 467-477.

2335 Lennartsson, W. (1989). Energetic (0.1-to 16-keV/e) magnetospheric ion composition at different levels
2336 of solar F10. 7. *Journal of Geophysical Research: Space Physics*, *94*(A4), 3600-3610.

2337 Lennartsson, W., and Sharp, R. D. (1985). Relative contributions of terrestrial and solar wind ions in the
2338 plasma sheet. *Advances in space research*, *5*(4), 411-414.

2339 Lennartsson, W., and E. G. Shelley (1986). Survey of 0.1- to 16-keV/e plasmasheet ion composition.
2340 Journal of *Geophysical Research,* 91, 3061–3076,doi:10.1029/JA091iA03p03061.

2341 Lennartsson, O. W., Klumpar, D. M., Shelley, E. G., & Quinn, J. M. (1993). Experimental investigation of
2342 possible geomagnetic feedback from energetic (0.1 to 16 keV) terrestrial O+ ions in the
2343 magnetotail current sheet. *Journal of Geophysical Research: Space Physics*, *98*(A11), 19443-19454.

2344 Li, Q., Winglee, R. M., Wilber, M., Chen, L., and Parks, G. (2000). The geopause in relation to the plasma
2345 sheet and the low-latitude boundary layer: Comparison between Wind observations and
2346 multifluid simulations. Journal of *Geophysical Research*, 105(A2), 2563– 2587,
2347 doi:10.1029/1999JA900369.

2348 Li, W. Y., Andre, M., Khotyaintsev, Y. V., Vaivads, A., Fuselier, S. A., Graham, D. B., . . . Burch, J. (2017).
2349 Cold ionospheric ions in the magnetic reconnection outflow region. *Journal of Geophysical*
2350 *Research: Space Physics*, 122 (10), 10,194-10,202. doi: 10.1002/2017ja024287.

2351 Li, W. Y., Graham, D. B., Khotyaintsev, Y. V., Vaivads, A., André, M., Min, K., et al. (2020). Electron
2352 Bernstein waves driven by electron crescents near the electron diffusion region. *Nature*
2353 *Communications*, 11(1), 141.

2354 Li, K., Haaland, S., Eriksson, A., André, M., Engwall, E., Wei, Y., ... & Ren, Q. Y. (2013). Transport of cold
2355 ions from the polar ionosphere to the plasma sheet. *Journal of Geophysical Research: Space*
2356 *Physics*, *118*(9), 5467-5477.

2357 Liang, H., Ashour-Abdalla, M., Lapenta, G., & Walker, R. J. (2016). Oxygen impacts on dipolarization
2358 fronts and reconnection rate. *Journal of Geophysical Research: Space Physics*, *121*(2), 1148-1166.

2359 Liang, H., Lapenta, G., Walker, R. J., Schriver, D., El-Alaoui, M., & Berchem, J. (2017). Oxygen acceleration
2360 in magnetotail reconnection. *Journal of Geophysical Research: Space Physics*, *122*(1), 618-639.

2361 Liao, J., Cai, X., Kistler, L. M., Clauer, C. R., Mouikis, C. G., Klecker, B., & Dandouras, I. (2014). The
2362 relationship between sawtooth events and O+ in the plasma sheet. *Journal of Geophysical*
2363 *Research: Space Physics*, *119*(3), 1572–1586. http://doi.org/10.1002/2013JA019084

2364 Liao, J., Kistler, L. M., Mouikis, C. G., Klecker, B., Dandouras, I., & Zhang, J. C. (2010). Statistical study of
2365 O+ transport from the cusp to the lobes with Cluster CODIF data. *Journal of Geophysical Research:*
2366 *Space Physics*, *115*(A12).

2367 Liao, J., Kistler, L. M., Mouikis, C. G., Klecker, B., & Dandouras, I. (2012). Solar cycle dependence of the
2368 cusp O+ access to the near-Earth magnetotail. *Journal of Geophysical Research: Space*
2369 *Physics*, *117*(A10).

2370 Liao, J., Kistler, L. M., Mouikis, C. G., Klecker, B., & Dandouras, I. (2015). Acceleration of O+ from the cusp
2371 to the plasma sheet. *Journal of Geophysical Research: Space Physics*, *120*(2), 1022-1034.

2372 Liemohn, M. W., Moore, T. E., & Craven, P. D. (2007). Geospace activity dependence of cold, streaming
2373 ions in the near-Earth magnetotail. *Journal of atmospheric and solar-terrestrial physics*, *69*(1-2),
2374 135-141.

2375 Lindstedt, T., Y. V. Khotyaintsev, A. Vaivads, M. André, H. Nilsson, and M. Waara (2010). Oxygen
2376 energization by localized perpendicular electric fields at the cusp boundary. *Geophysical Research*
2377 *Letters*, 37, L09103, doi:10.1029/ 2010GL043117.

2378 Liu, Y., Kistler, L. M., Mouikis, C. G., Klecker, B., & Dandouras, I. (2013). Heavy ion effects on substorm
2379 loading and unloading in the Earth's magnetotail. *Journal of Geophysical Research: Space*
2380 *Physics*, *118*(5), 2101-2112.

2381 Liu, Y. H., & Hesse, M. (2016). Suppression of collisionless magnetic reconnection in asymmetric current
2382 sheets. *Physics of Plasmas*, *23*(6), 060704.

2383 Liu, Y.-H., M. Hesse, P. A. Cassak, M. A. Shay, S. Wang, and L.-J. Chen(2018). On the collisionless
2384 asymmetric magnetic reconnection rate, *Geophysical Research Letters*,45(8), 3311–3318,
2385 doi:10.1002/2017GL076460.

2386 Liu, Y. H., M. Hesse, F. Guo, W. Daughton, H. Li, P. A. Cassak, & M. A. Shay (2017). Why does Steady-
2387 State Magnetic Reconnection have a Maximum Local Rate of Order 0.1?, *Physical Review*
2388 *Letters*,118(8), 1–6,doi:10.1103/PhysRevLett.118.085101.

2389 Liu, Y. H., C. G. Mouikis, L. M. Kistler, S. Wang, V. Roytershteyn, & H. Karimabadi (2015). The heavy ion
2390 diffusion region in magnetic reconnection in the Earth's magnetotail. Journal of *Geophysical*
2391 *Research,*120(5), 3535–3551, doi:10.1002/2015JA020982.

2392 Lopez, R. E. (2016). The integrated dayside merging rate is controlled primarily by the solar wind. *Journal*
2393 *of Geophysical Research: Space Physics*, *121*(5), 4435-4445.

2394 Louarn, P., N. Andre, C. M. Jackman, S. Kasahara, E. A. Kronberg, & M. F. Vogt (2015). Magnetic
2395 Reconnection and Associated Transient Phenomena Within the Magnetospheres of Jupiter and
2396 Saturn, *Space Science. Reviews, 187*, 181–227, doi:10.1007/s11214-014-0047-5.

2397 Lund, E. J., Nowrouzi, N., Kistler, L. M., Cai, X., & Frey, H. U. (2018). On the Role of Ionospheric Ions in
2398 Sawtooth Events. *Journal of Geophysical Research: Space Physics*, *123*(1), 665–684.
2399 http://doi.org/10.1002/2017JA024378

2400 Lybekk, B., A. Pedersen, S. Haaland, K. Svenes, A. N. Fazakerley, A. Masson, M. G. G. T. Taylor, and J.-G.
2401 Trotignon (2012). Solar cycle variations of the Cluster spacecraft potential and its use for electron
2402 density estimations. *Journal of Geophysical Research: Space Physics*, 117, A01217,
2403 doi:10.1029/2011JA016969.

2404 Maggiolo, R., and Kistler, L. M. (2014). Spatial variation in the plasma sheet composition: Dependence
2405 on geomagnetic and solar activity. *Journal of Geophysical Research: Space Physics*, *119*(4), 2836-
2406 2857.

2407 Markidis, S., Lapenta, G., Bettarini, L., Goldman, M., Newman, D., & Andersson, L. (2011). Kinetic
2408 simulations of magnetic reconnection in presence of a background O+ population. *Journal of*
2409 *Geophysical Research: Space Physics*, *116*(A1).

2410 Masters, A., J. P. Eastwood, M. Swisdak, M. F. Thomsen, C. T. Russell, N. Sergis, et al. (2012). The

2411 importance of plasma β conditions for magnetic reconnection at Saturn's magnetopause.
2412 *Geophysical Research Letters*, *39*, L08103, doi:10.1029/2012GL051372.

2413 Moore, T. E., Chandler, M. O., Fok, M. C., Giles, B. L., Delcourt, D. C., Horwitz, J. L., & Pollock, C. J. (2001).
2414 Ring currents and internal plasma sources. *Space Science Reviews*, *95*(1-2), 555-568.

2415 Moore, T. E., C. R. Chappell, M. O. Chandler, P. D. Craven, B. L. Giles, C. J. Pollock, et al. (1997). High-
2416 altitude observations of the polar wind, *Science*, 277, 349–351,
2417 doi:10.1126/science.277.5324.349.

2418 Moore, T.E. and Delcourt, D.C. (1995). The geopause. *Reviews of Geophysics*, *33*(2), pp.175-209.

2419 Moore, T.E., Fok, M. C., Chandler, M. O., Chappell, C. R., Christon, S. P., Delcourt, D. C., et al. (2005).
2420 Plasma sheet and (nonstorm) ring current formation from solar and polar wind sources. *Journal of*
2421 *Geophysical Research: Space Physics*, *110*(A2).

2422 Moore, T. E., and J. L. Horwitz (2007). Stellar ablation of planetary atmospheres, *Reviews of Geophysics*,
2423 45, RG3002, doi:10.1029/2005RG000194.

2424 Mouikis, C. G., Kistler, L. M., Liu, Y. H., Klecker, B., Korth, A., & Dandouras, I. (2010). H+ and O+ content
2425 of the plasma sheet at 15–19 Re as a function of geomagnetic and solar activity. *Journal of*
2426 *Geophysical Research: Space Physics*, *115*(A12).

2427 Nagai, T., Johnson, J. F. E., & Chappell, C. R. (1983). Low-energy (< 100 eV) ion pitch angle distributions in
2428 the magnetosphere by ISEE 1. *Journal of Geophysical Research: Space Physics*, *88*(A9), 6944-6960.

2429 Nagai, T., Fujimoto, M., Saito, Y., Machida, S., Terasawa, T., Nakamura, R., et al. (1998). Structure and
2430 dynamics of magnetic reconnection for substorm onsets with geotail observations. *Journal of*
2431 *Geophysical Research: Space Physics*, 103 (A3), 4419-4440. doi: 10.1029/97ja02190.

2432 Nilsson, H., E. Engwall, A. Eriksson, P. A. Puhl-Quinn, and S. Arvelius (2010). Centrifugal acceleration in
2433 the magnetotail lobes, *Annales Geophysicae*, 28, 569, doi:10.5194/angeo-28-569-2010

2434 Nilsson, H., Waara, M., Marghitu, O., Yamauchi, M., Lundin, R., Reme, H., et al. (2008). An assessment of
2435 the role of the centrifugal acceleration mechanism in high altitude polar cap oxygen ion outflow,
2436 *Annales Geophysicae*, 26, 145, doi: 10.5194/angeo-26-145-2008

2437 Nishida, A., T. Mukai, T. Yamamoto, Y. Saito, and M. Kokubun (1996). Magnetotail convection in
2438 geomagnetically active times, 1. distance to the neutral lines, *Journal of Geophys. Geomagn*., 48,
2439 489, doi:10.5636/jgg.48.489

2440 Nosé, M., Ieda, A., & Christon, S. P. (2009). Geotail observations of plasma sheet ion composition over
2441 16 years: On variations of average plasma ion mass and O+ triggering substorm model. *Journal of*
2442 *Geophysical Research: Space Physics*, *114*(A7).

2443 Ogawa, Y., I. Häggström, S. C. Buchert, K. Oksavik, S. Nozawa, M. Hirahara, et al. (2009). On the source of
2444 the polar wind in the polar top- side ionosphere: First results from the EISCAT Svalbard radar,
2445 *Geophysical Research Letters*, 36, L24103, doi:10.1029/2009GL041501.

2446 Parker, E. N. 1973 The reconnection rate of magnetic fields. *Astrophys. J.* 180, 247.

2447 Peroomian, V. and Ashour-Abdalla, M. (1995). Relative contribution of the solar wind and the auroral
2448 zone to near-Earth plasmas. *GEOPHYSICAL MONOGRAPH-AMERICAN GEOPHYSICAL UNION*, *93*,
2449 pp.213-218.

2450 Peroomian, V., El-Alaoui, M., Abdalla, M.A. and Zelenyi, L.M. (2007). A comparison of solar wind and
2451 ionospheric plasma contributions to the September 24–25, 1998 magnetic storm. *Journal of*
2452 *atmospheric and solar-terrestrial physics*, *69*(3), pp.212-222.

2453 Peterson, W. K., L. Andersson, B. C. Callahan, H. L. Collin, J. D. Scudder, and A. W. Yau (2008). Solar-
2454 minimum quiet time ion energization and outflow in dynamic boundary related coordinates.
2455 *Journal of Geophysical Research: Space Physics*, 113, A07222, doi:10.1029/2008JA013059.
2456 Peterson, W. K., H. L. Collin, O. W. Lennartsson, and A. W. Yau (2006). Quiet time solar illumination
2457 effects on the fluxes and characteristic energies of ionospheric outflow. *Journal of Geophysical*
2458 *Research: Space Physics*, 111, A11S05, doi: 10.1029/2005JA011596.
2459 Phan, T. D., Paschmann, G., Gosling, J. T., Oieroset, M., Fujimoto, M., Drake, J. F., & Angelopoulos, V.
2460 (2013). The dependence of magnetic reconnection on plasma β and magnetic shear: Evidence
2461 from magnetopause observations. *Geophysical Research Letters*, *40*(1), 11-16.
2462 Pollock, C. J., Burch, J. L., Henderson, M. G., Jahn, J. M., Mccomas, D. J., Mende, S. B., et al. (2003). The
2463 role and contributions of energetic neutral atom (ENA) imaging in magnetospheric substorm
2464 research. In *Magnetospheric Imaging—The Image Prime Mission* (pp. 155-182). Springer,
2465 Dordrecht.
2466 Runov, A., Angelopoulos, V., Artemyev, A., Birn, J., Pritchett, P. L., & Zhou, X.-Z. (2017). Characteristics of
2467 ion distribution functions in dipolarizing flux bundle: Event studies. *Journal of Geophysical*
2468 *Research: Space Physics*, 122 (6), 5965-5978. doi: 10.1002/2017ja024010.
2469 Sandel, B. R., J. Goldstein, D. L. Gallagher, and M. Spasojevic (2003). Extreme Ultraviolet Imager
2470 Observations of the Structure and Dynamics of the Plasmasphere. *Space Science Reviews*, 109,
2471 25–46, doi:10.1023/B:SPAC.0000007511.47727.5b.
2472 Sauvaud, J.-A., R. Lundin, H. Rème, J. P. McFadden, C. Carlson, G. K. Parks, et al. (2001). Intermittent
2473 thermal plasma acceleration linked to sporadic motions of the magnetopause, first Cluster results,
2474 *Annales Geophysicae*, 19, doi:10.5194/angeo-19-1523- 2001.
2475 Schillings, A., Slapak, R., Nilsson, H., Yamauchi, M., Dandouras, I., & Westerberg, L. G. (2019). Earth
2476 atmospheric loss through the plasma mantle and its dependence on solar wind parameters. *Earth,*
2477 *Planets and Space*, *71*(1), 1-13.
2478 Schunk, R. W., Raitt, W. J., & Banks, P. M. (1975). Effect of electric fields on the daytime high-latitude E
2479 and F regions. *Journal of Geophysical Research*, *80*(22), 3121-3130.
2480 Schunk, R. W. (2007). Time-dependent simulations of the global polar wind. Journal of *atmospheric and*
2481 *solar-terrestrial physics*, *69*(16), 2028-2047.
2482 Seki, K., Hirahara, M., Hoshino, M., Terasawa, T., Elphic, R. C., Saito, Y., et al, (2003). Cold ions in the hot
2483 plasma sheet of Earth's magnetotail. *Nature*, *422*(6932), 589-592.
2484 Shay, M. A., Drake, J. F., & Swisdak, M. (2007). Two-scale structure of the electron dissipation region
2485 during collisionless magnetic reconnection. *Physical review letters*, *99*(15), 155002.
2486 Shay, M. A., Drake, J. F., Denton, R. E., & Biskamp, D. (1998). Structure of the dissipation region during
2487 collisionless magnetic reconnection. *Journal of Geophysical Research: Space Physics*, 103 (A5),
2488 9165-9176. doi: 10.1029/97ja03528.
2489 Shay, M. A., T. D. Phan, C. C. Haggerty, M. Fujimoto, J. F. Drake,K. Malakit, P. A. Cassak, and M. Swisdak
2490 (2016). Kinetic signatures of the region surrounding the X line in asymmetric (magnetopause)
2491 reconnection. *Geophysical Research Letters*, 43, 4145–4154, doi:10.1002/2016GL069034.
2492 Sheeley, B. W., Moldwin, M. B., Rassoul, H. K., & Anderson, R. R. (2001). An empirical plasmasphere and
2493 trough density model: CRRES observations. *Journal of Geophysical Research: Space*
2494 *Physics*, *106*(A11), 25631-25641.
2495 Shelley, E. G., Johnson, R. G., and R. D. Sharp (1972). Satellite observations of energetic heavy ions
2496 during a geomagnetic storm. Journal of *Geophysical Research: Space Physics*, 77(31), 6104-6110.

Shen, Y., D. J. Knudsen, J. K. Burchill, A. D. Howarth, A. W. Yau, D. M. Miles, H. G. James, G. W. Perry, and L. Cogger (2018). Low-altitude ion heating, downflowing ions, and elf waves in the return current region. *Journal of Geophysical Research: Space Physics*, 123(4), 3087–3110, doi:10.1002/2017JA024955.

Slapak, R., M. Hamrin, T. Pitkänen, M. Yamauchi, H. Nilsson, T. Karlsson, A. Schillings (2017). Quantification of the total ion transport in the near-Earth plasma sheet. *Annales Geophysicae*, Volume 35, Issue 4, 2017, pp.869-877, doi:10.5194/angeo-35-869-2017.

Slapak, R., H. Nilsson, L. G. Westerberg (2015) O+ transport in the dayside magnetosheath and its dependence on the IMF direction, *Annales Geophysicae*, 33(3), 301-307, doi:10.5194/angeo-33-301-2015.

Slapak, R., A. Schillings, H. Nilsson, M. Yamauchi, L.-G. Westerberg, and I. Dandouras (2017). Atmospheric loss from the dayside open polar region and its dependence on geomagnetic activity: implications for atmospheric escape on evolutionary timescales, *Annales Geophysicae*, 35(3), 721–731, doi:10.5194/angeo-35-721-2017.

Spasojevic, M., and Sandel, B. R. (2010). Global estimates of plasmaspheric losses during moderate disturbance intervals. In *Annales Geophysicae*, 28(1), 27-36.

Sorathia, K. A., V. G. Merkin, A. Y. Ukhorskiy, R. C. Allen, K. Nykyri, and S. Wing (2019). Solar wind ion entry into the magnetosphere during northward IMF. *Journal of Geophysical Research: Space Physics*, *124*(7), 5461-5481.

Spinnagr, S. F., Hesse, M., Tenfjord, P. Norgren, C., Kolsto, H. M., Kwagala, N. K., and Jorgensen, T. M. (2020). The micro-macro coupling of mass-loading symmetric magnetic reconnection with cold ions. *Geophysical Research Letters*, submitted.

Strangeway, R. J., R. E. Ergun, Y. J. Su, C. W. Carlson, and R. C. Elphic (2005). Factors controlling ionospheric outflows as observed at intermediate altitudes. *Journal of Geophysical Research,* 110, A03221, doi: 10.1029/2004JA010829

Su, Y.-J., J. L. Horwitz, T. E. Moore, B. L. Giles, M. O. Chandler, P. D. Craven, M. Hirahara, and C. J. Pollock (1998). Polar wind survey with the Thermal Ion Dynamics Experiment/Plasma Source Instrument suite aboard POLAR. *Journal of Geophysical Research*, 103, 29,305–29,338, doi:10.1029/98JA02662.

Su, Y. J., Borovsky, J. E., Thomsen, M. F., Elphic, R. C., & McComas, D. J. (2000). Plasmaspheric material at the reconnecting magnetopause. *Journal of Geophysical Research: Space Physics*, *105*(A4), 7591-7600.

Svenes, K. R., B. Lybekk, A. Pedersen, and S. Haaland (2008). Cluster observations of near-Earth magnetospheric lobe plasma densities – a statistical study. *Annales Geophysicae*, 26, 2845 – 2852.

Swisdak, M., M. Opher, J. F. Drake, & F. Alouani Bibi (2010). The vector direction of the interstellar magnetic field outside the heliosphere. *Astrophysical Journal*, *710*(2), 1769 –1775, doi:10.1088/0004-637X/710/2/1769.

Swisdak, M., B. N. Rogers, J. F. Drake, & M. A. Shay (2003). Diamagnetic suppression of component magnetic reconnection at the magnetopause. *Journal of Geophysical Research*, *108*(A5), 1218, doi:10.1029/2002JA009726.

2537 Tenfjord, P., M. Hesse, C. Norgren, S. F. Spinnangr, and H. Kolstø (2019),The Impact of Oxygen on the
2538 Reconnection Rate. *Geophysical ResearchLetters*, 46(12), 6195–6203,
2539 doi:10.1029/2019GL082175.10

2540 Tenfjord, P., N. Østgaard, S. E. Haaland, K. Snekvik, K. M. Laundal, J. P.Reistad, et al. (2018). How the IMF
2541 By Induces a Local By Component During Northward IMF Bz and Characteristic Timescales. *Journal*
2542 *of Geophysical Research: Space Physics*, 123(5), 3333–3348, doi:10.1002/2018JA025186.

2543 Tenfjord, P., Hesse, M., Norgren, C., Spinnangr, S. F., Kolstø, H., & Kwagala, N. (2020). Interaction of Cold
2544 Streaming Protons with the Reconnection Process. *Journal of Geophysical Research: Space*
2545 *Physics*, *125*(6), e2019JA027619.

2546 Thorne, R. M. (2010). Radiation belt dynamics: The importance of wave-particle
2547 interactions. *Geophysical Research Letters*, *37*(22).

2548 Toledo-Redondo, S., André, M., Khotyaintsev, Y. V., Lavraud, B., Vaivads, A., Graham, D. B., et al. (2017).
2549 Energy budget and mechanisms of cold ion heating in asymmetric magnetic reconnection. *Journal*
2550 *of Geophysical Research: Space Physics*, *122*(9), 9396-9413.

2551 Toledo-Redondo, S., André, M., Khotyaintsev, Y. V., Vaivads, A., Walsh, A., Li, W., et al. (2016a). Cold ion
2552 demagnetization near the X-line of magnetic reconnection. *Geophysical Research Letters*, *43*(13),
2553 6759-6767.

2554 Toledo-Redondo, S., André, M., Vaivads, A., Khotyaintsev, Y. V., Lavraud, B., Graham, D. B., et al.
2555 (2016b). Cold ion heating at the dayside magnetopause during magnetic
2556 reconnection. *Geophysical Research Letters*, *43*(1), 58-66.

2557 Toledo-Redondo, S., Dargent, J., Aunai, N., Lavraud, B., André, M., Li, W., et al. (2018). Perpendicular
2558 current reduction caused by cold ions of ionospheric origin in magnetic reconnection at the
2559 magnetopause: Particle-in-cell simulations and spacecraft observations. *Geophysical Research*
2560 *Letters*, *45*(19), 10-033.

2561 Toledo-Redondo, S., Lavraud, B., Fuselier, S. A., André, M., Khotyaintsev, Y. V., Nakamura, N., et al.
2562 (2019). Electrostatic spacecraft potential structure and wake formation effects for
2563 characterization of cold ion beams in the Earth's magnetosphere. *Journal of Geophysical Research:*
2564 *Space Physics*, 124, 10048– 10062. doi:10.1029/2019JA027145

2565 Toledo-Redondo, S., A. Vaivads, M. André, and Y. V. Khotyaintsev (2015). Modification of the Hall physics
2566 in magnetic reconnection due to cold ions at the Earth's magnetopause. *Geophysical Research*
2567 *Letters*,42(15), 6146–6154, doi:10.1002/2015GL065129.

2568 Torkar, K., R. Nakamura, M. Tajmar, C. Scharlemann, H. Jeszenszky, G. Laky, et al. (2016), Active
2569 Spacecraft Potential Control Investigation. *Space Science Reviews*, 199, 515–544,
2570 doi:10.1007/s11214-014-0049-3.

2571 Varney, R.H., Wiltberger, M., Zhang, B., Lotko, W. and Lyon, J., 2016a. Influence of ion outflow in
2572 coupled geospace simulations: 1. Physics-based ion outflow model development and sensitivity
2573 study. *Journal of Geophysical Research: Space Physics*, *121*(10), pp.9671-9687.

2574 Varney, R.H., Wiltberger, M., Zhang, B., Lotko, W. and Lyon, J., 2016b. Influence of ion outflow in
2575 coupled geospace simulations: 2. Sawtooth oscillations driven by physics-based ion
2576 outflow. *Journal of Geophysical Research: Space Physics*, *121*(10), pp.9688-9700.

2577 Vasyliunas, V. M. (1975). Theoretical models of magnetic field line merging. *Reviews of*
2578 *Geophysics*, *13*(1), 303-336.

2579 Vasyliunas, V. M., (1983). Plasma distribution and flow, in *Physics of the Jovian Magnetosphere*, edited
2580 by A. J. Dessler, pp. 395-453, Cambridge University Press, New York.

Vernisse, Y., Lavraud, B., Faganello, M., Fadanelli, S., Sisti, M., Califano, F., et al. (2020). Latitudinal Dependence of the Kelvin-Helmholtz Instability and Beta Dependence of Vortex-Induced High-Guide Field Magnetic Reconnection. *Journal of Geophysical Research: Space Physics*, *125*(5), e2019JA027333.

Vines, S. K., Fuselier, S. A., Trattner, K. J., Burch, J. L., Allen, R. C., Petrinec, S. M., et al., (2017). Magnetospheric ion evolution across the low-latitude boundary layer separatrix. *Journal of Geophysical Research: Space Physics*, *122*(10), 10-247.

Walsh, B. M., Sibeck, D. G., Nishimura, Y., & Angelopoulos, V. (2013). Statistical analysis of the plasmaspheric plume at the magnetopause. *Journal of Geophysical Research: Space Physics*, *118*(8), 4844-4851.

Wang, S., Kistler, L. M., Mouikis, C. G., Liu, Y., & Genestreti, K. J. (2014). Hot magnetospheric O+ and cold ion behavior in magnetopause reconnection: Cluster observations. *Journal of Geophysical Research: Space Physics*, *119*(12), 9601-9623.

Wang, S., Kistler, L. M., Mouikis, C. G., & Petrinec, S. M. (2015). Dependence of the dayside magnetopause reconnection rate on local conditions. *Journal of Geophysical Research: Space Physics*, *120*(8), 6386-6408.

Westerberg, L.-G. (2019). Earth atmospheric loss through the plasma mantle and its dependence on solar wind parameters. *Earth, Planets and Space*, 71(1), doi:10.1186/s40623-019-1048-0

Welling, D. T., André, M., Dandouras, I., Delcourt, D., Fazakerley, A., Fontaine, D., et al. (2015). The Earth: Plasma sources, losses, and transport processes. *Space Science Reviews*, *192*(1-4), 145-208.

Welling, D.T., Barakat, A.R., Eccles, J.V., Schunk, R.W. and Chappell, C.R. (2016). Coupling the generalized polar wind model to global magnetohydrodynamics: Initial results. *AGU Monograph.* Series

Welling, D.T., Jordanova, V.K., Zaharia, S.G., Glocer, A. and Toth, G. (2011). The effects of dynamic ionospheric outflow on the ring current. *Journal of Geophysical Research: Space Physics*, *116*(A2).

Welling, D.T. and Liemohn, M.W. (2014). Outflow in global magnetohydrodynamics as a function of a passive inner boundary source. *Journal of Geophysical Research: Space Physics*, *119*(4), pp.2691-2705.

Welling, D.T. and Zaharia, S.G. (2012). Ionospheric outflow and cross polar cap potential: What is the role of magnetospheric inflation?. *Geophysical research letters*, *39*(23).

Whipple, E. C. (1981). Potentials of surfaces in space, Rep. Prog. Phys., 44, 1197–1250, doi:10.1088/0034-4885/44/11/002

Wilken, B., Q. G. Zong, I. A. Daglis, T. Doke, S. Livi, K. Maezawa, Z. Y. Pu, S. Ullaland, and T. Yamamoto (1995). Tailward flowing energetic oxygen ion bursts associated with multiple flux ropes in the distant magnetotail: GEOTAil observations. *Geophysical Research Letters*, 22(23), 3267–3270, doi:10.1029/95GL02980.

Winglee, R.M., 1998. Multi-fluid simulations of the magnetosphere: The identification of the geopause and its variation with IMF. *Geophysical research letters*, *25*(24), pp.4441-4444.

Winglee, R. M., Chua, D., Brittnacher, M., Parks, G. K., & Lu, G. (2002). Global impact of ionospheric outflows on the dynamics of the magnetosphere and cross-polar cap potential. *Journal of Geophysical Research: Space Physics*, *107*(A9), SMP-11.

Winglee, R. M., & Harnett, E. (2011). Influence of heavy ionospheric ions on substorm onset. *Journal of Geophysical Research: Space Physics*, *116*(A11).

Wiltberger, M., Lotko, W., Lyon, J.G., Damiano, P. and Merkin, V. (2010). Influence of cusp O+ outflow on magnetotail dynamics in a multifluid MHD model of the magnetosphere. *Journal of Geophysical Research: Space Physics*, *115*(A10).

Wygant, J. R., Cattell, C. A., Lysak, R., Song, Y., Dombeck, J., McFadden, J., et al. (2005). Cluster observations of an intense normal component of the electric field at a thin reconnecting current sheet in the tail and its role in the shock-like acceleration of the ion fluid into the separatrix region. *Journal of Geophysical Research: Space Physics*, 110 (A9). doi: 10.1029/2004ja010708.

Xu, Y., Fu, H. S., Norgren, C., Toledo-Redondo, S., Liu, C. M., & Dong, X. C. (2019). Ionospheric cold ions detected by mms behind dipolarization fronts. *Geophysical Research Letters*, 46 (14), 7883-7892, doi:10.1029/2019gl083885.

Yamada, M., R. Kulsrud, and H. Ji (2010). Magnetic reconnection. *Reviews of Modern Physics*, 82(1), 603–664, doi:10.1103/RevModPhys.82.603.

Yamauchi (2019). Terrestrial ion escape and relevant circulation in space. *Annales Geophysicae*, 37, 1197-1222.

Yau, A. W., T. Abe, M. André, A. D. Howart and W. K. Peterson (2020). Ionospheric ion acceleration and transport, Space Physics and Aeronomy Collection Volume 2: Magnetospheres in the Solar System, Geophysical Monograph, Published 2021 by John Wiley & Sons, DOI: 10.1002/9781119507512

Yau, A. W., T. Abe, and W. K. Peterson (2007). The polar wind: Recent observations. Journal of Atmospheric and Solar-Terrestrial Physics, 69, 1936–1983, doi: 10.1016/j.jastp.2007.08.010.

Yau, A. W., and M. André (1997). Sources of Ion Outflow in the High Latitude Ionosphere. *Space Science Reviews*, 80, 1–25, doi:10.1023/A:1004947203046.

Yau, A.W., Peterson, W.K., & Abe, T. (2017). Measurements of ion outflows from the Earth's ionosphere, In Magnetosphere-Ionosphere Coupling in the Solar System, Geophysical Monograph 222, First Edition. American Geophysical Union. Published by John Wiley & Sons, Inc.

Young, D. T., Balsiger, H., & Geiss, J. (1982). Correlations of magnetospheric ion composition with geomagnetic and solar activity. *Journal of Geophysical Research: Space Physics*, *87*(A11), 9077-9096.

Young, D. T., Burch, J. L., Gomez, R. G., De Los Santos, A., Miller, G. P., Wilson, P., ... & Pollock, C. J. (2016). Hot plasma composition analyzer for the magnetospheric multiscale mission. *Space Science Reviews*, *199*(1-4), 407-470.

Zhang, B., Brambles, O. J., Wiltberger, M., Lotko, W., Ouellette, J. E., & Lyon, J. G. (2016). How does mass loading impact local versus global control on dayside reconnection?. *Geophysical Research Letters*, *43*(5), 1837-1844.

Zhang, B., Brambles, O. J., Cassak, P. A., Ouellette, J. E., Wiltberger, M., Lotko, W., & Lyon, J. G. (2017). Transition from global to local control of dayside reconnection from ionospheric-sourced mass loading. *Journal of Geophysical Research: Space Physics*, *122*(9), 9474-9488.

Zhang, B., Brambles, O. J., Lotko, W., & Lyon, J. G. (2020). Is nightside outflow required to induce magnetospheric sawtooth oscillations. *Geophysical Research Letters*, 47, e2019GL086419. doi : 10.1029/2019GL086419

Zheng, Y., Moore, T.E., Mozer, F.S., Russell, C.T. and Strangeway, R.J. (2005). Polar study of ionospheric ion outflow versus energy input. *Journal of Geophysical Research: Space Physics*, *110*(A7).

2665 Zong, Q. G., B. Wilken, J. Woch, T. Mukai, T. Yamamoto, G. D. Reeves, et al. (1998),Energetic oxygen ion
2666 bursts in the distant magnetotail as a product of intense substorms: Three case studies. *Journal of*
2667 *Geophysical Research*, 103(A), 20,339–20,364, doi:10.1029/97JA01146.